NTNU

Norwegian University of
Science and Technology

The Influence of Water Content and Mineralogy on the Shear Strength of two Petrographically Contrasting Norwegian Tills

Emilie Olsen Hauge

Geotechnology
Submission date: June 2018
Supervisor: Bjørn Frengstad, IGP
Co-supervisor: Arnfinn Emdal, IBM
Erin Lindsay, IBM

Norwegian University of Science and Technology
Department of Geoscience and Petroleum

Abstract

The influence of mineralogical controlled properties and water content on the shear strength of two petrographically contrasting Norwegian till soil types are evaluated within this thesis. A total of ten samples have been collected. Six originating from the Precambrian bedrock region in the county of Møre & Romsdal and four samples derived from the Cambro-Silurian metamorphic rock region in Trøndelag county. Samples have been collected both inside and outside of landslide scars and analyzed in regard to material properties.

Conducted examinations include field investigations, grain size distribution analysis of material finer than 16 mm, mineralogical analysis, shape and angularity analysis and investigation of dry of optimum water content. The results from these analyses were used to explain differences in the shear strength parameters found by conduction of shear box tests on three of the samples. The samples were tested in both dry condition and with a dry of optimum water content.

The angle of friction found by shear box testing ranges from 22.8 to 35.4°. The samples from the valley Innfjorden in the Precambrian bedrock province exhibit in general a higher frictional angle compared to the sample from Gauldalen in the Cambro-Silurian province. Analysis of a limited number of samples imply a connection between the bedrock geology and material parameters, such as particle shape and mineralogy. Furthermore, results from the shear tests indicate an influence of material properties on the shear strength.

The material properties of the samples collected inside and outside of landslide channels show no substantial differences. The only variation is a lower degree of grading of the grains in the samples from inside a channel. In dry condition the samples display the same shear strength properties. When water is added, the out of channel sample exhibits a higher frictional angle.

The change in the shear strength, as a result of added water is not analogous for all the samples. A reason for this might be the different effects of water on the density of the samples. However, the shear stress – displacement curves of unsaturated soil show a lower frictional resistance compared to dry material.

Sammendrag

I denne oppgaven er det sett på påvirkningen av mineralogisk bestemte faktorer og vanninnhold på skjærstyrken til to typer morene med ulik bergartsopprinnelse. Det er samlet inn ti prøver, seks hentet fra Innfjorden i Møre og Romsdal, mens fire kommer fra Gauldalen i Trøndelag. Geologien i Innfjorden er dominert av Prekambrisk grunnfjell bestående av ulike typer gneiser, mens det i Gauldalen er Kambro-Siluriske metamorfe bergarter. Prøvene er hentet fra både utenfor og inne i skredløp og analysert for å undersøke sammenhengen mellom materialegenskaper og utløsning av skred.

Utførte analyser inkluderer feltundersøkelser, kornfordelingsanalyse av material finere enn 16 mm, mineralogisk analyse, analyse av kornform og flisighet og undersøkelse av optimalt vanninnhold. Det er sett på sammenhengen mellom materialegenskapene og forskjeller i skjærstyrkeparametere funnet gjennom tester i skjærboks. Tre ulike prøver er testet både i tørr og umettet tilstand.

Friksjonsvinkelen ble gjennom skjærboksforsøk funnet til å variere mellom 22.8 – 35.4°. Prøvene fra Innfjorden viser generelt en høyere friksjonsvinkel sammenlignet med prøvene fra Gauldalen. Resultater fra analyser av den begrensede prøvemengden impliserer en sammenheng mellom berggrunnsgeologien og material egenskapene til morenen, slik som kornform og mineralogi. Det er også en sannsynlig sammenheng mellom materialegenskaper og skjærstyrke.

Forskjellen i materialegenskapene til prøver samlet utenfor og innenfor skredbaner viser ingen tydelige forskjeller. Eneste markante forskjellen er lavere gradering av kornfordelingen i prøvene tatt fra skredkanaler i forhold til prøver hentet utenfor. I tørr tilstand har prøvene i og utenfor skredbaner de samme skjærstyrkeparameterne. Ved testing av fuktig materiale har prøven hentet utenfor skredbanen den største friksjonsvinkelen.

Endringen av friksjonsvinkel ved tilsetning av vann til prøvene er ikke samsvarende for alle prøvene. En årsak til dette kan være den ulike effekten av vann på tettheten til prøvene. Skjærstyrke – forskyvingsgrafen for umettet material viser derimot en lavere friksjonsmotstand sammenlignet med tørt materiale.

Preface

This master thesis was written the spring semester of 2018 as a continuation of the project report delivered in December 2017 at the Department of Geoscience and Petroleum at the Norwegian University of Science and Technology. The master thesis constitutes 30 credits.

The Project report and master thesis have been conducted in collaboration with the Department of Civil and Environmental Engineering, NTNU and is a part a of PhD candidate Erin Lindsay's research within "Landslides triggered by hydro-meteorological processes". This is one of the research areas within "Klima 2050", a Centre for Research-based Innovation (SFI).

First of all, I would like to thank my main supervisor Professor Bjørn Frengstad and co-supervisors Assistant Professor Arnfinn Emdal and Phd. Candidate Erin Lindsay for help and support. I specially want to thank Erin for letting me take part in her project and for help with the field work. I would also like to thank Gunnar Vistnes, Phd. Candidate Øystein Lid Opsal, Marte Maria D. Jermstad, Håkon Havskjold and Odd Corneliussen for assistance and guidance regarding the laboratory tests. In addition, I must thank Lena Rubensdotter at NGU for valuable input and guidance with the theoretical part of the thesis.

At last, I want to thank all my fellow students for five remarkable years at NTNU.

Emilie Olsen Hauge

Trondheim 11.06.18

Table of contents

List of figures

List of tables

1 Introduction

1.1 Background

No other natural hazard causes as many fatalities as landslides and avalanches in Norway (Amundsen, 2009). During the last 500 years, a total of 3500 landslide events were registered, resulting in more than 4000 fatalities (Furseth, 2006). A landscape dominated by valleys created by glacial activity causes large topographical differences which facilitate landslide events.

Water induced landslides in the form of debris flows and soil slides occur regularly in Norwegian valley slopes. As water infiltrates the ground surface, stabilizing forces between the soil particles are reduced. The stabilizing forces are related to frictional- and cohesive forces and are dependent on several factors including soil type, degree of compaction, grain size distribution and grain shape (Høeg et al., 2014). A large quantity of the soil cover in Norway consists of till soils (Selmer-Olsen, 1977). However, scientific research performed within this field is scarce and most of the research was conducted in the 1970's and 1980's (Jørgensen, 1977, Haldorsen and Kruger, 1990, Haldorsen et al., 1983). A recent study of till soils in relation to shear strength and geological properties has been conducted by (Opsal, 2017, Opsal, 2018). These papers do however not consider the influence of the soil water content, which affects the shear strength of soil materials (Lu and Likos, 2004).

A changing climate causes an expected increase in the frequency of extreme precipitation events. In addition to this, the amount of precipitation during such events is calculated to rise. If these predictions are correct, the occurrence of rainfall induced landslides might become more frequent in the future (Hanssen-Bauer, 2015).

The damages caused by landslides and the future predictions have resulted in more research within this field. Klima 2050, a Centre for research-based Innovation (SFI) hosted by SINTEF and financed by the Research Council of Norway and 20 partners is one of them. Klima 2050 has the aim to reduce the societal risks caused by climate change. Buildings and infrastructure are particularly vulnerable to such risks. Adaption to the changes in climate is essential, hence Klima 2050 will concentrate on development of new solutions to withstand the changes in weather and gradual changes in climate. One of the four main research areas within Klima 2050 is "Landslides triggered by hydro- meteorological processes" (SFI, 2017).

1.2 Problem description

The hydro-mechanical properties of till soils may vary depending on factors including source material mineralogy, deposition process, degree of physical, chemical, or biological weathering, freezing, vegetation, groundwater conditions and degree of saturation. These properties affect the capacity of the soil to absorb and transport water, as well as the strength properties relevant to slope stability. Therefore, they influence the threshold limits for slope stability.

The objective of this master project is to investigate the shear strength of two petrographically contrasting tills found in areas with known debris flow hazard. The relation between shear strength and water content as well as between shear strength and mineralogical factors will be emphasized.

This includes

- Collection of field samples from both inside and outside of landslide scars
- Description of the undisturbed till at the field sites, including layering, weathering, compaction, cementation, cohesion, etc.
- Study of grain size distribution and coefficient of uniformity
- Description of the mineralogy, especially the mica content, and the grain shapes from areas with contrasting bedrock geology
- Testing the shear strength of till samples with varying water content

2 Theory

2.1 Unsaturated soil mechanics

The soil that covers the ground surface can be subdivided into saturated and unsaturated soil based on the water content. In contrast to the saturated soil, which consist of the two phases solids and fluids, the unsaturated soil also contains air. Negative pore-water pressures relative to the air-pore pressure is characteristic for unsaturated soils. The air-water interface called the contractile skin is important then assessing unsaturated soil mechanics (Fredlund and Morgenstern, 1977). The depth of the groundwater table, and thus the thickness of the unsaturated zone is strongly dependent upon the local climate and topography (Brattli, 2009). The soil above the groundwater table can be separated into the "Dry zone", the "Two-phase zone" and the "Capillary zone", as illustrated in figure 2.1 The soil within the capillary zone has a high water content, but is characterized as a part of the unsaturated zone (Fredlund et al., 2012).

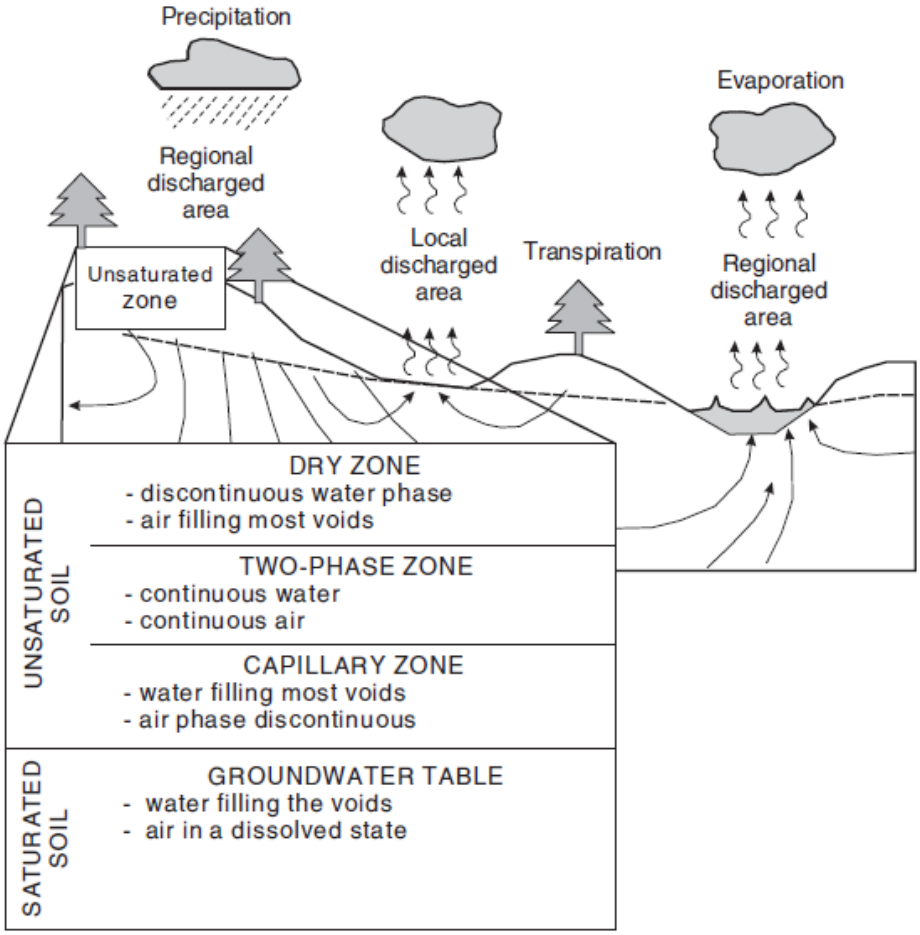

Figure 2.1: Hydrologic cycle and soil subsections (Fredlund et al., 2012).

Grain size and shape reflect the mineralogical composition, length and type of transportation and type of deposition of the soil. Increasing distance of transport by water usually results in increased rounding of grains. Smaller particles tend to have failure along crystal atomic planes and are therefore more platy than larger grains (Santamarina and Cho, 2004). The porosity of a soil is affected by the size and shape of grains, the degree of compaction and cementation and is given by:

$$n = \frac{V_p}{V} \quad 2.1$$

Where V_p represents the volume of pores and V the total volume of the sample. The void ratio, e is the ratio of the volume of pores to the volume of solids, V_s (Terzaghi et al., 1996).

$$e = \frac{Vp}{Vs} \quad 2.2$$

Increasing amount of fine particles in a soil will reduce the porosity and increase the density by occupying space between larger grains. Angular grains will on the other hand result in lower density and higher void ratio (Mitchell and Soga, 2005).

2.1.1 Soil suction

The high degree of saturation in the capillary zone can be explained by the capillary phenomena. Capillary rise of water in soil can be described by use of a capillary tube with the lower end submerged into water. Water is drawn upwards in the tube until pressure equilibrium is reached. The upper end of the water column is in the shape of a cup and is called the meniscus. The angle between the meniscus and the wall of the tube is called the contact angle, α. The water surface film, otherwise known as the contractile skin acts as the boundary between water and air. Tensile stress, called surface tension, T_s is working on the contractile skin. The surface tension is a result of strength differences in the forces acting on the water molecules, as illustrated in Figure 2.2 (Terzaghi, 1943, Fredlund et al., 2012).

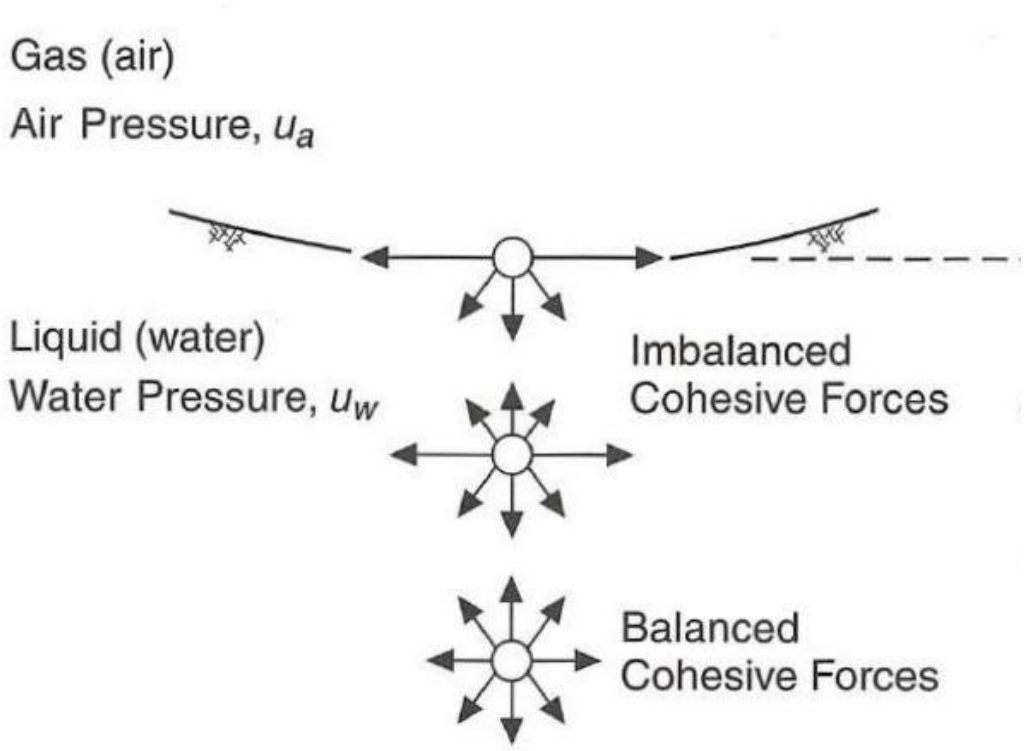

Figure 2.2: Forces acting on an air-water interface (Lu and Likos, 2004).

Tension forces are oriented parallel to the skin surface. The tensile stress causes the skin to attain an elastic behavior and a pressure difference between the air and the water phase. A change in stress in the contractile skin can result in soil volume changes, change in water content and shear strength. The vertical component of the surface tension, F is responsible for holding the weight of the water at a height, h_c.

$$F = 2\pi r T_s cos\alpha = \pi r^2 h_c p_w g \qquad \text{(N/m)} \qquad 2.3$$

This effect and the components in equation 2.3., except the density of water, ρ_w are illustrated in Figure 2.3 (Terzaghi, 1943, Fredlund et al., 2012).

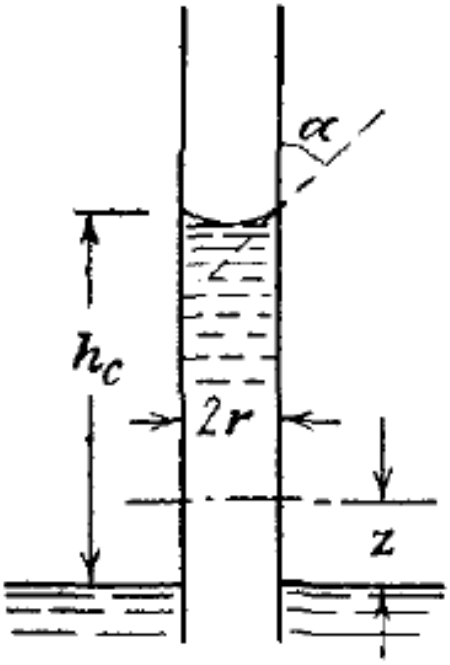

Figure 2.3: Water in a capillary tube (Terzaghi, 1943).

The capillary tube can be compared to the pores in soils with small pore sizes. The capillary forces cause a rise of water above the groundwater table. The height of the capillary rise increases with decreasing pore size. The stresses from the contractile skin cause a compressive force on the surrounding particles, resulting in a negative pore-water pressure. The pressure becomes more negative with decreasing soil saturation (Terzaghi, 1943, Fredlund et al., 2012).

In addition to capillary forces there are electrical forces working on the particle contacts. These forces include electrical repulsive and Van der Waals attraction forces, which strength decreases with increased interparticle distance (Santamarina, 2003). The forces occur close to the solid-liquid interface and are most prominent for fine grained soils. Electrical repulsive forces are a consequence of the negative charge on mineral surfaces. The attractive Van der Waals forces occur by interactions between particle and water molecules. A low water content results in a thin water film surrounding the soil particles, and thus increased importance of the Van der Waals attractive forces. The effect of electrical forces is most prominent around clay minerals with high surface charge and large surface area. The capillary force, together with repulsion and attraction forces are combined to matric suction. Matric suction is controlled by the water content of the soil. An increasing water content is followed by a decrease in matric suction (Lu and Likos, 2004).

Matric suction constitutes one out of two components in the total soil suction in unsaturated soil. The second component is caused by a decrease in relative humidity, due to dissolved salts in the pore water, and is called osmotic suction, π. The effect of osmotic suction is generally very low, and is therefore often neglected. The total suction, ψ is defined as

$$\Psi = (u_a - u_w) + \pi \qquad \text{(Pa)} \qquad 2.4$$

where

u_a = pore-air pressure

u_w = pore-water pressure

(u_a-u_w) = matric suction

π = osmotic suction (Fredlund et al., 2012).

The suction in soils ranges from 0 to 1 000 000 kPa, depending on the degree of saturation. This correlation is illustrated in Figure 2.4 for different types of soils. The straight lines which intersect the suction axis at complete saturation represents the soil specific air-entry value. The air-entry value is the pressure difference between air and fluid required for desaturation of the largest pores (Vanapalli et al., 1999).

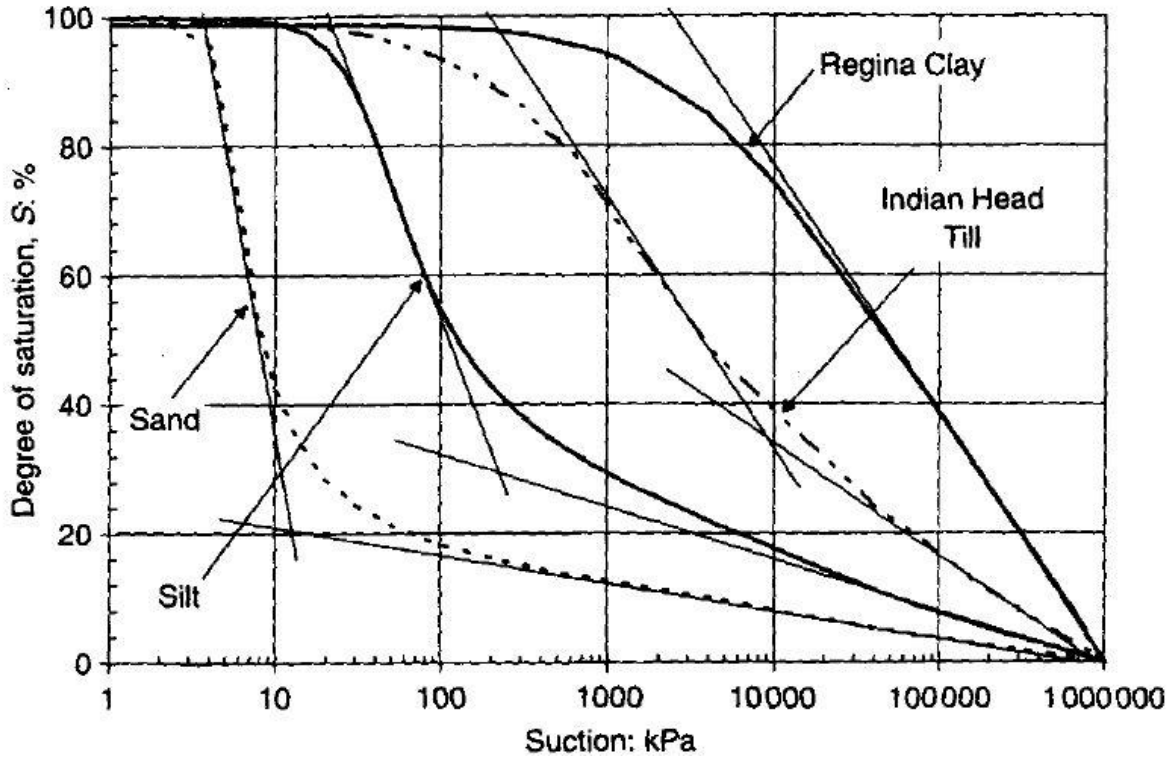

Figure 2.4: Suction in relation to degree of saturation of different types of soil (Vanapalli et al., 1999).

Mineralogy of the soil is the main controlling factor regarding particle size, shape and surface characteristics. The interaction with water is also affected by the mineralogy (Mitchell and Soga, 2005). Studies on concrete aggregates have shown that flaky grains increase the water absorption capacity and causes a lower compressibility compared to rounded particles (Adom-Asamoah and Afrifa, 2010). The grain size distribution is important, as the ability to retain water and buildup of pore pressures are higher in fine grained soils than coarse grained soil (Vanapalli et al., 1999).

Clay minerals are smaller than 0.002 mm and consists of aluminum silicates created by chemical weathering of silicate minerals. Kaolinite, illite and montmorillonite are the main groups of clay minerals. These minerals can bind a large amount of water to the surface (Selmer-Olsen, 1980). Thus, an increasing amount of clay minerals present in a soil causes a rising plasticity, larger potential for swelling and shrinking, reduction of the hydraulic conductivity, greater compressibility, larger cohesion and lower internal angle of friction. This can be explained by the layered structure, the large surface area and negative surface charge of these minerals (Mitchell and Soga, 2005).

Mica is a group of silicate minerals that are characterized by a thin sheet structure, a high degree of shine and low hardness. The main types are muscovite and biotite. Muscovite is white of color, while biotite is black due to iron. Biotite is easily weathered into rust-colored grains. Biotite and hornblende have a large capacity to absorb water on the surface, compared to cubical grains, such as feldspar grains (Selmer-Olsen, 1980, Selmer-Olsen, 1977). Experiments performed by Novikov and Miskovsky (2009) on aggregates for construction purposes show that increasing content of free mica in the fine fraction results in an increase in the capillarity. The greatest effect was observed in samples with a content of mica exceeding 20%. Minerals such as illite and chlorite, with similar characteristics as mica are expected to have a similar effect. Studies have shown that the size of the mica grains have a great importance in relation to the influence in the porosity. A content of coarse mica of 20% in a sand can increase the porosity by 70%. The same effect was not observed in sand with mica minerals of finer fractions (Selmer-Olsen, 1977).

In summary, the soil is divided into two sections depending on the soil water content. Within the unsaturated zone capillary and electrical forces induces matric suction. The amount of suction in a soil is dependent on the soil water content and ranges from zero in saturated soil to

1 000 000 kPa in soil with a low water content. Particle size, shape and surface characteristics are strongly dependent on the mineralogy. Flaky grains, such as mica have a larger water absorption ability than rounded grains.

2.1.2 Stress conditions and shear strength of soils

Saturated soil

A change in the degree of saturation creates a difference in the stresses acting on the soil matrix. Terzaghi (1943) defined effective stress as the stress state variable for saturated soils beneath the groundwater table. It describes the stress acting on the soil skeleton:

$$\sigma' = \sigma - u_w \qquad \text{(kPa)} \qquad 2.5$$

where

σ’ = effective normal stress
σ = total normal stress
u_w = pore-water pressure

Shearing resistance of soils is a consequence of resistance to movement at interparticle contacts due to bonds between grains and particle interlocking. The area of contact between soil particles depends on the effective normal force acting on the material. These resistant forces increases with increasing particle contact area and results in an increased shear resistance (Terzaghi et al., 1996).

Slope failure along a planar sliding surface is described by the Mohr-Coulomb failure criterion. The shear resistance of a saturated soil along the surface at the time of failure is given by:

$$\tau = c' + (\sigma - u_w)\, tan\, \phi' \qquad \text{(kPa)} \qquad 2.6$$

where

τ = shear resistance on the sliding surface at the time of failure
$(\sigma - u_w)$ = mean effective normal stress on the surface at time of failure
ϕ’ = effective internal friction angle
c’ = effective cohesion
u_w = pore-water pressure at failure

Equation 2.6 and the failure envelope in Figure 2.5 describes the relationship between the shear strength of a soil and the effective stress. The slope of the failure envelope defines the angle of internal friction, while the interception with the y-axis equals the effective cohesion. The point of interception between the failure envelope and the Mohr circles represents the stress conditions on the sliding surface at the time of failure. The shear strength envelope illustrates the amount of shear stress a saturated soil can withstand before failure occurs (Fredlund et al., 2012).

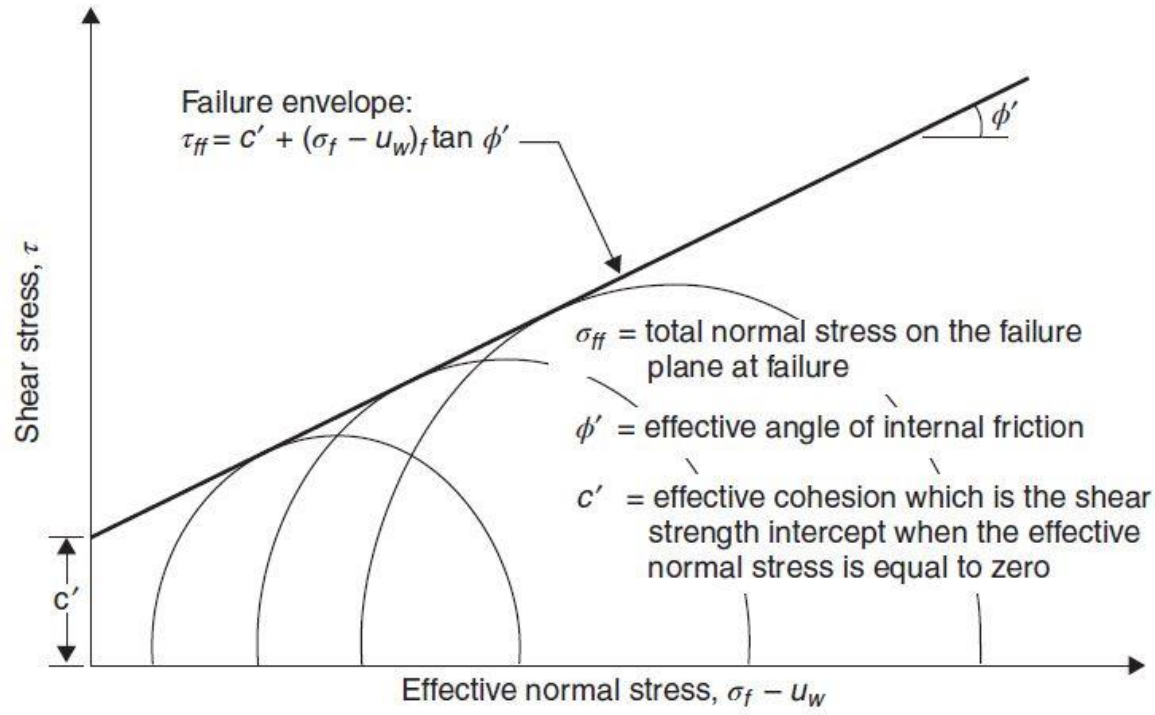

Figure 2.5: Mohr Coulomb failure envelope for saturated soil (Fredlund et al., 2012).

Unsaturated soil

When studying unsaturated soil, additional factors needs to be considered. As the pores contain both air and fluid, the pore-air pressure and the difference between the pore-air and pore-water pressure needs to be incorporated (Lu and Likos, 2004). Regarding unsaturated soils there exists three main approaches for describing the stress state. The first is "*The modified effective stress approach*" based on the work by Bishop (1959). Secondly, Fredlund and Morgenstern (1977) presented "*The independent stress state variable approach*" (Lu and Likos, 2006).

The modified effective stress approach is based on the effective stress equation:

$$\sigma' = (\sigma - u_a) + \chi(u_a - u_w) \quad \text{(kPa)} \quad 2.7$$

where

($\sigma - u_a$) = net normal stress

($u_a - u_w$) = matric suction

χ = effective stress parameter

The effective stress parameter, χ is a material variable depending on the degree of saturation. In dry soil, $\chi = 0$ and in completely saturated soil, $\chi = 1$. Determination of the effective stress parameter in relation to soil saturation has proved difficult. Based on the Mohr-Coulomb criterion the failure conditions can be described by:

$$\tau_f = c' + \left[(\sigma - u_a)_f + \chi_f (u_a - u_w)_f\right] tan\phi' \quad \text{(kPa)} \quad 2.8$$

Where τ_f represents the shear strength and f indicates the stress acting on the failure plane (Lu and Likos, 2004).

The independent stress state variable approach is defined as:

$$\tau = c' + (\sigma_f - u_a) \tan \phi' + (u_a - u_w) \tan \phi^b \quad \text{(kPa)} \quad 2.9$$

where

c´ = effective cohesion

($\sigma_f - u_a$) = net normal stress on the failure plane

u_a = pore-air pressure on the failure plane

ϕ' = angle of internal friction

($u_a - u_w$) = matric suction on the failure plane

ϕ^b = rate of increase in shear strength in relation to a change in matric suction

When completely saturated the pore-water pressure will approach the pore-air pressure and the matric suction reduces to zero. Hence, equation 2.9 transforms into the equation for saturated soil. Equation 2.9 can be plotted in three dimensions, as illustrated in Figure 2.6. The tangent to the Mohr circles at failure is named the extended Mohr-Coulomb failure envelope. It defines the shear strength of unsaturated soil. The shear strength of saturated soils is illustrated by the interception line between the extended failure envelope and the frontal plane. For unsaturated soils with constant matric suctions larger than zero, the failure plane is given by:

$$\tau = c + (\sigma_f - u_a) tan\phi' \qquad \text{(kPa)} \qquad 2.10$$

Where the parameter c equals the total cohesion intercept. The failure envelope can be both linear or curved. The cohesion, c and the slope angles ϕ' and ϕ^b are the shear strength parameters of the soil. Influencing factors, such as density, mineral composition, void ratio, stress history and strain rate are incorporated in these parameters (Fredlund et al., 2012, Fredlund et al., 1978).

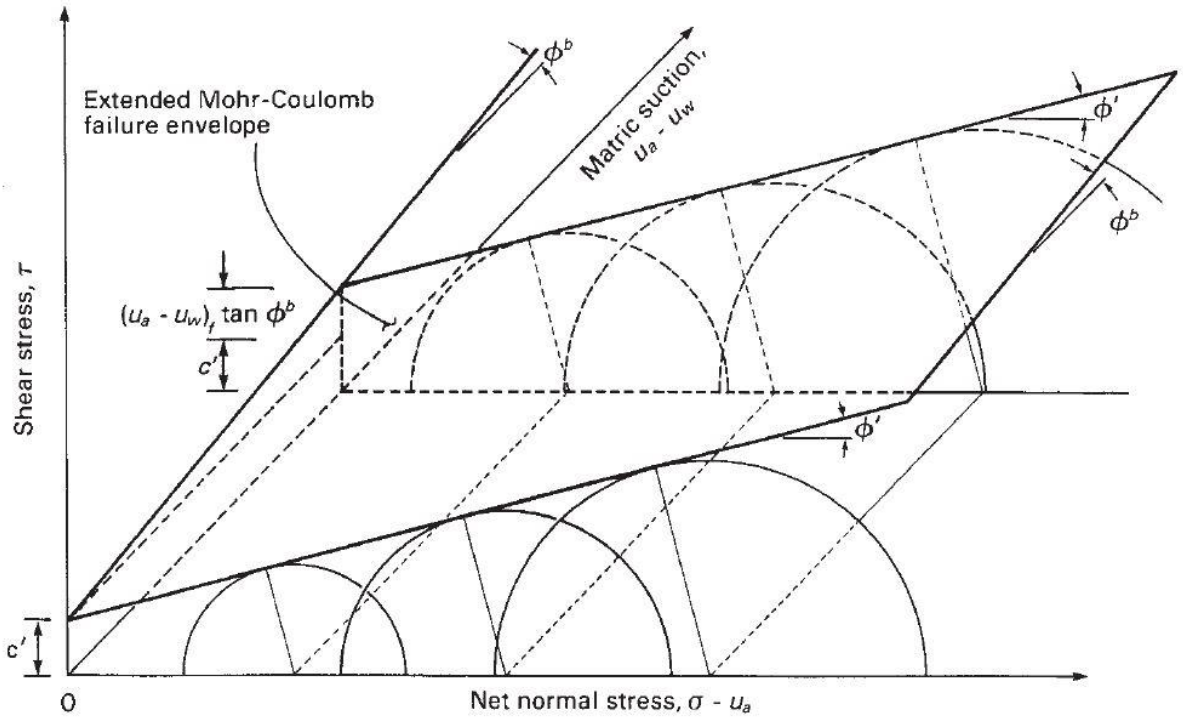

Figure 2.6: Extended Mohr-Coulomb failure envelope for unsaturated soil (Fredlund et al., 2012).

The shear strength of the soil increases with an increase in matric suction. The amount of increase is determined by the angle ϕ^b, which generally equals the internal friction angle ϕ' (Fredlund et al., 2012). The internal friction angle can be assumed to be independent of the matric suction in the range of 0-500 kPa. Which is the range where most practical problems for engineers occur (Vanapalli et al., 1996a).

Material properties

Effective stress, density and soil structure are the central factors determining the shear resistance of soils. Density is affected by the porosity, void ratio and water content. The void ratio is particularly important in relation to the area of interparticle contact. It is dependent on material properties such as grain size, shape, surface roughness and strength. Hence, the mineralogical composition, which controls these parameters has an indirect influence on the shear strength of soils (Terzaghi et al., 1996).

The cohesion parameter, c´ in equation 2.11. represents interparticle bonding. This includes van der Waals forces, electrical forces, salt bridges, and cementation between particles. The degree of saturation, grain size distribution and density are in addition incorporated into the parameter c´ (Sidle and Ochiai, 2006). Cementation of grains occur due to precipitation of dissolved minerals and salts in the pore-water. Cementation normally occurs in the upper unsaturated zone and is also connected to biological and chemical activities. Cementation strengthens the interparticle contacts and increases shear strength of the soil in the range of tens to hundreds of kPa (Lu and Godt, 2013, Novotný and Klimeš, 2014).

Cementation due to chemical precipitation is sparse in Norwegian soils. However, iron and calcite does in some locations cause increasing binding between grains. Precipitation of iron occurs mainly in the leached horizon, caused by groundwater containing humus which results in a reduction of Fe^3-compounds to soluble Fe^2-compounds. The iron oxides are transported by percolating water into the underlying soil, where it is precipitated due to reaction with oxygen rich capillary water or groundwater (Selmer-Olsen, 1980). Precipitation of calcite minerals in the soil or in surrounding bedrock fills the pore spaces between grains. The degree of increased strength of the soil depends on the precipitated amount, which is highly variable. In addition to iron and calcite, other types of mineral precipitation occur in Norwegian soils. These are usually found at a larger depth, for example precipitation of quartz (Selmer-Olsen, 1977).

The frictional resistance between the grain contacts is expressed by the internal friction angle ϕ', which defines at which gradient the sediments are stable. Slope stability increases with increasing internal frictional angle, which is a function of surface roughness, shape and size of grains. Figure 2.7 illustrates that coarse, angular grains have the highest frictional angle (Selmer-Olsen, 1977).

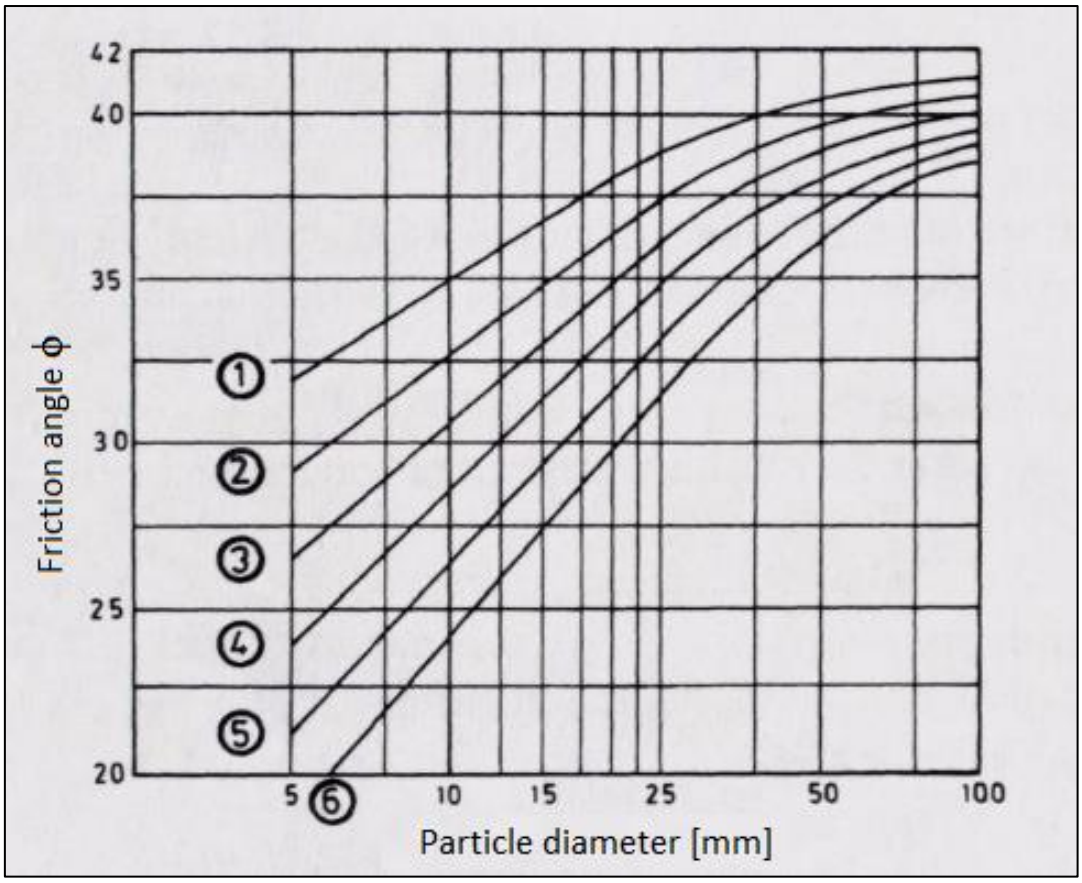

Figure 2.7: Particle size and shape in relation to the friction angle. 1: very angular, 2: moderately angular, 3: Slightly angular, 4: Slightly rounded, 5: Moderately rounded 6: Well rounded. Modified from Selmer-Olsen (1977).

A study performed by Li (2013), concluded that an increased coarse fraction results in a higher shear strength. Surface roughness is dependent on the strength, texture and hardness of the particle surface. These parameters are determined by the crystal structure of the minerals. Friction angles of a selection of minerals are given in Table 2.1 (Terzaghi et al., 1996).

Table 2.1: Sliding friction angle of minerals in water. Modified from Terzaghi et al. (1996)

Mineral	**Frictional resistance, ϕ´(degrees)**
Quartz	22-35
Feldspar	36-38
Hornblende	31
Calcite	31-34

The surface of mica minerals is among the smoothest natural occurring mineral surfaces. On sheet minerals such as muscovite, biotite, chlorite and clay minerals, water acts as a lubricant reducing the frictional strength. The sheets are held together by electrostatic forces. The forces are weak and cleavage occurs easily. The sheet structure of mica minerals causes mixtures of sand and silt with a small amount of mica to have high compressibility when loaded , similarly to clay minerals (Mitchell and Soga, 2005). The presence of water on the particle surfaces of massive minerals such as quartz, calcite and feldspar results in an anti-lubricating effect and increasing frictional coefficients. This effect decreases with increased surface roughness (Horn and Deere, 1962).

The shear strength of a soil is also affected by the hardness of particles. Crushing hardness is roughly equal to the scratching hardness defined by Moh´s scale: 1. Talc, 2. Gypsum, 3. Calcite, 4. Fluorite, 5. Apatite, 6. Orthoclase, 7. Quartz, 8. Topaz, 9. Corundum, 10. Diamond (NS-EN 12670, 2001). Quartz, with a scratch hardness of 7 is thus resistant to crushing. Silt and clay minerals are not very susceptible to breaking and the particle size distribution has minor impact on the degree of crushing (Hardin, 1985).

Novotný and Klimeš (2014) and Fragaszy et al. (1992) performed several shear box tests on till soils and found that individual large particles flow within the soil matrix and have little impact on the shear strength. Direct shear tests on clay and sand mixtures show that the shear strength depends on the relative concentration of the two grain sizes. The shear resistance of a material with a sand content larger than 75%, by weight, were dominated by the frictional resistance between the sand grains. With a sand content ranging between 75 – 40% the shear resistance depends upon a combination of the shear strength of the clay and the frictional resistance. Less than 40% sand content in a mixture resulted in a shear strength controlled by the properties of clay (Vallejo and Mawby, 2000).

Compaction of the soil increases the number of particles per unit volume, thus increasing the area of interparticle contacts and the shear strength. The term dry density is used to describe the degree of compaction. It is dependent on the compaction effort applied and the moisture content. This is explained by formation of a surface film surrounding the particles. As the water film increases in thickness lubrication between particles rises, which results in a higher packing density. Further increase in water content will at a certain point result in a larger distance between the particles, and decreasing density. The moisture content at the maximum dry density is called the optimum moisture content (Aysen, 2002, Whitlow, 2001). The optimum moisture content is influenced by the grain size distribution, shape of grains and the amount and type of

fine particles present (Das and Sawicki, 2001). Vanapalli et al. (1996b) found that soil tested at optimum or wet of optimum moisture content exhibit a higher shear strength than soil tested at dry of optimum. A greater shear strength is explained by a higher matric suction, created by a larger amount of wetted interparticle contacts.

The degree of dilation during shear of dense granular soils under low pressure is high. Particles push and move around the surrounding grains. The inter-movement of particles causes an additional resistance to the frictional angle. The degree of dilatancy increases by increasing density, grain size and the degree of flakiness. In soils with a loose character, the shear stress might cause a negative dilatancy. Grains will mobilize and create a greater density. At greater pressures movement relative to adjacent particles becomes more difficult when the pressure increases. Thus, the interparticle movement is replaced by particle crushing. Crushing of particles is controlled by particle strength, shape, size and porosity. In well graded and strong material, such as till, particle crushing only occurs at high pressures (Terzaghi et al., 1996, Selmer-Olsen, 1977).

In summary, shear resistance in a soil is caused by bonds between grains and interparticle locking. The Mohr-Coulomb failure criterion describes the shear failure along a sliding surface. When considering saturated soils, the criterion includes cohesion, normal effective stress, pore-water pressure and internal friction angle. Resulting in a failure envelope describing the amount of shear stress a soil can withstand before failure. Several approaches exists for assessment of the stress state of unsaturated soils:

- The modified effective stress approach
- The independent stress state variable approach

These approaches all includes the degree of saturation and matric suction in the evaluation. Resulting in an extended Mohr-Coulomb failure envelope where the shear strength increases with increasing matric suction.

The mineralogy of the material is determinative for the shear strength as it controls the size, shape, roughness and strength of grains. These factors influence on the internal friction angle of the soil.

2.2 Norwegian tills

The sediments covering the Norwegian land-surface were mainly deposited by glaciers during the last glaciation, Weichsel. The degree of glacial erosion depended on the glacier thickness and the velocity of flow. The direction of movement was towards the marginal zones, as illustrated in Figure 2.8 (Selmer-Olsen, 1980).

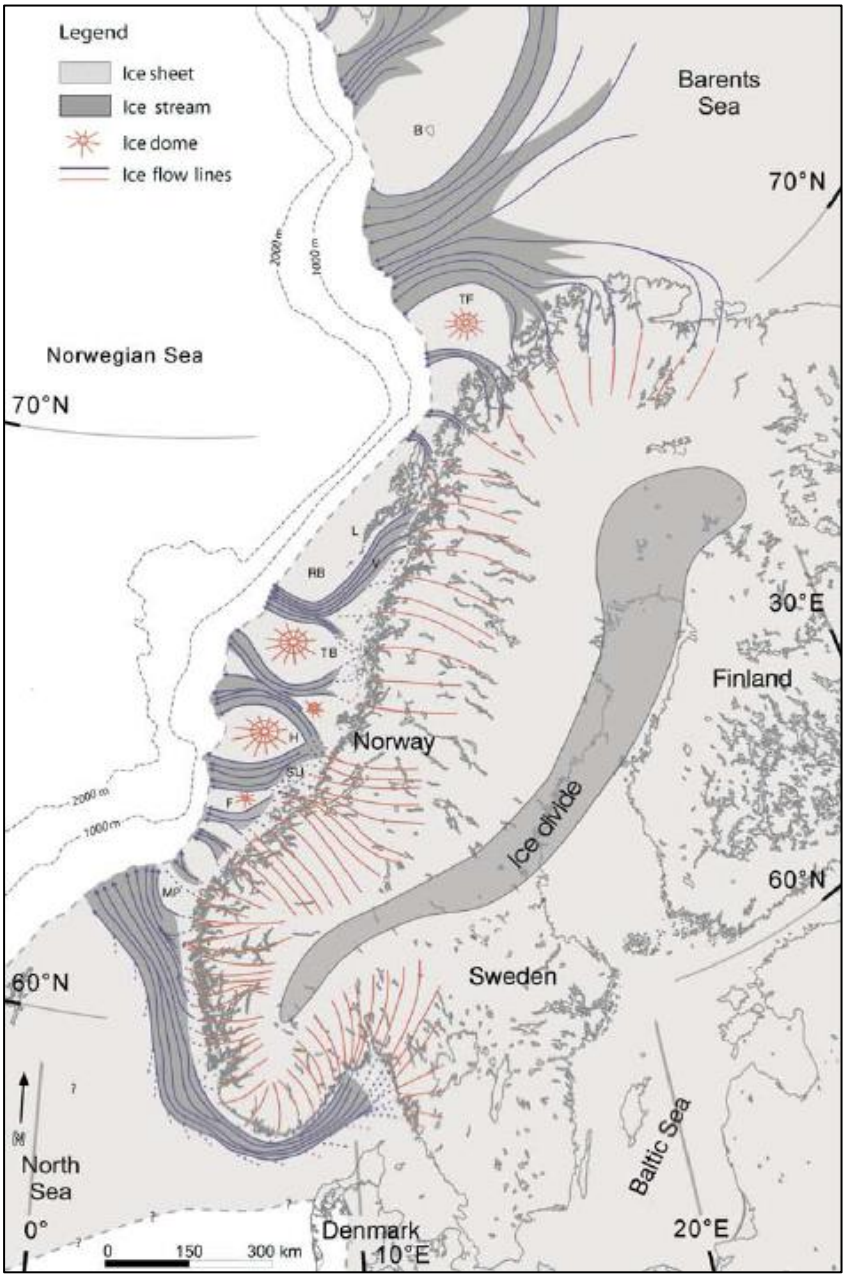

Figure 2.8: The glacier flow directions during the last glacial period. Modified from Ottesen et al. (2005).

Tills are characterized as poorly sorted sediments with a high degree of compaction. The tills are generally highly influenced by the geologic composition within 0-2 km, which indicates a short transport distance (Selmer-Olsen, 1977). Glacial erosion of the land surface has resulted in a bedrock with a low degree of weathering and a distinct boundary between the bedrock and the overlying soil (Høeg et al., 2014).

Tills were deposited by different processes which resulted in diverse properties. Differentiation by type of deposition through investigation of till deposits in the field is difficult. Boulton (1972) divided the depositional processes into:

Subglacial tills:	Melt-out till
	Lodgment till
Supraglacial tills:	Flow till
	Melt-out till

Lodgment tills are normally characterized by a high degree of consolidation resulting from the pressure inflicted by the overlying glacier. Following the deglaciation, the top soil surface has been subjected to repeated freezing and thawing cycles producing a 1-2 meter thick “active layer” with a loose character (Bargel et al., 2011). It is this looser layer that usually fails when a landslide occurs (Høeg et al., 2014).

The Norwegian tills can be divided into two main groups based on the grain size distribution. Figure 2.9 shows the difference in particle size of 3000 till samples. The two zones of higher concentration are marked and represents the two main groups. Tills derived from Cambro-Silurian metamorphic sedimentary rocks have a higher content of fine grains than the tills derived from Precambrian bedrock. The fines content was found to be above 35% for Cambro-Silurian and 15-25% for Precambrian derived tills (Jørgensen, 1977). The difference in the content of fine particles can be explained by the fact that sedimentary rocks are weaker and more easily crushed. In addition they have a higher content of minerals such as chlorite and mica compared to hard and strong metamorphic rocks (Selmer-Olsen, 1977).

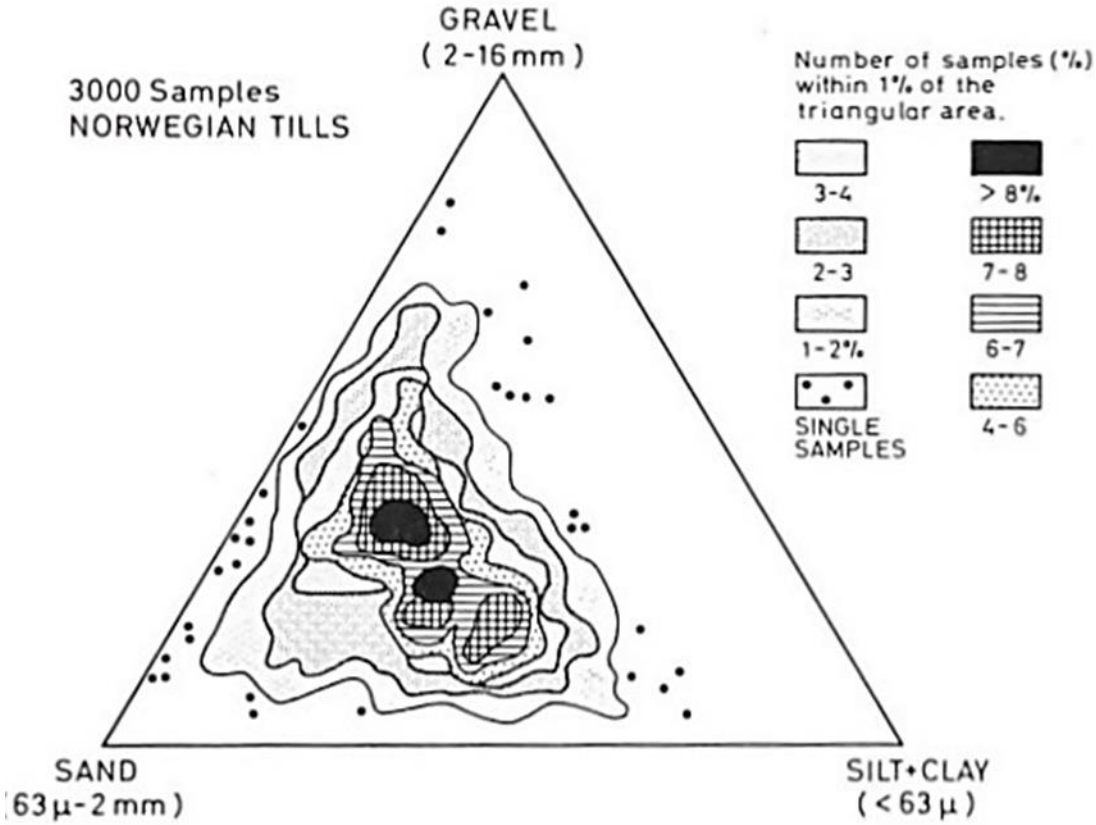

Figure 2.9: Grain size distribution of 3000 till soil samples collected in Norway (Jørgensen, 1977).

Opsal (2018) verified the results presented by Jørgensen (1977) regarding the content of fines in relation to bedrock origin. Tills derived from Precambrian rocks in the southernmost part of Norway were found to have a fine content of 21% on average. The Cambro-Silurian derived tills in Trøndelag have on average a 36% fines content. The distribution of Norwegian geological units is illustrated in Figure 2.10. The Cambro Silurian sedimentary metamorphic rocks are a result of the formation of the Caledonian mountain range. Typical rock types include sedimentary rocks of late Precambrian and Cambro-Silurian age, in addition to magmatic rocks. Precambrian bedrock mainly consists of gneiss, granite and other magmatic and metamorphic rocks (Ramberg et al., 2007). The Norwegian rocks are generally strong and coarse grained, which results in tills with a typical clay content of less than 10 %. In addition to bedrock origin, the mode and distance of transportation also influences on the grain size distribution. Increasing transport distance coincide with increasing content of coarse silt and medium sand fractions, in addition to a higher content of monocrystalline grains (Jørgensen, 1977). Outwash of silt and clay by melt water during the deglaciation may have created a coarser grain size distribution than in the original deposit (Selmer-Olsen, 1977).

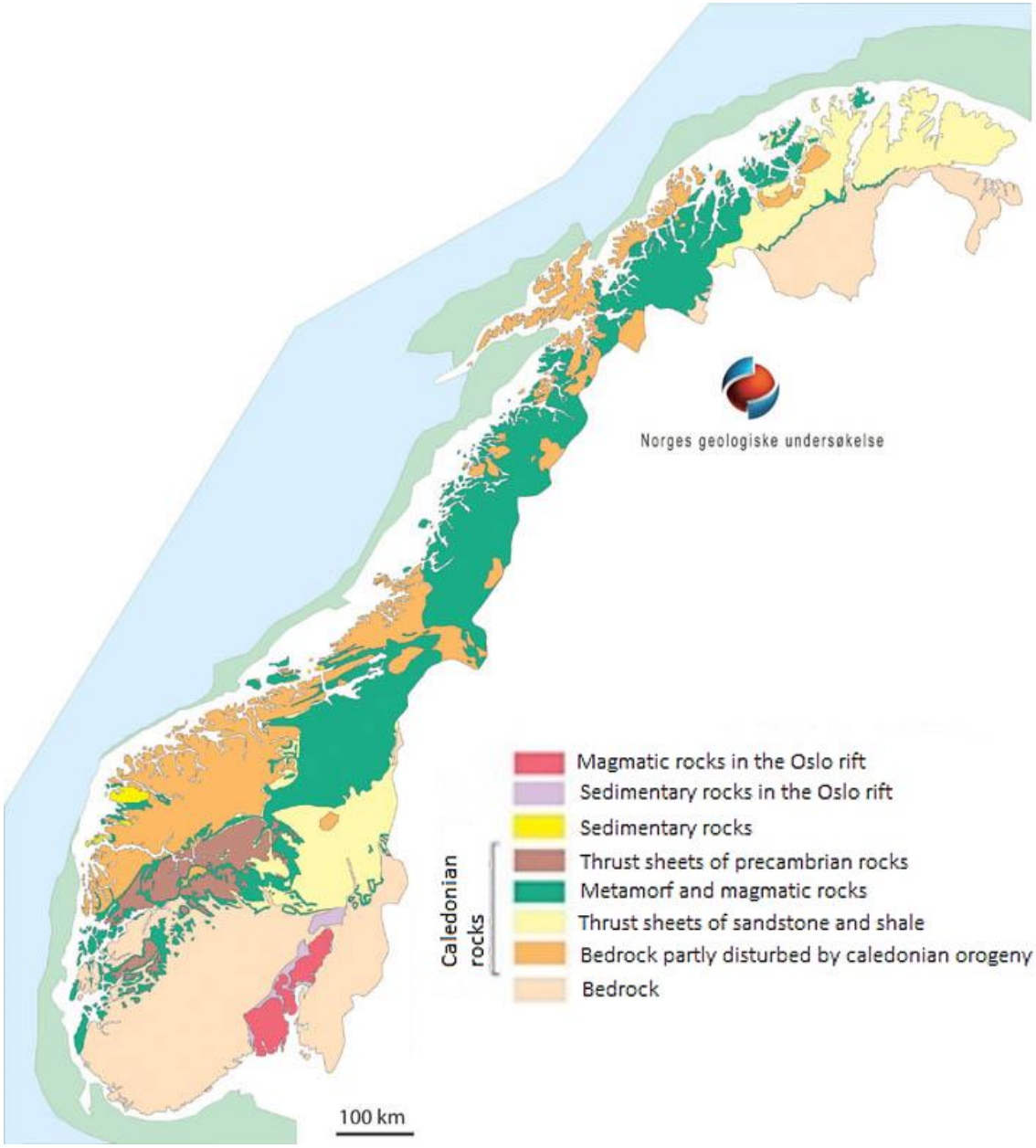

Figure 2.10: Norwegian geological units. Modified after NGU (2017a).

The clay fraction in Norwegian tills mainly consist of crushed rock aggregates (Raade, 2017). Opsal (2017) investigated the mineralogy of the fraction 0.5-1mm in till samples collected from various locations in the southern part of Norway. The mineral content of samples collected from the Western Precambrian region were dominated by plagioclase, but with a significant content of quartz. Samples collected from the Cambro-Silurian region were dominated by quartz, with smaller amounts of plagioclase. The presence of mica minerals was greatest in the Cambro-Silurian region, as illustrated by the provinces G (Precambrian region) and E (Cambro-Silurian region) in Figure 2.11.

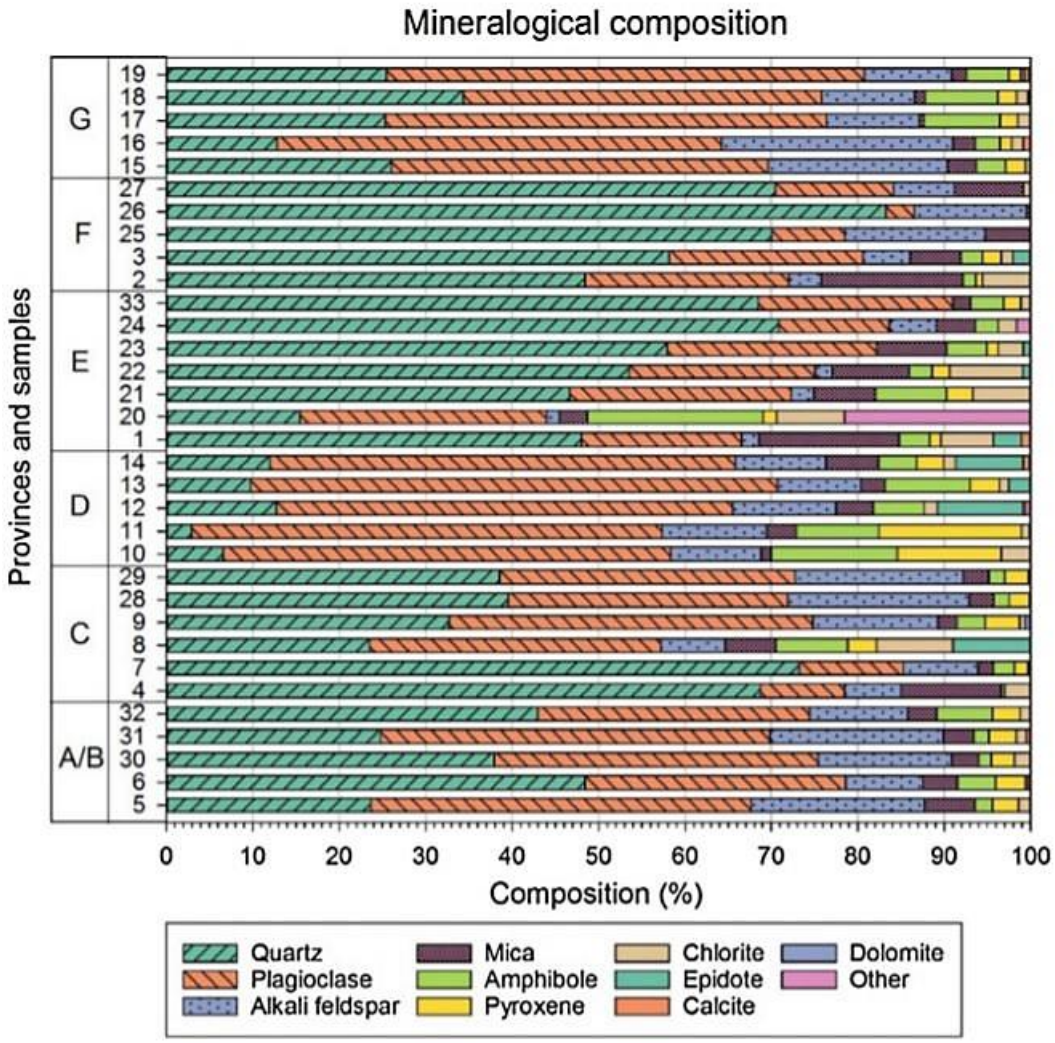

Figure 2.11: Mineralogical composition of Norwegian till samples (Opsal, 2018).

In summary, a large amount of the Norwegian sediments consists of glacial till soils deposited after the last glaciation. Tills are well graded, highly compacted and strongly influenced by the local bedrock geology. The Norwegian tills can be separated into two main types based on the grain size distribution; tills derived from Precambrian bedrock and tills derived from Cambro-Silurian sedimentary rocks. The Norwegian tills have generally a low content of fines, but the Cambro-Silurian derived tills usually contain more fines compared to the Precambrian derived.

2.2.1 Shear strength of tills

Opsal (2017) conducted shear testing on 33 dry samples of till soil in a large-scale shear box. Each sample was tested three times under the applied normal stresses 100, 200 and 300 kPa. Investigations of the samples from different bedrock regions show a correlation between average angle of friction, average shear stresses and the bedrock geology. Results show that tills derived from Precambrian rocks generally have a higher internal friction angle compared to tills originating from weaker rocks, such as sandstone. Sample number 23, derived from Cambro-Silurian rocks had a friction angle of 36.5 degrees. The Precambrian derived sample, number 18 had a friction angle of 38 degrees. These results are similar to results from testing of samples from the respective regions, and can thus be expected to be representative for the till soil types.

Further investigations on the till samples show that the shear strength of Norwegian tills is controlled by a combination of geological parameters. A correlation between the grain size distribution, the mineralogical composition and the angle of friction were found. The particle shape influences on the initial shear resistance (Opsal, 2018).

(Vanapalli et al., 1996b) performed direct shear tests on consolidated glacial till soil. The tests were performed with water contents dry of optimum, optimum and wet of optimum. Three different normal stresses were applied with varying suction. The shear strength in relation to matric suction was found to be non-linear.

The lower undisturbed parts of soil profiles in till have a high degree of consolidation resulting in a large cohesion parameter (Høeg et al., 2014). A high frequency of events has been registered in the months of May and June, highlighting the importance of depth of freezing and saturation caused by thawing (Dahl et al., 1981).

Research undertaken by Dahl et al. (1981) concludes that high permeable layers of sorted material can have a major influence on the slope stability. In combination with vertical fractures, these layers can contribute to slope failure in deeper parts of the soil profile. Investigations on the fracture density in till shows that the amount of fractures is high in the upper part of the soil, but decreases with depth. The near surface factures have a strike parallel to the slope surface, thought to be a consequence of processes after deglaciation. The fractures influence on the stability by facilitating increased percolation of water downward in the soil, where rapid pore-pressure increase can occur. In addition to this, the shear strength of fractures is normally lower compared to for compact material.

Minerology

The mineralogical composition of tills is dependent on the grain size distribution. The quartz content decreases with decreasing grain sizes, while the content of feldspar and sheet minerals increases. Mineralogy of tills are not only controlled by bedrock geology, but also by the till-forming processes. Lodgment tills are found to have a higher content of finer fractions compared to melt-out till. This is thought to be a result of glacial abrasion (Haldorsen, 1983).

Sand grains of quartz from glacial environments are generally very angular in shape. Larger grains are characterized by conchoidal fractures, while smaller grains will have flat cleavage surfaces. Glacial grinding can alter the grain shapes and the size and shape of the grains might be highly variable. Weathering and diagenesis causes smoothening of sharp edges. The flat cleavage surfaces might be modified by precipitation of minerals and pore-water. As quartz grains decrease in size, they become more reactive and chemical reactions causes round grains (Krinsley and Doornkamp, 2011).

The amount of clay minerals increases with increasing degree of weathering. Chemical weathering alters minerals, such as biotite and calcite. However, there is generally a low degree of chemical weathering in Norway compared to other parts of the world (Selmer-Olsen, 1977).

Cementation of soil at a depth of 0.5-1.0 meter caused by percolation of water and transport of minerals through the permeable upper part of a soil profile is common. This cementation may create an impermeable boundary where pore-pressures tend to build up (NVE, 2014).

In addition to material properties numerous external factors will influence on the stability of a slope. An unstable and landslide prone slope is covered by a layer of soil and the slope angle normally is greater than 25 degrees. For the landslide to occur, a triggering mechanism has to exist (Bargel et al., 2011). Vegetation, slope shape, degree of weathering, frequency of freeze/thaw cycles and groundwater conditions are other external factors that influences on the stability of the upper soil layers (Høeg et al., 2014).

In summary, studies have shown that the shear strength of soils is mainly controlled by the grain size distribution, mineralogical composition, the angle of friction. Layers and fractions in the soil can have a large influence on the strength. Precambrian derived tills show a higher shear strength than tills originating from weaker sedimentary rocks.

3 Description of study sites

Till samples were collected from two valleys in Norway. The locations, shown by red markers in Figure 3.1 were chosen to investigate the two main types of Norwegian tills, defined by Jørgensen (1977). To examine the spatial variation of soil properties in relation to landslide events, samples have been collected from both inside and outside of landslide channels. A total of ten samples, from five different landslide channels were collected. Six of the samples were gathered from Innfjorden and four from Gauldalen.

The selection of study sites was based on bedrock geology, type of soil, previous landslide activity and the ease of access. As previously mentioned, it is difficult to distinguish between different depositional processes while investigating in-situ (Haldorsen and Kruger, 1990). The mode of deposition has for this reason not been considered.

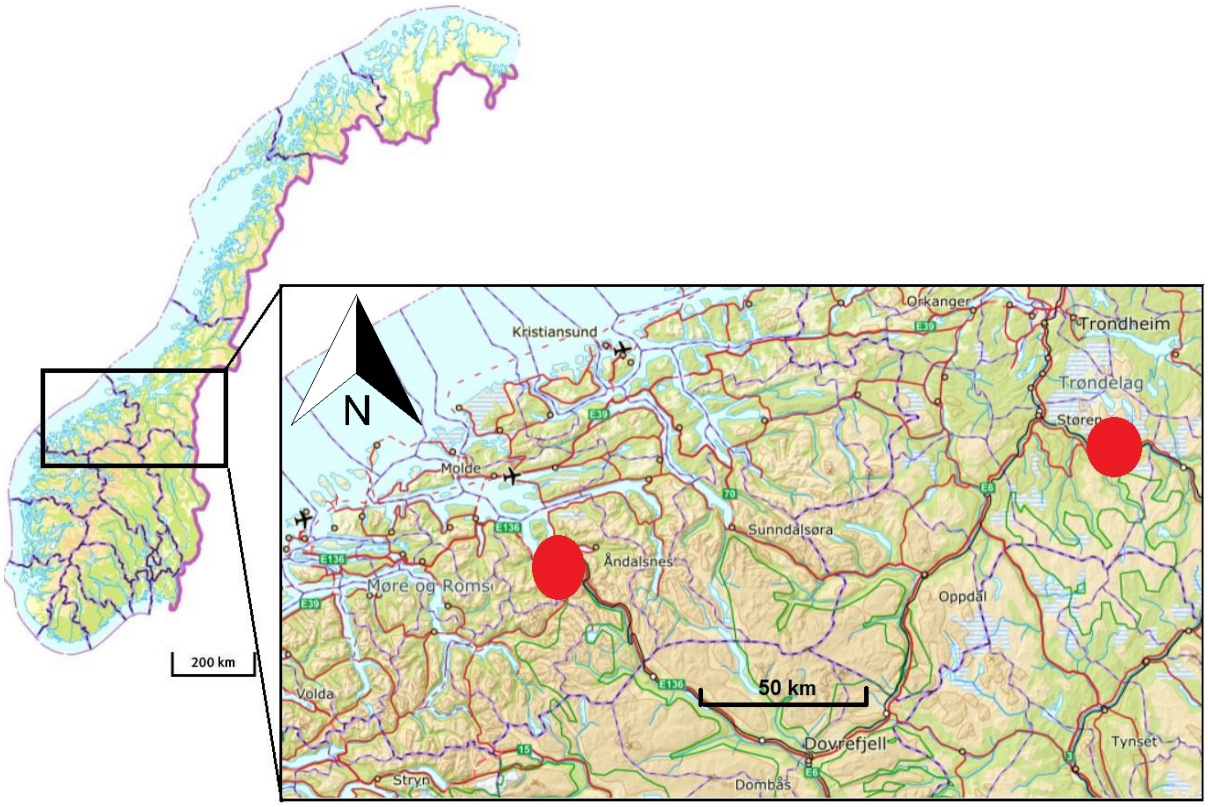

Figure 3.1: Innfjorden and Gauldalen marked by red points. Modified from (Kartverket, 2017)

3.1 The Precambrian region

The sampling sites in the Precambrian region are situated in Innfjorden, close to Åndalsnes in Møre & Romsdal on the west coast of Norway. The locations are marked on Figure 3.2 and are surrounded by deep valleys and fjords.

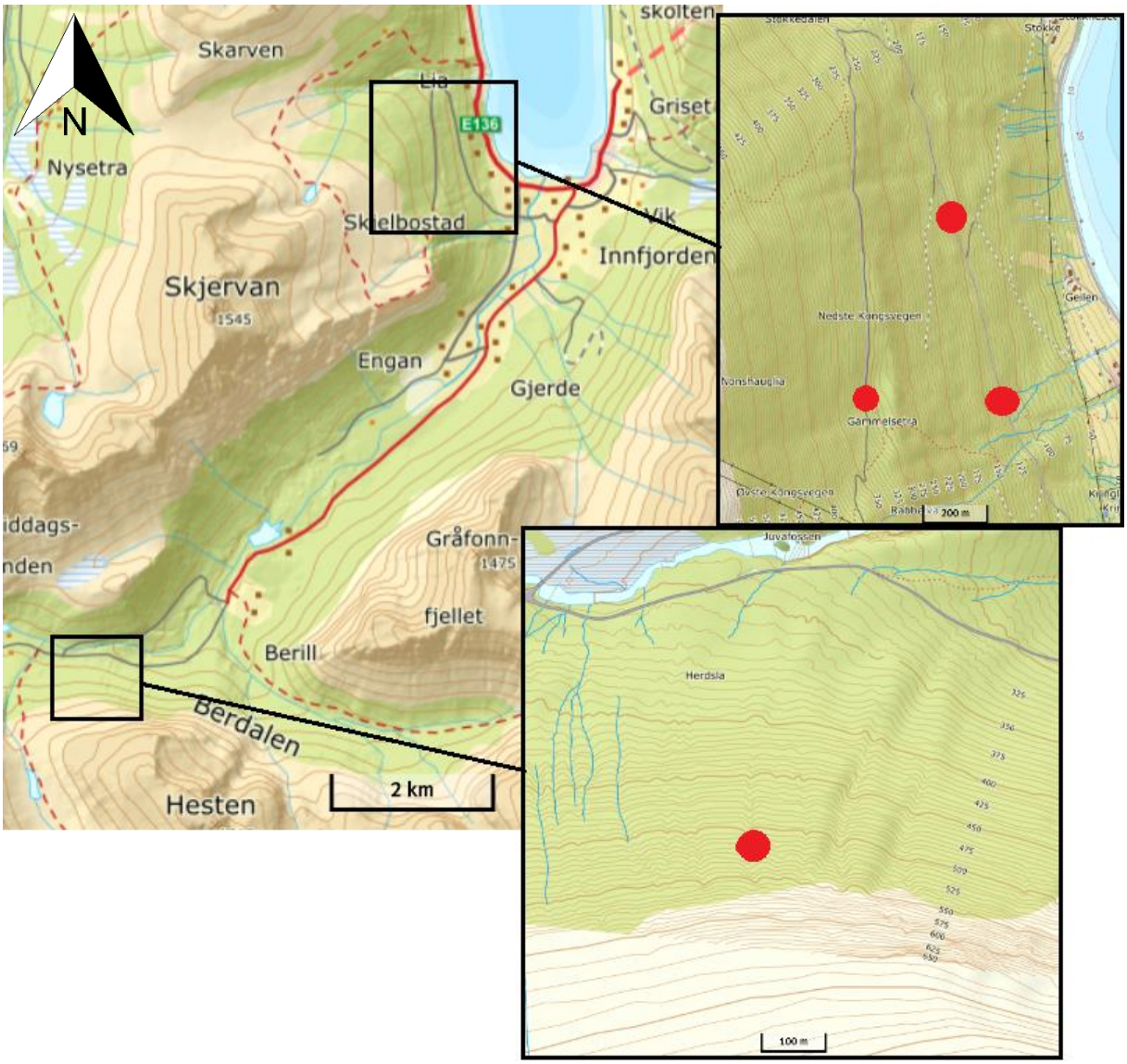

Figure 3.2: Sampling locations in Innfjorden marked by red points. Modified from (Kartverket, 2017).

3.1.1 Bedrock and Quaternary geology

Innfjorden lies within "*The western gneiss region"* where the most common rock types are various kinds of granitic gneisses and migmatites. A geological bedrock map in the scale of 1:250 000 covers the area, as shown in Figure 3.3. The granitic to dioritic gneisses and migmatites were created by metamorphosis of magmatic and sedimentary rocks during the Caledonian orogenesis 1700 to 1500 million years ago (Ramberg et al., 2007). In general, gneiss is a medium to coarse grained rock with grains of the size 2-5mm. The main minerals are quartz and feldspar, with smaller amounts of biotite and amphibole. Migmatites are a mixture of magmatic and metamorphic gneiss (Price et al., 2012).

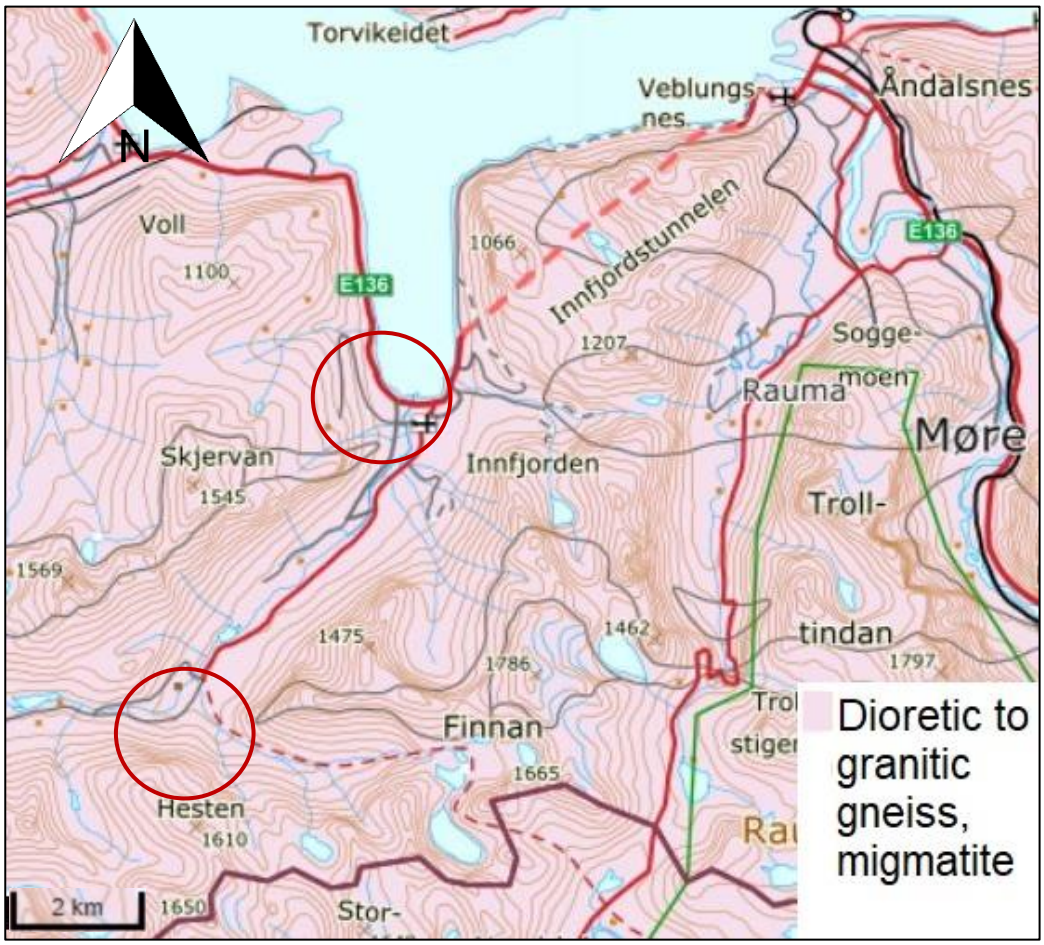

Figure 3.3: Bedrock geology in the area surrounding Innfjorden, Møre & Romsdal. Modified after (NGU, 2017a).

The main direction of glacier flow during the late-Weichselian ice age was orientated north-west, as illustrated in Figure 2.8 (Ottesen et al., 2005). As previously mentioned, till soils are highly influenced by the surrounding geology as illustrated in Figure 3.4 (Selmer-Olsen, 1977). Thus, the most interesting bedrock geology in relation to mineralogical composition of the collected samples are the bedrock lying within a few km upstream of the sampling locations. The marine limit in the area is at approximately 115 masl (NGU, 2017c).

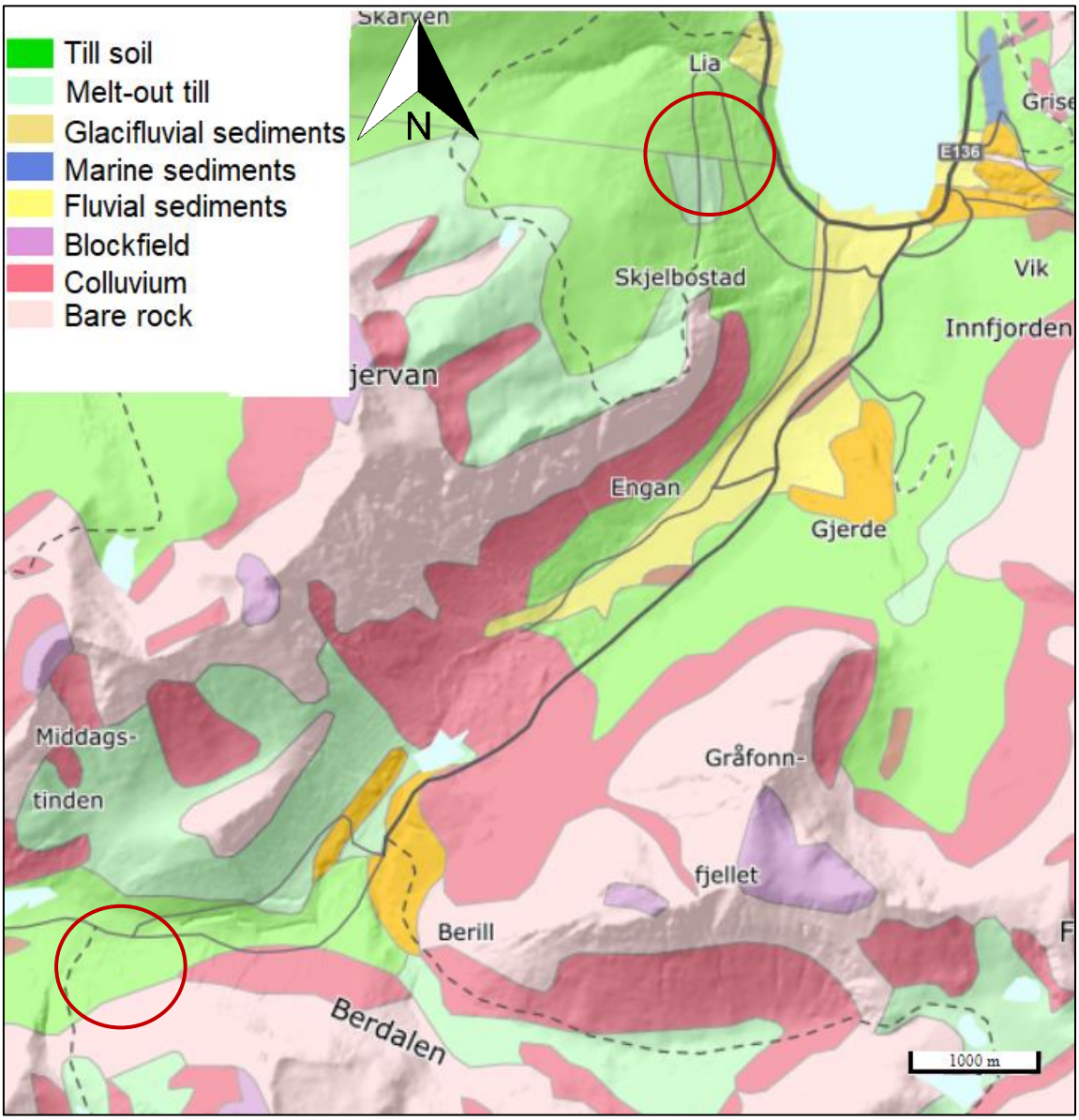

Figure 3.4: Soil distribution map of Innfjorden. Modified from (NGU, 2017d).

3.1.2 Climate

Due to transport of warm water by the Golf current and warm air by winds, the Norwegian climate is warmer compared to other places situated at the same longitude. The climatic variations within Norway are in addition large compared to the aerial size. This can be explained by the mountains which protect the inland and creates a difference in the amount of annual precipitation on the west coast compared to the inland. Innfjorden has a coastal climate and the area receives approximately 1000-1500mm of precipitation each year. The mean annual temperature in Ålesund is 6,7 °C, with 1,3 °C in January and 13,2 °C in August (Dannevig and Harstveit, 2013).

3.1.3 Location 1

The first location is located in the south end of Innfjorden, at a hight of 510 masl. The samples were collected on a west facing slope covered by a thick moraine deposit in the lower part and colluvium in the upper (NGU, 2017d). The soil distribution is illustrated in Figure 3.4. Field work and sampling were performed the 24th of October.

Figure 3.6 shows the channel which was investigated. The date and time of the landslide event are unknown, as the event has not been registered in NVE-Atlas. A light vegetation cover indicates that the event occurred a few years ago. The slope gradient at the point of initiation was approximately 40°, as seen in Figure 3.5. The slope gradient increases upslope where the soil cover gives way for bedrock in the overlying parts of the slope and the rockfall hazard was evident. Figure 3.5 is based on a digital terrain model with 10 meters accuracy. The maps illustrating the slope angle does not show smaller variations. The width of the channel was about 4 meters, but it narrows below the initiation area. Rock was visible in the top center of the channel and the thickness of surrounding soil deposit was variable (1,5-3m). Vegetation in the slope consisted of grass, moss and small birch trees (1-2 m) that showed signs of heavy snow cover during winter.

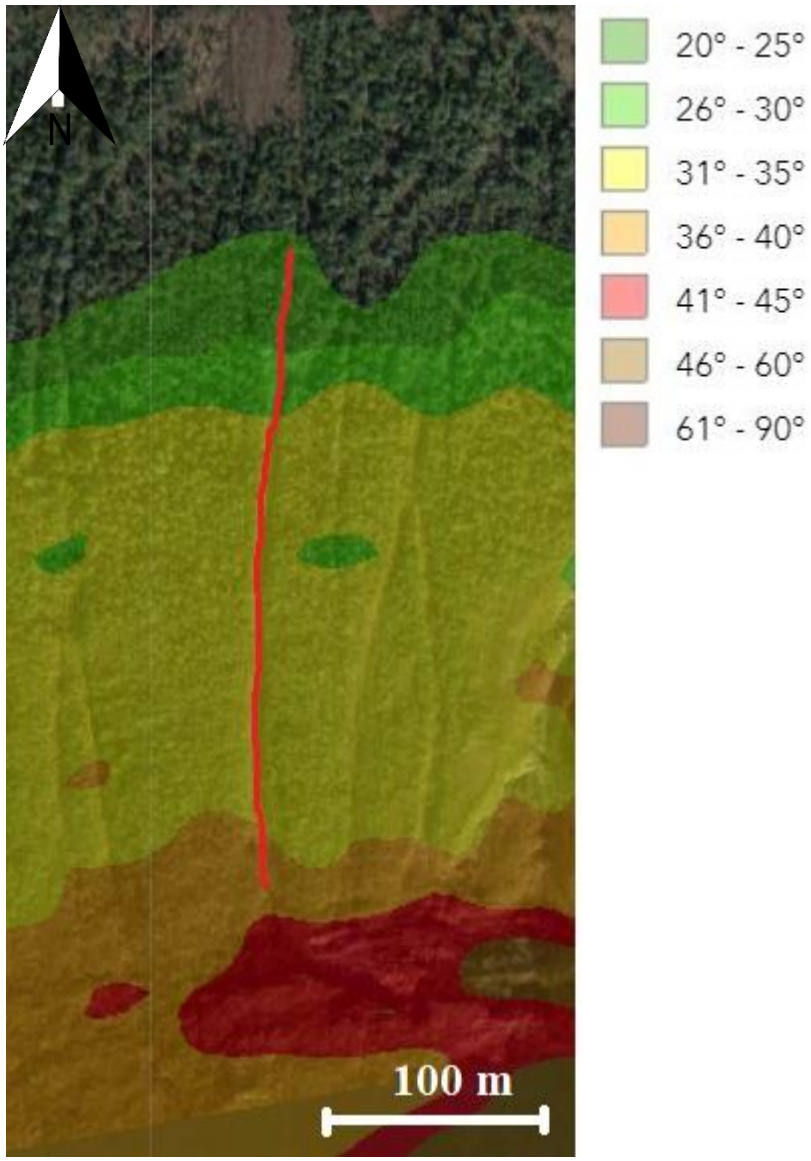

Figure 3.5 Slope gradient at location 1. Modified from NGI (2017).

The surface in the slope was rough with several thresholds of lower gradient. A small slope slip close to the channel originated from one of these thresholds. The channel was defined by levees with a height of approximately 1,5 meters (Figure 3.6 and Figure 3.7). The “out of channel” sample was collected approximately 5 meters to the side of the channel (Hauge, 2017).

Figure 3.6: Channel in location 1

Figure 3.7: Vegetation and rockfall in channel 1.

3.1.4 Location 2

The second location is located at an east facing slope in the outer parts of valley. Sampling and field work were performed the 24th of October. Vegetation in the area consists of dense forest with approximately 20-meter-high trees of various types. According to information registered at NVE-atlas (NVE, 2017) the first event in this channel occurred after heavy rainfall September 11th 1991. A farm house and a barn further downslope were destroyed, luckily no one were injured. The channel is shown in Figure 3.9.

Figure 3.8: The upper channel is channel 3, the lower is channel 2.Modified from Kartverket (2017).

The “in-channel” sample was collected 10 meters above the road at a height of 125 masl. The channel is displayed in Figure 3.9 and was approximately 4 meters deep, but without obvious levees. The sample was collected in the upper left side, below the vegetation cover. No bedrock was visible, and the channel floor was covered by cm – dm size rocks and sand. A small stream was running in the center. The slope profile did not change considerably upslope, as shown in Figure 3.11 (Hauge, 2017).

Figure 3.9: The channel at location 2.

The “out-off channel” sample was collected from a soil slip 5 meters above the road at a height of 310 masl. The slope gradient in the area was between 25-30 degrees. The soil slip is shown in Figure 3.10, where the sample was collected below the vegetation.

Figure 3.10: The "out-off" channel sample in location 2 was collected below the vegetation cover in the upper part of the soil slip.

3.1.5 Location 3

Location 3 is located 520 meters north of where the location 2 “in-channel” sample was collected. Due to the short distance between the locations, the vegetation was identical. The sample was collected October 25th.

The event is not registered in the NVE-atlas. Figure 3.8 shows that the point of initiation lies close to the forest road. Figure 3.11 shows that the slope gradient ranges between 31-35°. The channel was of the same character as the channel in location 2, with steep sides and no visible bedrock. The slope at the sampling point was about 30 degrees. (Hauge, 2017).

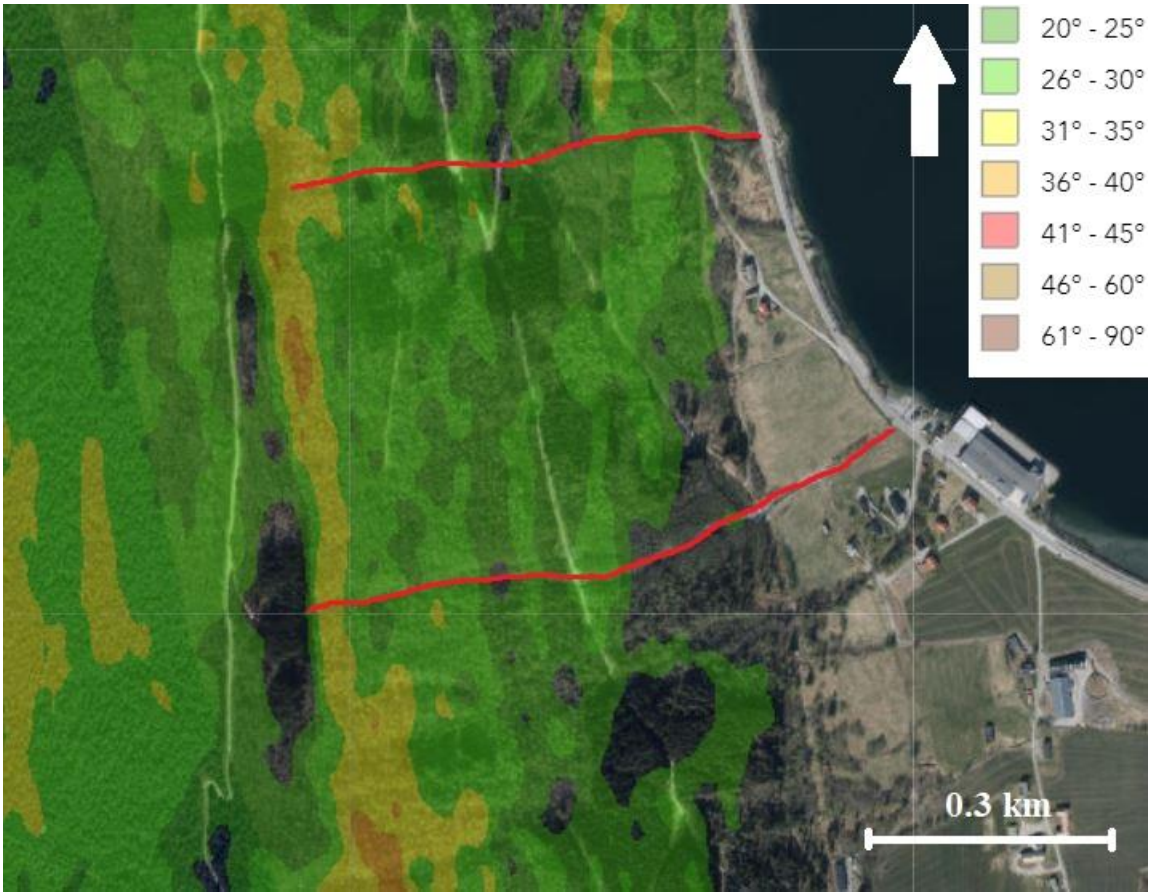

Figure 3.11: The slope gradient. Modified from NGI (2017).

The channel was roughly 2 meters deep with larger rocks in the center. The “in-channel” sample was collected about 0.75 – 1.4 meters below the vegetation on the channel wall. The channel is displayed in Figure 3.12 (Hauge, 2017).The “out-off” channel sample was collected 5 meters to the side of the channel, marked by the shovel in Figure 3.13.

Figure 3.12: The channel in location 3.

Figure 3.13: The out of channel sample in location 3 were collected from where the white shovel is located.

3.2 The Cambro-Silurian region

Study locations in the Cambro-Silurian region lies within Gauldalen, an east-west orientated valley in Trøndelag. The locations are marked in Figure 3.14. The field work was performed in dry weather the 3rd of November.

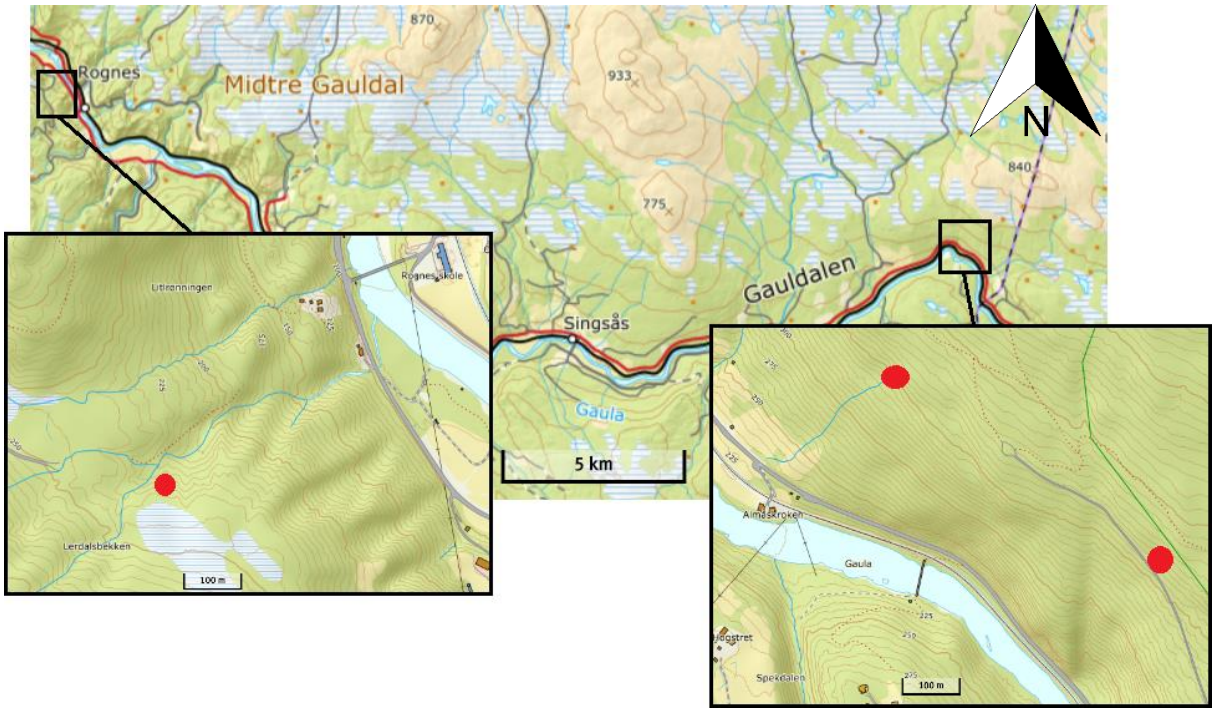

Figure 3.14: Locations in Gauldalen marked by red points. Location five is shown in the map to the left and location four to the right. Modified from (Kartverket, 2017).

3.2.1 Bedrock and Quaternary geology

Approximately 425 million years ago, the continents of Laurentia and Baltica collided. Baltica was submerged beneath trust sheets originating from Laurentia, other small continents lying between and the oceanic seafloor. Thus, the rocks that are found in the Cambro-Silurian region today include greenstone, gabbro, metasandstone, mica-schist and phyllite (Ramberg et al., 2007). Greenstone, also known as metabasalt, is a green colored metamorphic basalt. The main minerals are plagioclase, pyroxene, epidote and amphibole. It contains grains smaller than 0,1mm of chlorite, albite and actinolite. Phyllite is a metamorphic rock with a schistose structure. A strong foliation with oriented mica sheets and small-scale folding and veins of quarts are common. Phyllites are characterized by grains smaller than 0,1mm.

Quartz and muscovite are the main components. Mica-schist is a metamorphic rock of a higher degree of metamorphosis than phyllite. The grain size is medium, from 0,1-2mm. The main minerals include quartz and mica, and smaller amounts of feldspar, chlorite and apatite. Gabbro is a magmatic, coarse grained rock. Typical minerals include plagioclase and pyroxene, with smaller amounts of magnetite and olivine (Price et al., 2012, Garmo, 1995).

Figure 3.15 and Figure 3.16 shows the bedrock geology at location 4 and 5. The dominating rocks are metasandstone, mica-schist and amphibolite. The geological maps are produced by The Geological Survey of Norway, NGU and are in the scale 1:250 000 (NGU, 2017a). The large scale results in a low accuracy. A line, indicating the border between two independent maps is seen in Figure 3.15 and Figure 3.16. The interpretation of the rock types has been performed by two different geologists with unequal opinions. Thus, the boarder between the independent maps does not fully correspond.

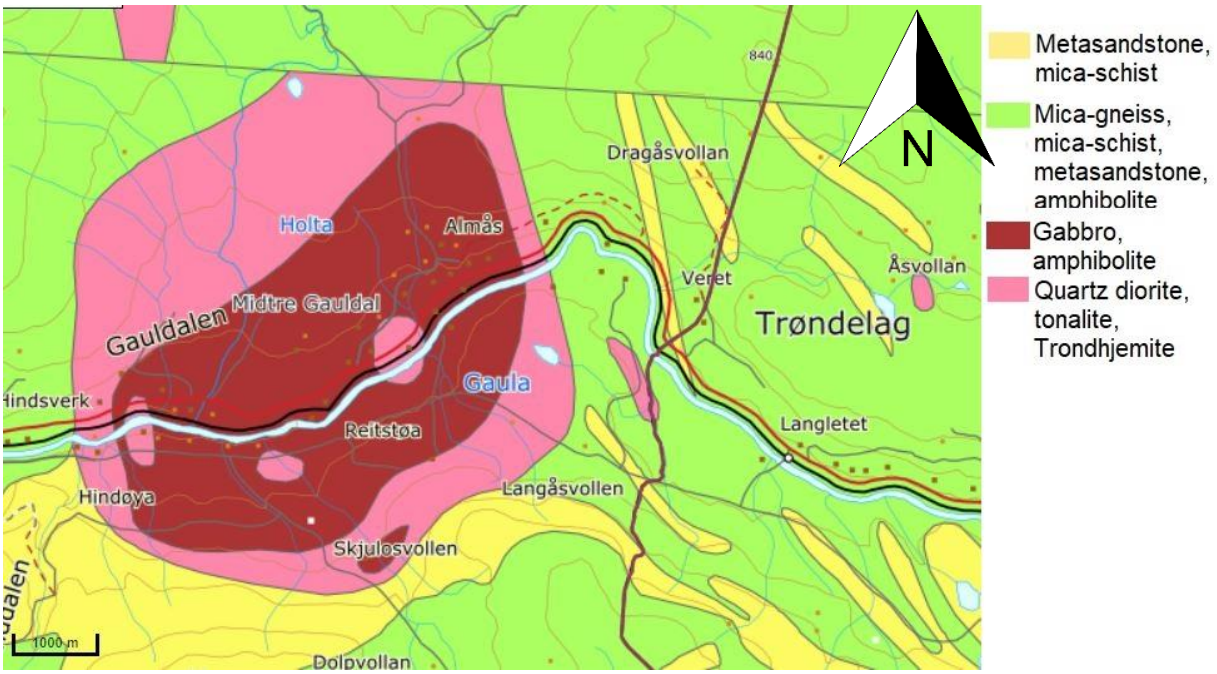

Figure 3.15: Bedrock geology surrounding location 4. Scale: 1:2500 00. Modified from (NGU, 2017a).

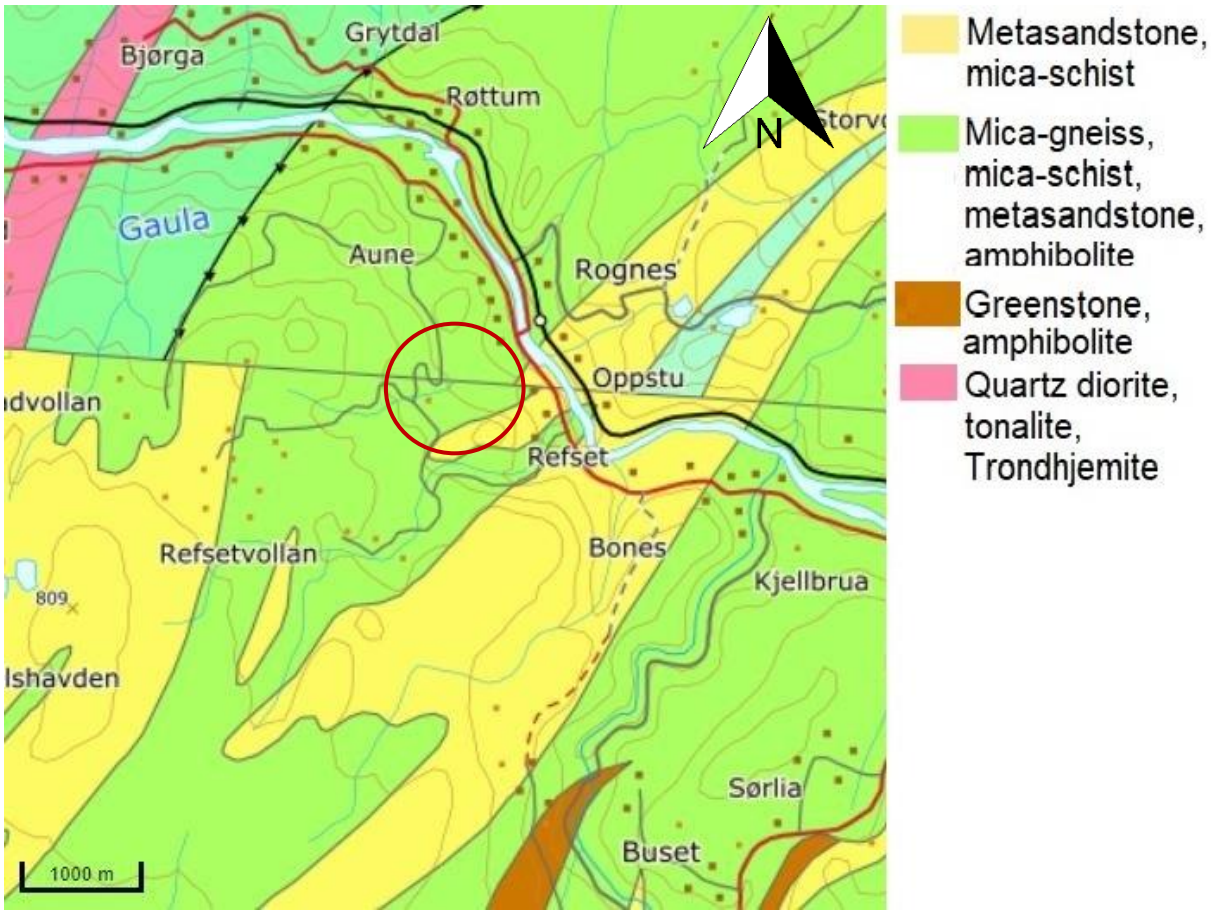

Figure 3.16: Bedrock geology surrounding location 5. Scale: 1:250 000. Modified from (NGU, 2017a)

The main direction of glacier flow in the area during the last ice age was towards the north-west. A clayey till is found below 1-5m of sandy till, separated by a transition zone. The clayey till is mostly found in deep narrow valleys and depressions in the terrain (Reite, 1994). The marine limit in the valley ranges between 180-200 masl. (NGU, 2017c). A large amount of landslide events are registered in the valley (NVE, 2017). Figure 3.17 and Figure 3.18 are clippings from NGU's Quaternary geology maps in the scale 1:250 000 (NGU, 2017d). Similar to the bedrock geology maps, these maps must be used with care as the accuracy is low.

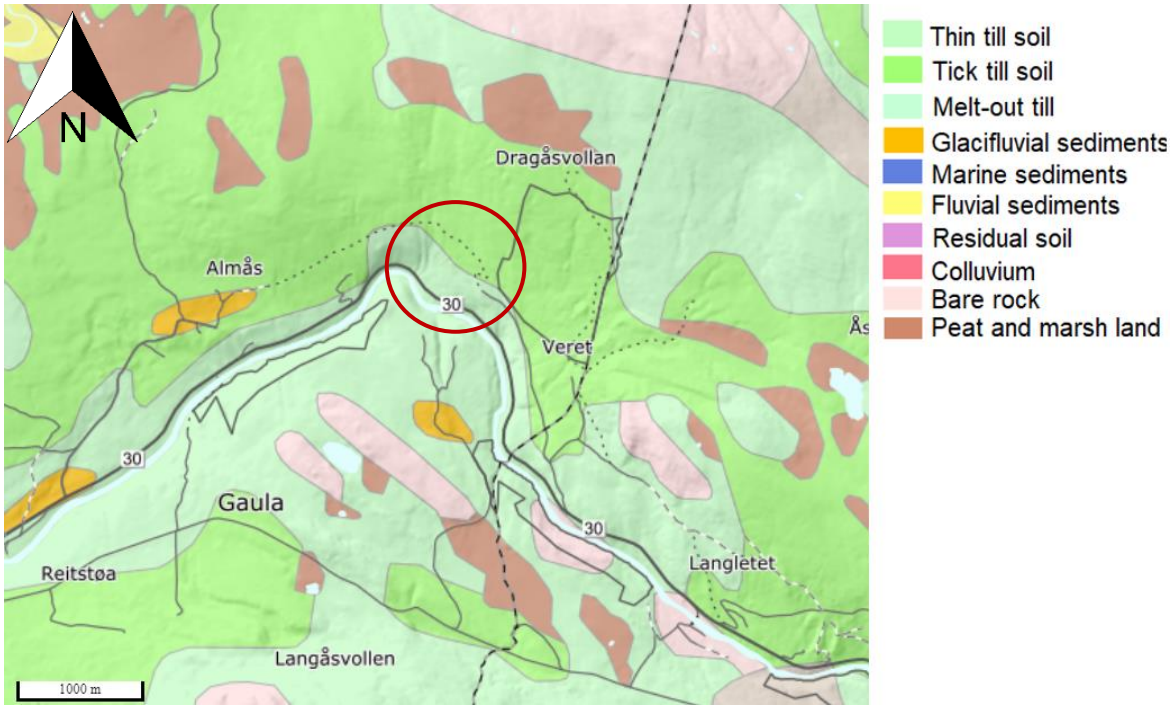

Figure 3.17: Quaternary map of the area surrounding location 4. Modified from (NGU, 2017d).

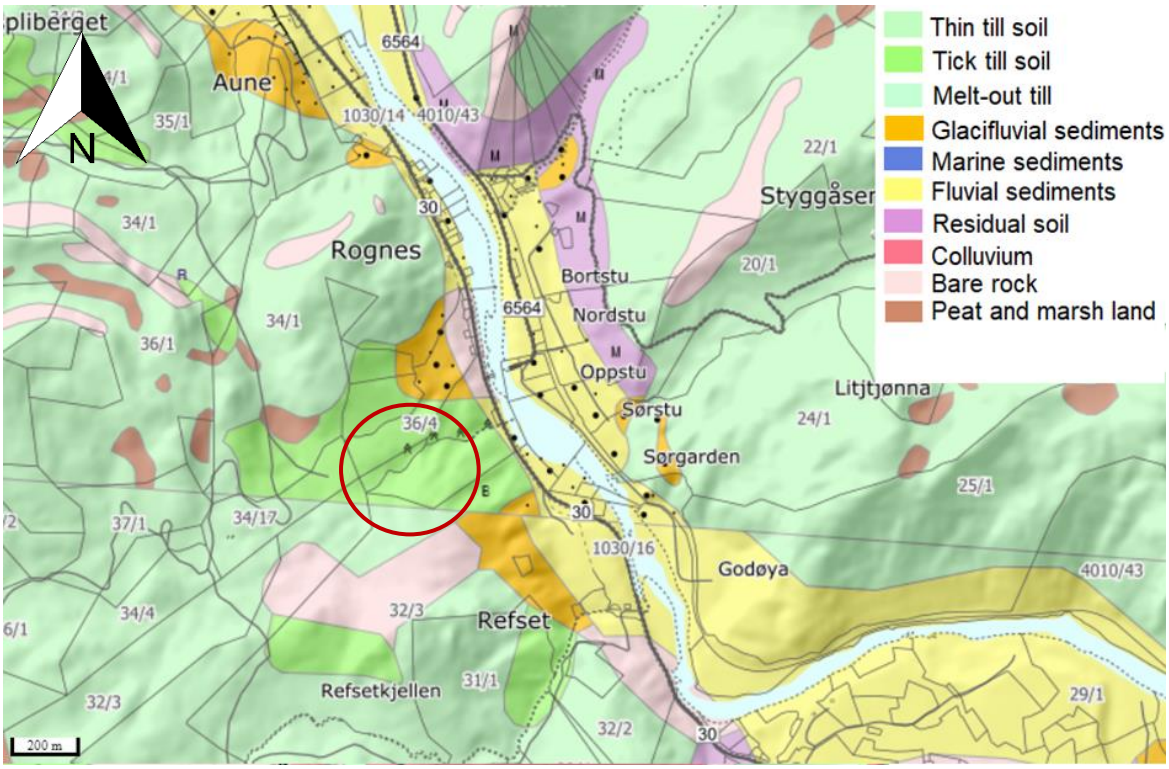

Figure 3.18: Quaternary map of location 5. Modified from (NGU, 2017d).

3.2.2 Climate

Gauldalen is located inland and is protected by the mountains. Thus, the area receives about 750-1000mm annual precipitation. Temperatures in the area are typical for a continental climate with cold winters and warm summers. The mean annual air temperature for Røros is 0,3°, with January as the coldest month (-11,2°) and July as the warmest (11,4°) (Dannevig and Harstveit, 2013).

3.2.3 Location 4

August 13th, 2013 a soil slide occurred 10 km east of Singsås in Gauldalen. Large amounts of masses were deposited on the road and on the property of a farm situated at the foot of the slope (NVE, 2017b). According to precipitation measurements at Kotsøy measurement station, about 20 km west for the landslide event, the amount of rainfall the day before and the day of the event were respectively 23,9 mm and 8,8 mm. The recorded rainfall amount the previous days were minor. The annual precipitation in the area is about 910 mm (Yr, 2017).

The slide was initiated at a height of ~360 masl. Vegetation in the area consisted of dense forest in a rough terrain. The point of initiation lies below a steep cliff and rock was visible in the channel. Figure 3.19 shows the back scarp of the slide which was ~ 1 meter high and the width of the channel was ~5 meters. The slope gradient above the cliff was gentle and covered by birch and spruce trees and wet marsh land. Below the cliff the slope gradient is approximately 45 degrees for 20 meters, before the gradient decreased drastically, as shown in Figure 3.20.

The “in-channel sample” was collected at the side of the channel wall, 5 meters below the back scarp. The “out-off channel” sample was collected in a road cut ~650 meters south east of the slide initiation point. The soil cover was very thin in the area, which made it difficult to obtain a representative sample closer to the channel. The slope in the road cut was ~30 degrees and the vegetation of the same kind as where the slide occurred. Large weathered blocks of mica schist were observed in close distance to the sampling point (Hauge, 2017).

Figure 3.19: The back scarp of the channel in location 4.

Figure 3.20 Slope gradient at location 4. Modified from NGI (2017).

3.2.4 Location 5

Location 5 is situated at a north facing slope at 240 masl. close to Rognes in Gauldalen. Several events are registered from the same slope, one April 29th 2000, another September 24th 2004 and the most recent April 9th 2014 (NVE, 2017). Weather records from the closest meteorological station, 6.5 km from Rognes, show that the events that took place in April occurred in relation to increased temperatures, which probably caused substantial snowmelt. The event in September 2004 occurred after three days of heavy precipitation. The total amount of rainfall during these three days were 68 mm (NRK, 2017). Due to difficulty accessing the channels, the samples were collected in a watershed above these scars. The vegetation was dominated by large spruce trees and moss. Deforestation was ongoing at the location and a large area was cleared. The slope gradient at the sampling location was about 20-25 degrees, with varying slope gradient in the surrounding area (Figure 3.21). The "in-channel" sample was collected in a small channel with running water. The channel was about 1 meter deep and contained running water (Figure 3.22). The "out-off channel" sample was collected in a road cut 20 meters to the side of the channel (Hauge, 2017).

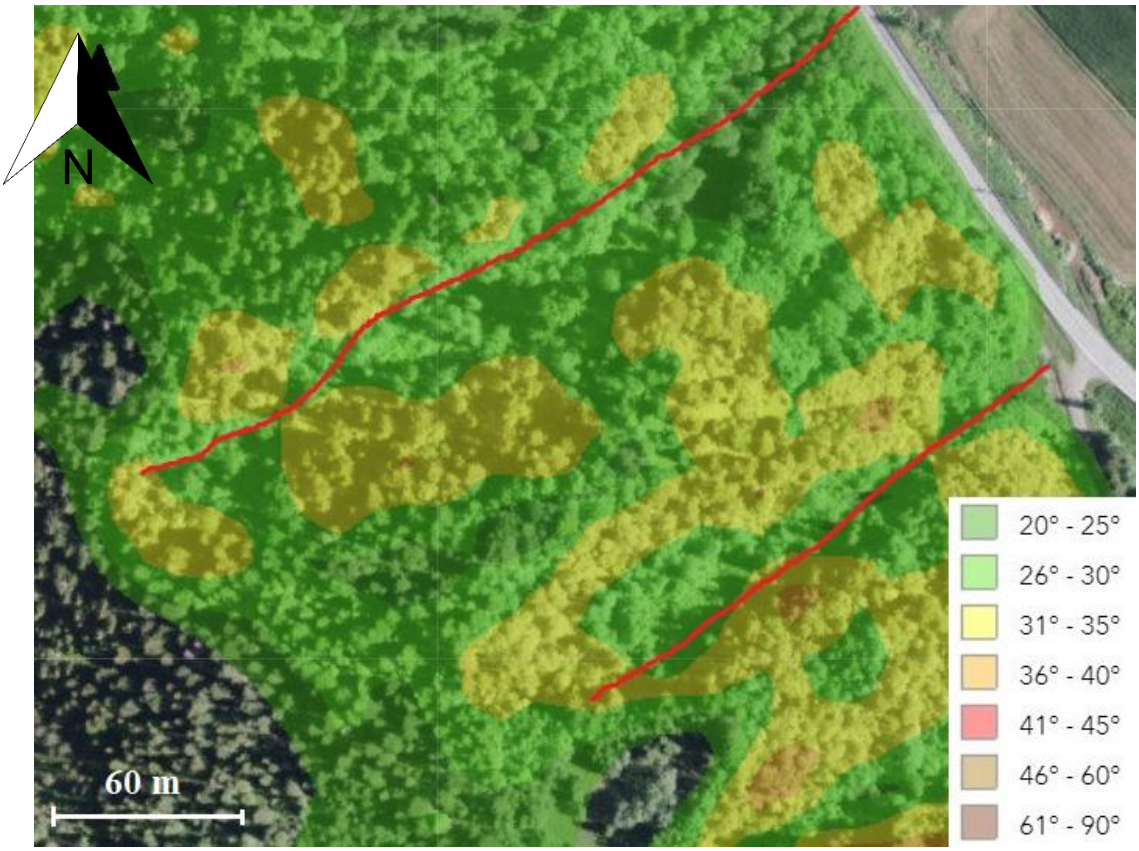

Figure 3.21 Slope gradient at location 5. Modified from NGI (2017).

Figure 3.22: The in-channel sample in location 5

4 Methods

Properties known to influence on the shear strength of soils were investigated though various methods in the laboratory. The theory in Chapter 2 of this thesis discuss the importance of several different properties, such as grain size distribution, mineralogy, particle shape and water content.

4.1 Field investigations

The selection of sampling locations was performed based on NGU's bedrock (NGU, 2017b) and quaternary map (NGU, 2017d). NVE Atlas (NVE, 2017), an online service provided by The Norwegian water and energy resources directorate, NVE was used to find the locations of previous landslide activity. A online map provided by the Norwegian Geotechnical Institute, NGI was used to evaluate the slope gradient (NGI, 2017).

The collection of samples and field investigations were conducted the fall semester of 2017. The field visit to Innfjorden was October 24th -25th, while Gauldalen was visited November 3rd. Samples were collected from both inside and outside of landslide scars. The depth of sampling ranged from 20 cm – 2 m, dependent on the depth of the ease of access, depth of organic layer, the root zone and the fabric of the till. Larger rocks were removed from the sample. Special attention was given to description of the vegetation cover, slope profile, surface relief, degree of compaction, fabric of the deposits and depth to bedrock. The locations were marked by use of GPS and soil profiles were made by use of a shovel. The dimensions and depth of sampling were measured with a folding ruler. The samples were of equal size, approximately 10 L.

4.2 Grain size distribution analysis

The grain size distribution analysis is based on the classification of particle fractions displayed in Table 4.1.

Table 4.1: Particle size fractions (NS-EN ISO 14688-1, 2002).

Soil fractions	Sub-fractions	Symbols	Particle sizes mm
Very coarse soil	Large boulder	LBo	> 630
	Boulder	Bo	> 200 to 630
	Cobble	Co	> 63 to 200
Coarse soil	Gravel	Gr	> 2,0 to 63
	Coarse gravel	CGr	> 20 to 63
	Medium gravel	MGr	> 6,3 to 20
	Fine gravel	FGr	> 2,0 to 6,3
	Sand	Sa	> 0,063 to 2,0
	Coarse sand	CSa	> 0,63 to 2,0
	Medium sand	MSa	> 0,2 to 0,63
	Fine sand	FSa	> 0,063 to 0,2
Fine soil	Silt	Si	> 0,002 to 0,063
	Coarse silt	CSi	> 0,02 to 0,063
	Medium silt	MSi	> 0,006 3 to 0,02
	Fine silt	FSi	> 0,002 to 0,006 3
	Clay	Cl	⩽ 0,002

Analysis of the grain size distributions was conducted after the standard given by the Norwegian Public Roads Administration in Handbook R210 (SVV, 2016). The size of the sample needed for the analysis is dependent on the largest grain size. Big blocks and rocks were removed from the sample at the time of sampling. The samples were first dried in an oven at 105 degrees Celsius and then weighted, before they were sieved on a 16mm sieve. Material smaller than 16mm was split into smaller portions and analyzed. Sieves with mesh sizes of 12.5mm, 9mm, 6.68mm, 4mm, 1.168mm, 0.589mm, 295µm, 147µm, 74µm and 38µm were used. The upper limit of 16mm was chosen to compare the results with the studies of Opsal (2018) and Jørgensen (1977). The fractions ranging from 38µm to 6.68mm were sieved for 30 minutes by a Rotap machine (Figure 4.1), while the fractions between 16mm to 6.68mm were separated using a larger industrial sieving machine.

Material <38 µm was analyzed by laser diffraction. The analysis was performed in a machine named Malvern Mastersizer 3000, Figure 4.2, which measures the intensity of dispersion of a laser beam passing through a dispersed sample. From this, the particle sizes are calculated. By use of this method the grain size is measured by the equivalent spherical diameter, in contrast to sieving where the grain size is measured by the second smallest direction of the particle (MalvernPanalytical, 2018).

Figure 4.1 Sieving of material > 38µm was performed by the Rotap machine

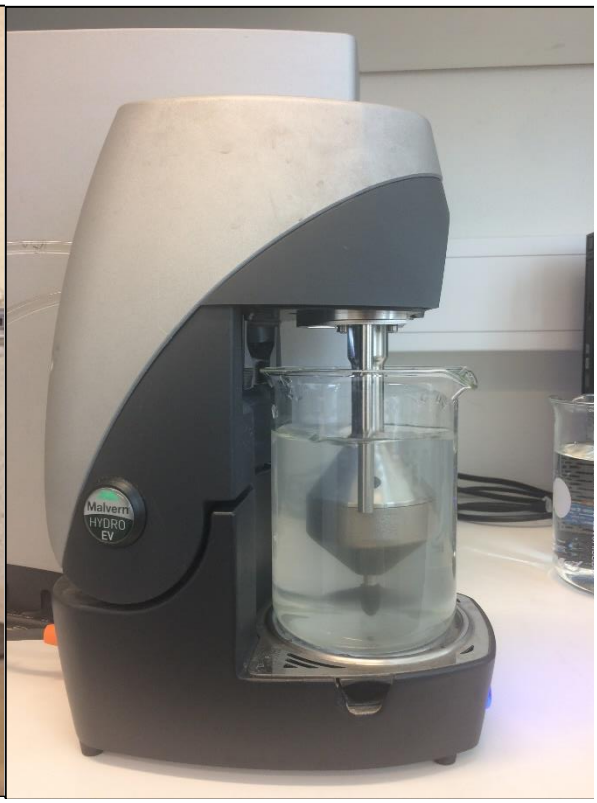

Figure 4.2 Grain size analysis of material <38µm were performed by the Malvern Mastersizer 3000.

The Malvern Mastersizer measures the grain fractions in percentage, while the dry sieving results in data in grams. The amount of material smaller than 38µm was thus calculated from percentage to grams by use of the amount of material passing the 38µm sieve.

The grain size distribution is characterized by use of the grading number, Cu.

$$C_u = \frac{d_{60}}{d_{10}} \quad 4.1$$

where

d_{60} = the grain size where 60 % of the material passes through.

d_{10} = the grain size where 10 % of the material passes through.

The material is considered as poorly graded if Cu < 6, medium graded if 6 < Cu > 15 and well graded if Cu > 15 (SVV, 2016).

4.3 Particle shape investigations and mineralogical analysis

Microscopic investigations

Microscopic investigations of dried material were performed to search for signs of cementation between grains. Indications of cementation are growth of mineralization surrounding the grains and fracture surfaces that may indicate previous bonding of grains (B. Frengstad, pers. comm., 2018).

4.3.1 Particle shape and surface texture

Flakiness index, FI

The flakiness index is based on the weight of particles passing through a grid sieve corresponding to the fraction of interest. The analysis was based on the standard NS-EN 933-3 (2012), but due to a lack of sieves of the correct mesh size smaller modifications were conducted. The investigated fractions were; 4/4.8, 4.8/6.6, 6.6/8, 8/9.5 and 9.5/12.5, while the correct fractions to the corresponding to the grid sieves were; 4/5, 5/6.3, 6.3/8, 8/10, 10/12.5. Sieving of material on a grid sieve is illustrated in Figure 4.3.

Figure 4.3: Grid sieve for determination of flakiness index

Shape index, SI

The shape index is defined as the ratio between the grain thickness and length. Five fractions, ranging from 4mm to 12.5mm were investigated in compliance with NS-EN 933-4 (2008). A selection of separated particles is shown in Figure 4.4.

Figure 4.4: Cubical grains to the left, elongated grains to the right. The paper squares are 0.5x0.5cm.

Angularity and surface texture

Parameter	Particle shape
Angularity/roundness	Very angular Angular Subangular Subrounded Rounded Well rounded
Form	Cubic Flat Elongate
Surface texture	Rough Smooth

Table 4.2: Particle angularity (NS-EN ISO 14688-1, 2002)

Grains can be sorted by degree of angularity as listed in Table 4.2. The dominating shape and surface texture were found for the fractions 4/5mm and 6.6/8mm. The degree of angularity is divided into four categories (Figure 4.5); angular, sub-angular, sub-rounded and rounded (Holtz and Kovacs, 1981). As described in NS-EN ISO 14688-1 (2002), two categories for surface texture were used; rough and smooth.

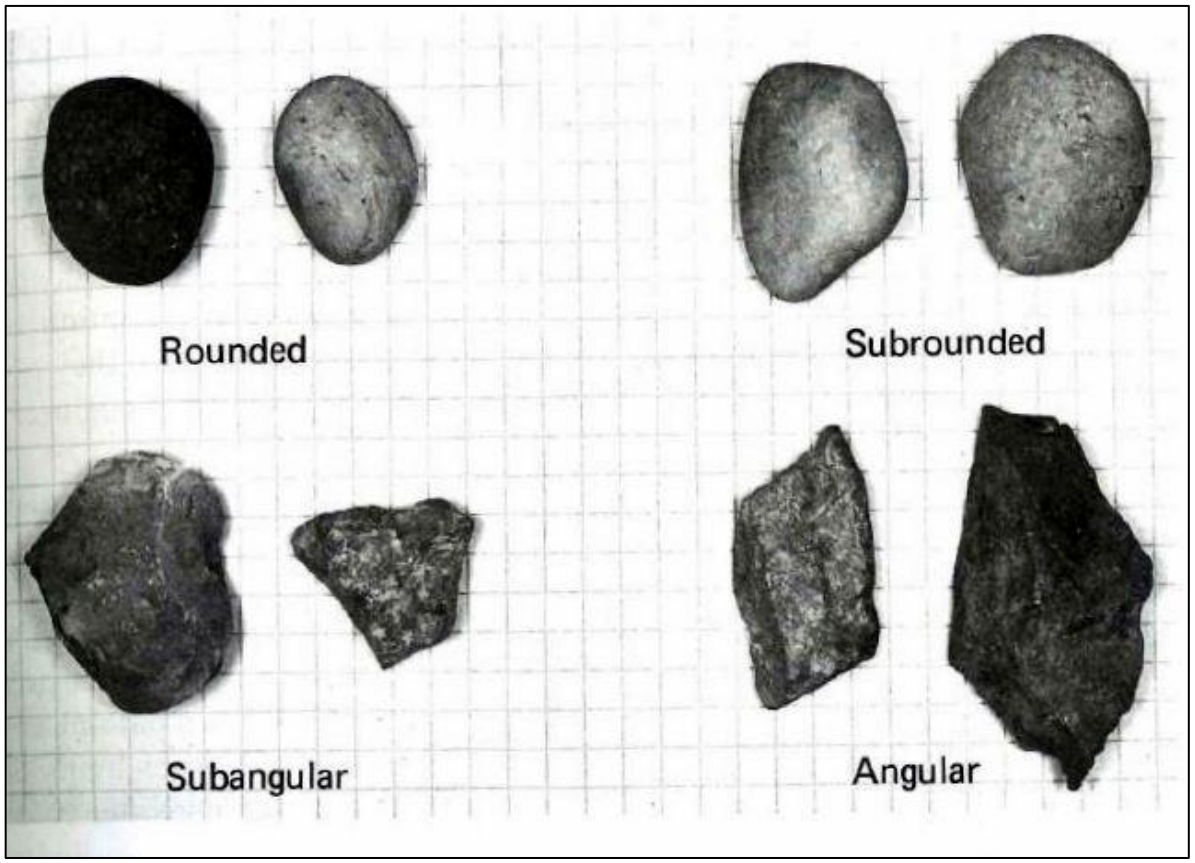

Figure 4.5: Categories for angularity (Holtz and Kovacs, 1981).

4.3.2 Mineralogical composition

Determination of the mineralogical composition or rock type of grains in the fractions of 4/5 mm and 6.6/8mm has been performed by visual inspection as described in (SVV, 2016). The inspection was performed on material extracted from the grain size analysis. Any occurrence and degree of surface coating was noted.

4.3.3 XRD analysis

The mineralogical composition of fractions smaller than 61µm was studied through XRD analysis. The material was divided into two fractions; 0-38µm and 38-61µm. The purpose of the XRD analysis was to determine the mineralogical composition to investigate the difference in mineralogy of silt and clay. Before testing, the samples were crushed down to 10 µm and placed on a glass plate, as shown in Figure 4.6.

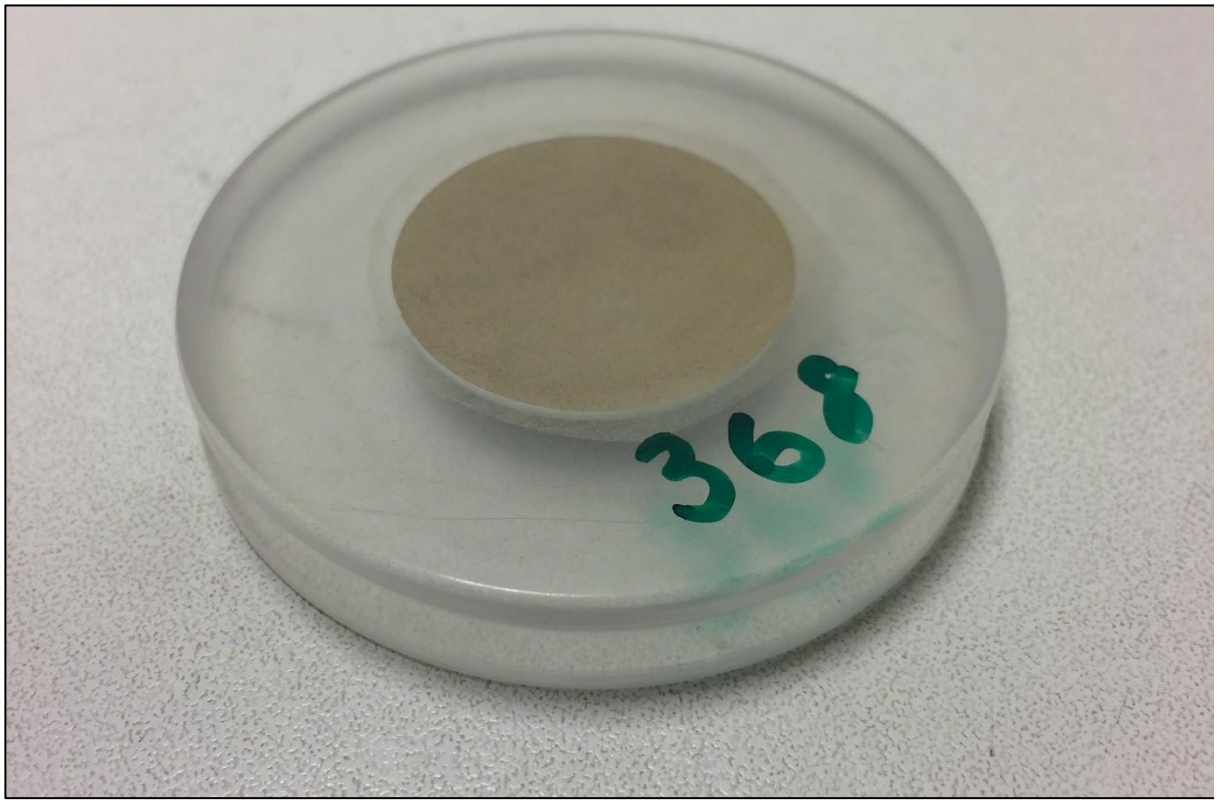

Figure 4.6: Sample ready for XRD-analysis

The general principle of an XRD-analysis involves the specific lattice structure of each mineral type. A laser beam of X-rays with wavelengths in the range of 0.01-100Å is used to measure the distance between atoms in the crystal structure of minerals. Since no minerals have the same spacing between the interatomic planes the crystal lattice can be identified. Figure 4.7 illustrates the diffraction of X-rays from the atomic planes in minerals. The X-rays with wavelength λ hits the crystal planes with an angle θ. The path length between the waves that hit different atomic planes must be a number of wavelengths $n\lambda$. In Figure 4.7 this difference equals BC + CD = $n\lambda$. Since BC = CD and CD = d sin θ, the minerals can be identified by:

$$n\lambda = 2d\ sin\ \theta \quad 4.2$$

This equation is known as Bragg's law, were d is the distance between atomic planes (Mitchell and Soga, 2005).

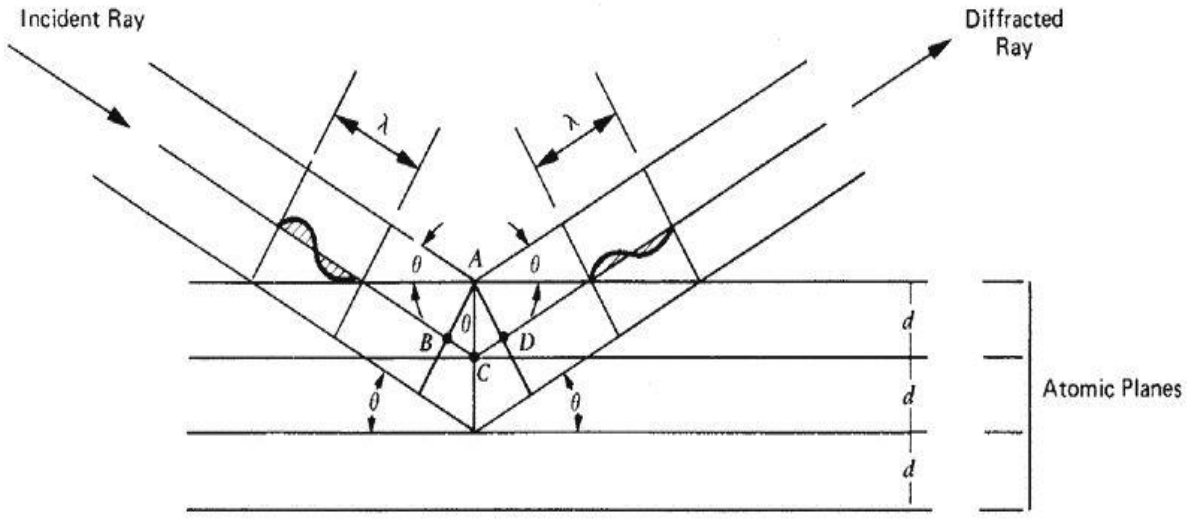

Figure 4.7: X-ray diffraction according to Bragg's law (Mitchell and Soga, 2005)

The XRD-analysis was performed at the chemical and mineralogical lab by Laurentius Tijhuis at the department of geoscience and petroleum, NTNU.

4.4 Optimum moisture content

The dry optimum moisture content of the specimens was found by a test called "draining method", which is a less time-consuming alternative to the standard proctor test. Initially the sample was dried and sieved to separate material smaller than 6.68 mm. A representative quantity of the sample was extracted by splitting and then weighted. Water was then added to the extracted sample and packed into a container, shown in Figure 4.8. The packing was conducted by 25 blows with an instrument made of glass. Each sample was packed three times. If water runs out from underneath the container during the third sequence, the sample is at optimum moisture content. If not, more water must be added.

To find the dry optimum moisture content of the three samples that were going to be tested in the shear box, the samples were split into 4 equally large parts. One of these four was split in two, where one of these parts were used to find the water content needed for optimum. The correct amount of water was then added to the rest of the sample. This test was conducted by Odd Corneliussen at the lab geological engineering laboratory at the department of geoscience and petroleum, NTNU.

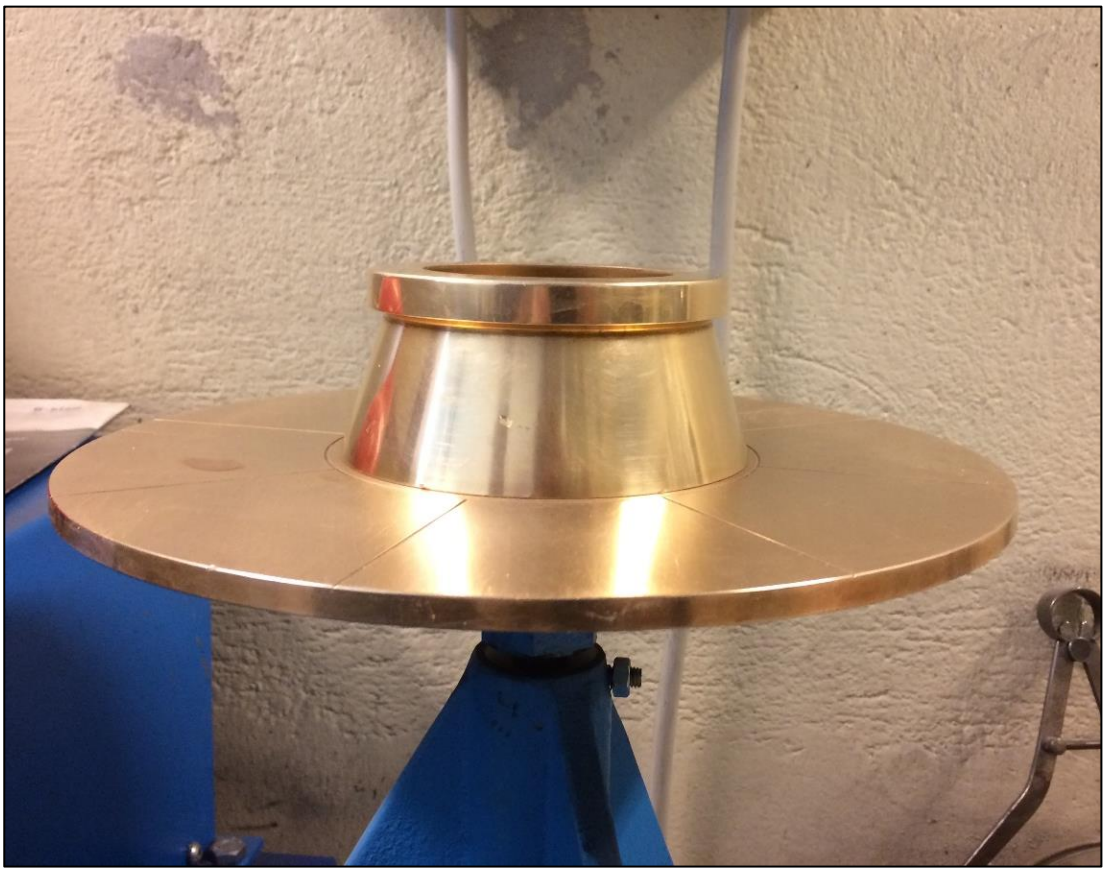

Figure 4.8: Container used to find the optimum moisture content

4.5 Shear box test

Shear tests of three samples were conducted by Marte Maria D. Jermstad and the author in the laboratory at the Department of Geoscience and Petroleum at the Norwegian University of Science and Technology. The tests were performed by use of an automatic large-scale shear box, SB2010 from Testconsult Ltd. The SB2010 is operated by a PC controller which logs and displays the test data. Shear stress, τ is automatically registered in kPA. The lateral and vertical load cell range are 0 to 100kN and the maximum vertical load is 1000 kPA. The maximum internal dimensions of the shear box are 305mm x 305mm x 150mm. The shear box apparatus is in compliance with BS 1377-7:1990 (Testconsult, 2012).

The procedure for shear box testing is based on the method for large scale shear box testing described by Opsal (2017). This procedure is customized to the specific shear box machine and till soil samples. The procedure is mainly based on the standards; BS 1377-7:1990 and ASTM D3080/D3080M-11. Modifications to the procedure presented by (Opsal, 2017) had to be undertaken for testing of unsaturated soil samples and at low normal stress.

A total of three samples were tested in the shear box. The reason for the restriction of three out of ten samples was the limited time to perform the tests. The chosen samples were two from location 2 in Innfjorden; one from inside the channel and one from outside. The third sample was from the channel at location 4 in Gauldalen. The samples were chosen with the purpose of investigating the difference between the inside and outside of a channel and the difference between samples from Innfjorden and Gauldalen.

First, the samples were dried in an oven at $110^{\circ}C \pm 5^{\circ}C$ for 24 hours, in compliance with ISO 17892-1 for a fine-grained soil. BS 1377-7:1990 recommends a maximum particle size of 20mm. Hence, samples were sieved on a 16mm sieve to remove larger particles.

After sieving the samples, each of the samples we weighted before individually tested in the shear box. Minor modifications had to be done on the shear box, as the volume of the samples were too small to fill the sample box. The bottom of the box was filled with sand retained in a strong mesh bag. Duct tape was used to prevent sample material from entering and from disappearing below the bag of sand, this is illustrated in Figure 4.9. The height of the sand fill was 7.5 cm.

Figure 4.9: The bottom of the shear box was filled with sand in a mesh bag and covered by dukt tape.

The first round of tests was conducted on dry material, while the second on material with a dry of optimum moisture content. Three different normal stresses were applied on both the dry and unsaturated samples, which is necessary to achieve the shear strength parameters. Experience from previous use of the shear box has shown that the degree of accuracy is low when applying normal stress below 50 kPa (Pers. Comm. G. Vistnes). As landslides in soils usually occur in shallow parts of the soil profile, where the normal stresses are considerably lower than 50 kPa, a steal beam was placed underneath the hydraulic valve, as shown in Figure 4.10. This prevented the machine from applying vertical load to the sample.

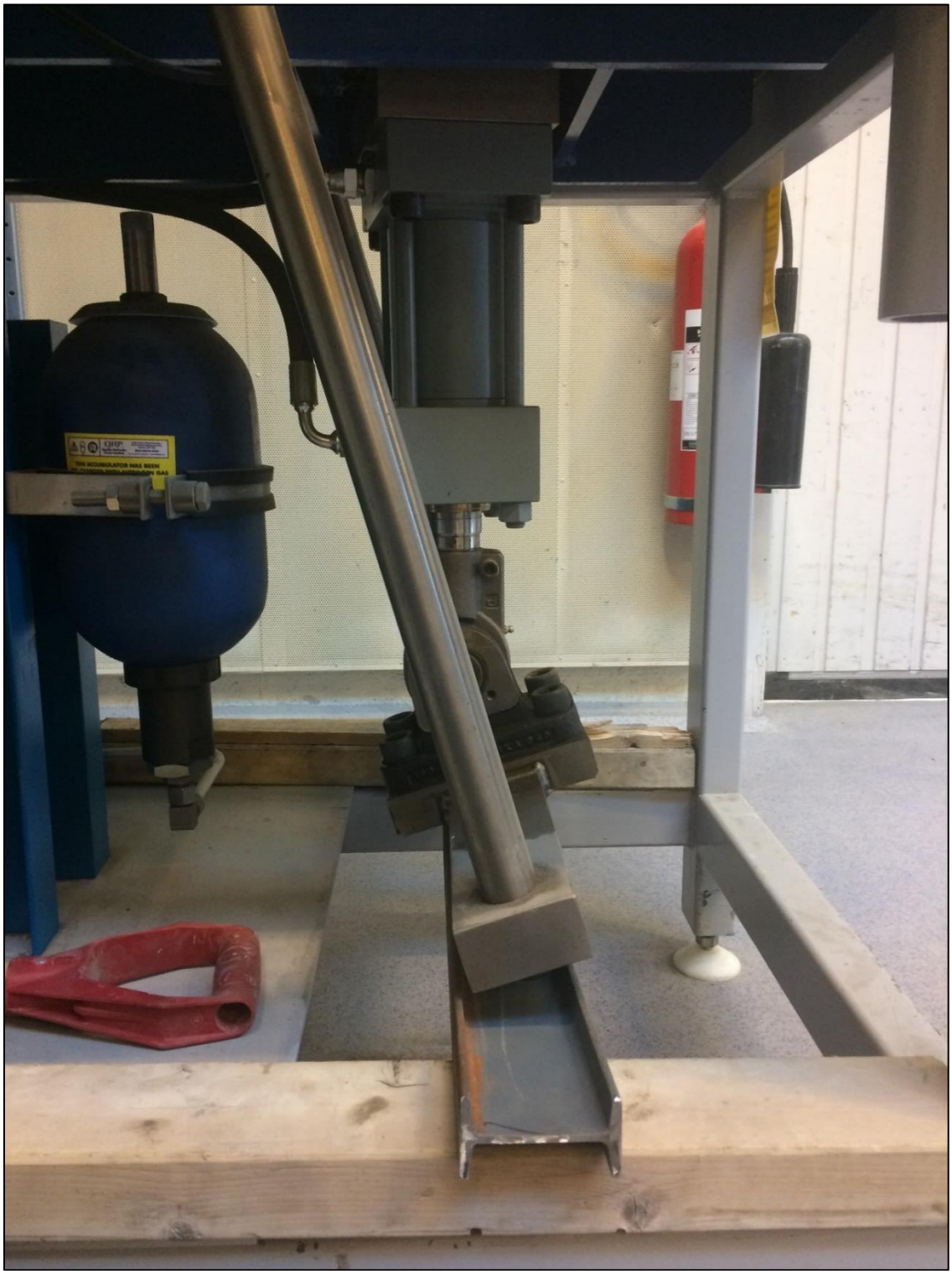

Figure 4.10: A steel beam is placed underneath the hydraulic valve.

Landslides in Norwegian soils usually occur in the upper 0.5-1 meters (Høeg et al., 2014). The impact of pore pressure is neglected at this depth and the vertical stress in the soil is thus given by:

$$\sigma_z = \gamma * z \qquad \text{(kPa)} \qquad 4.3$$

Where γ represents the soil density and z the depth below the surface (Emdal, 2013).

Table 4.3 Bulk density of till soils used in dam construction (Andersen et al., 2012).

	Dry (kN/m3)	**Unsaturated (kN/m3)**
Compacted	23	24
Poorly compacted	19	20

The bulk density of till soils used as filling in dams depends on the degree of compaction and the water content and are given in Table 4.3 (Andersen et al., 2012). These values correspond with the values 1.8-2.4 g/cm^3 for dry material given by Selmer-Olsen (1977) and with 20.8 and 22.7 kN/m^3 for dry and unsaturated material, as given by Terzaghi et al. (1996). The shear box machine SB2010 requires a minimum vertical load of 10 kPa to shear at the given rate. Normal loads of 14.13 kPa, 17.66 kPa and 21.19 kPa were applied by use of steel plates, with an individual weight of 33.5 kg, placed on top of the sample (Figure 4.11). The applied normal loads correspond to the depths (m):

Table 4.4 Depth in meters in a till soil corresponding to the applied normal load, density and moisture content.

	Dry		**Unsaturated**	
σ (kPa)	γ = 23	γ = 19	γ = 24	γ = 20
14.13	0.61	0.74	0.59	0.71
17.66	0.77	0.93	0.74	0.88
21.19	0.92	1.12	0.88	1.06

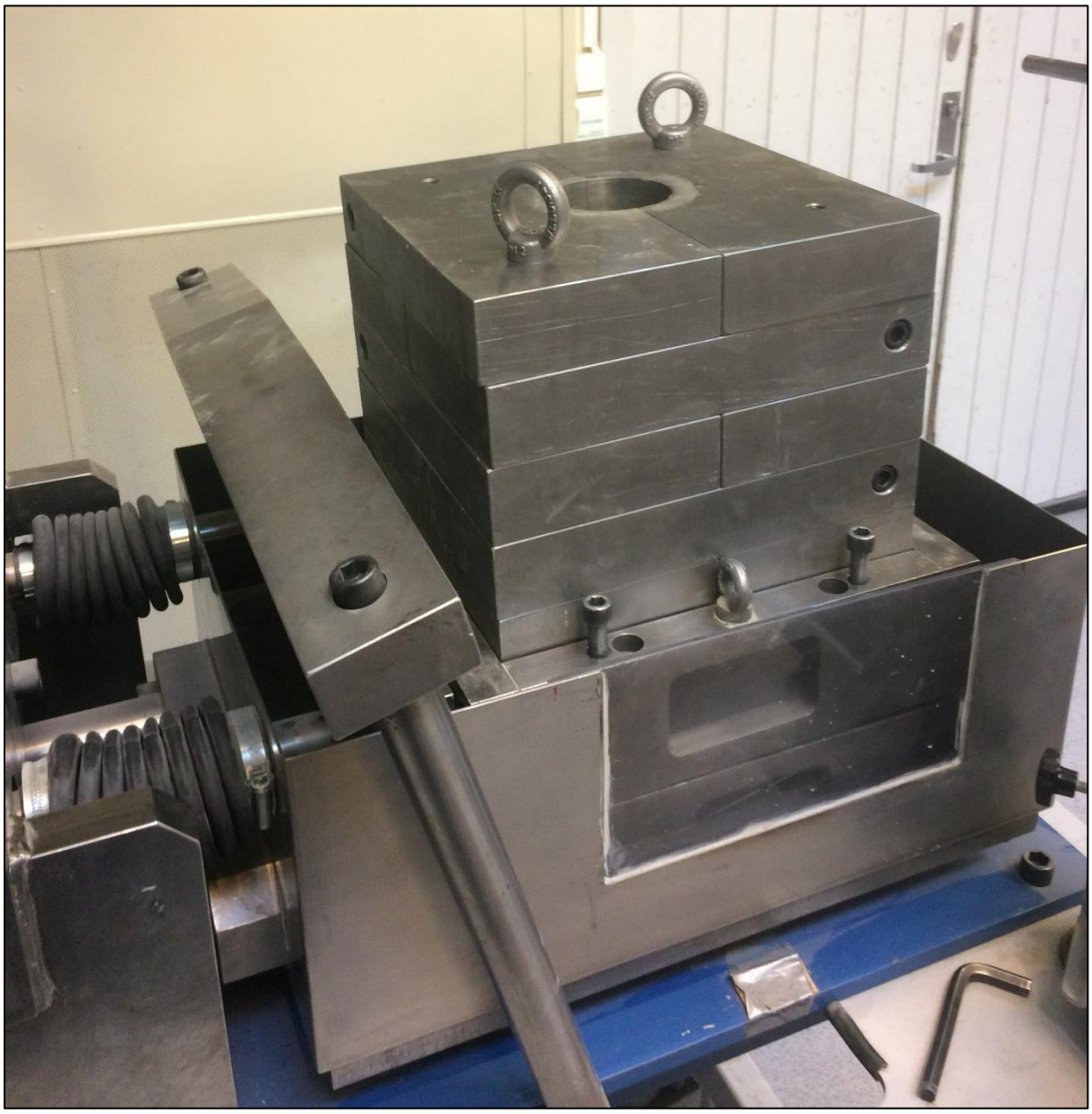

Figure 4.11: Steel plates were used to apply normal stess to the sample.

The shear box was filled by use of a hand scoop and the material poured into the center of the box to achieve a homogeneous distribution. The material was inserted in three vertical layers of corresponding thickness. Wooden tools, designed and built by PhD. canditate Øystein Lid Opsal was used to even out the layers. Compaction of each layer was performed by five drops of a 4kg kettlebell from approximately 20 cm height onto a steel plate. After compaction, a garden hand fork was used to scarify the layers, in two perpendicular directions, to prevent segregation. These procedures are shown in Figure 4.12 and Figure 4.13. The sample volume was calculated, using the measured depth from the top of the box to the sample surface. After

completion of the test, the material was weighted and combined with the volume to find the initial dry testing density, ρ_d of the sample.

The shear rate was set to 2.0 mm/min when testing dry material. The maximum shearing distance of the SB2010 is 50 mm (Testconsult, 2012). As described by Opsal (2017), such a long shear distance can result in spillage of material and reduced shearing area. A shear distance of 32 mm was chosen and will prevent this and is above the minimum shear distance of 30.5 mm, recommended by ASTM D3080/D3080M (2011). Between each test the sample was removed from the sample box and refilled by the same method as previously described.

Figure 4.12: Compaction of a layer

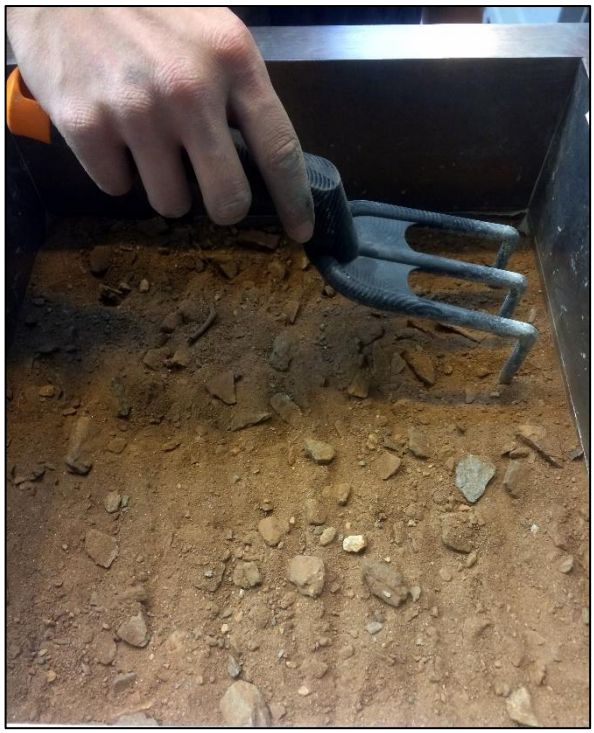

Figure 4.13: Scarification of a layer.

An identical procedure was performed when testing material with a water content dry of optimum. The only difference was the shear rate, which was set to 0.5mm/min as recommended by ISO 17892-10 (2004).

The shear stress is plotted against the normal load. Through linear regression a line is fitted to the points (Figure 4.14). The angle of friction is found by:

$$\varphi = tan^{-1}\frac{dy}{dx} \qquad (°) \qquad 4.4$$

The cohesion parameter is found by the point of intersection between the regression line and the y-axis, as illustrated in Figure 4.14.

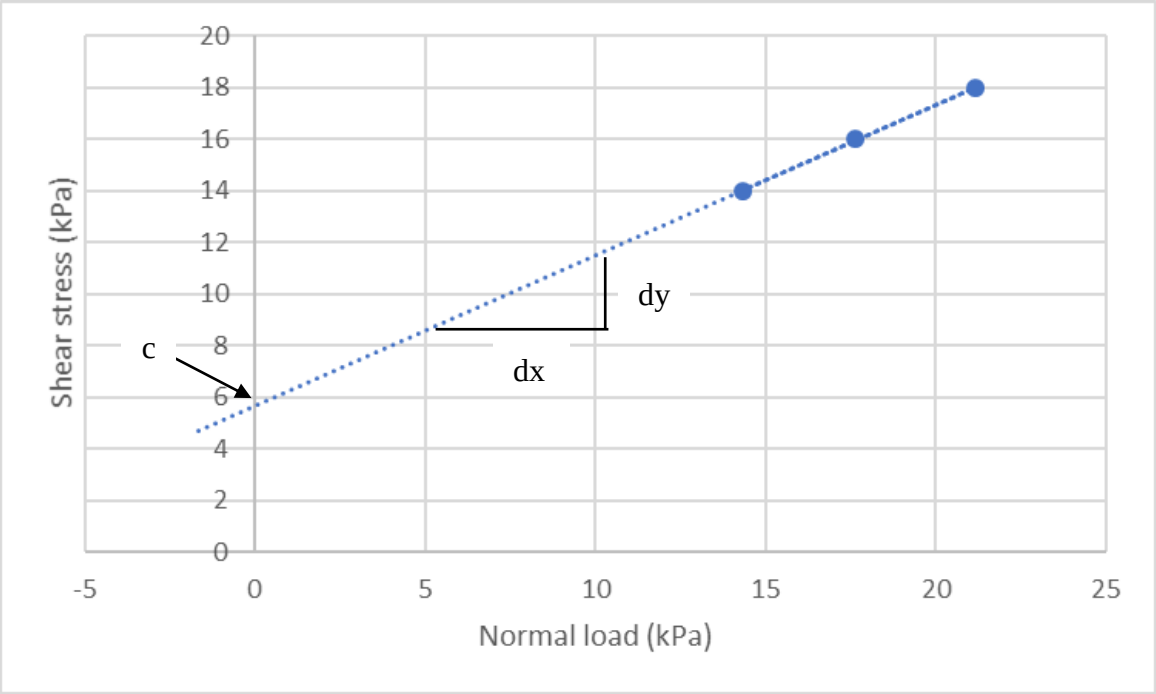

Figure 4.14 Linear regression gives a slope gradient (dy/dx) and an intersection point used to find the angle of friction, φ and the cohesion, c.

5 Results

The samples were given a name based on a number, by location. In addition, the letter A represents samples collected from inside a landslide channel, while B represents samples collected outside a channel. The “in-channel” samples (A) were collected from a profile in one of the channel walls. The “out-off channel” samples (B) were collected with various distances from the channels. Depending on ease of access, depth of soil cover and slope gradient. To investigate the spatial variability of landslide occurrence, the out of channel locations were of similar character to the terrain where the event occurred.

5.1 Field investigations

Ten samples were collected from five different locations during the field work. The sampling locations are marked in Figure 3.2 and in Figure 3.14. As the distance between particular sampling locations is minor, a few of the points represent both the inside and outside of a channel samples.

Table 5.1 Categories for evaluation of the degree of compaction in the field.

Degree of compaction	
Compact	A tool of metal or wood and a large amount of force were required to remove material from the profile.
Moderate	The material could easily be removed by use of a tool.
Loose	The material could be removed by use of hands/fingers.

The depth of sampling was measured from below the vegetation cover. The degree of compaction was evaluated based on the categories listed in Table 5.1.

Table 5.2: Results from field work. Modified from Hauge (2017).

	1		2		3		4		5	
	In	Out	In	Out	In	Out	In	Out	In	Out
Depth of sampling	30-70 cm	30-60 cm	20 - 100 cm	10 - 85 cm	75 - 200 cm	30 - 50 cm	50 - 80 cm	50 - 100 cm	50 - 100 cm	50 - 100 cm
Degree of compaction	Compact	Moderate	Moderate	Compact	Compact	Moderate/ Compact	Loose	Loose	Moderate	Compact
Grain size	Coarse	Coarse	Medium	Medium	Medium	Medium	Fine	Medium	Medium	Medium
Approximate amount of removed rocks (>5x5 cm)	40 %	50 %	20 %	20%	30 %	20 %	40 %	20 %	10-20 %	10-20%
Shape of larger rocks	Mostly tabular, some rounded	Tabular	Rounded	Rounded	Rounded	Rounded	Tabular	Tabular	Rounded/ Tabular	Rounded/ Tabular
Fractures	No	No	No	No	No	No	No	No	No	No
Layering	top 20 cm: dark organic layer	No	Top 20 cm: dark organic layer	Some cm thick brown/red horizontal lenses in the upper 50 cm	Sand in the upper 10 cm of the profile	Top layer consists of 20 cm of sand. Till below	Layer of larger rocks (10x10 cm) in the upper 40 cm. Brown color in upper 40 cm. Red below	10 cm thick red colored layer at 55 cm.	2-3 Cm thick layers of clay/silt	No
Other observations	Large boulders (20x20 cm) found in the profile		Moist soil, but no obvious seepage. Gray color	Dry conditions, grey color	Larger rocks with depth	Very compact at 30 cm, looser at 50 cm	Water seepage at 80 cm. Surface prallel orientation of larger rocks. Large amount of mica minerals.	Light brown/ red color. Larger rocks below vegetation cover.	Dark brown/grey color.	Brown color

Observations made during sampling in the field are listed in Table 5.2. A selection of the results is based on subjective evaluations. The approximate amount of removed rocks were decided by eye measurement and given in percentage of the sample volume, which was a 10 liters bucket. Only rocks larger than about 5x5 cm were removed from the sample. Figure 5.1 shows some of the removed rocks at location 1. Shape of larger rocks were determined by eye measurement and divided into rounded or tabular. Layering in the material were examined during and after excavation of the soil profile (Hauge, 2017). Figure 5.2 illustrates the profile in location 2B, where layers of red colored soil is visible.

Figure 5.1: Rocks removed when sampling at location 1.

Figure 5.2 Profile at location 2B. Red colored layers in the upper part. The length of the folding ruler is 1 meter.

Figure 5.3 and Figure 5.4 shows sample 2A and 4A, respectively. By visual inspection it is apparent that the sample from Innfjorden (2A) contains coarser material than the sample from Gauldalen (4A). The color difference is also evident. Sample 2A is grey of color, while sample 4A is red/brown. There was not observed any clear signs of cementation of the soil in the field. Larger grains were surrounded by finer particles. Roots penetrated the soil in all locations, but to different depths. The largest depth of root penetration was 70 cm below the vegetation cover.

Figure 5.3 Sample 2A before drying.

Figure 5.4 Sample 4A before drying.

5.2 Grain size distribution

The grain size analysis was performed on representative parts of the material collected in the field. The depth of each profile is listed in Table 5.1.

The grain size analysis was performed by two different methods, dry sieving and laser diffraction. The results from the two methods are collated into one curve in Figure 5.5, showing the cumulative grain size distribution for each sample. Table 5.3 and Figure 5.5 shows the grain size distribution in percentage of each fraction. The fractions used are based on the definition given by NS-EN ISO 14688-1 (2002). The two methods used for the analysis are based on different theories, resulting in a change in slope gradient at 38µm.

All samples have similar grain size distribution in the fine fractions. The content of clay is minor in all samples. The highest content is found in sample 4A, with 2.4%. All samples have a silt content below 30%. The largest differences are seen in the sand fraction and coarser. Sample 1A and 1B differs from the others with a content of medium gravel of 41 and 38%. The complete data from the grain size analysis is given in Appendix B.

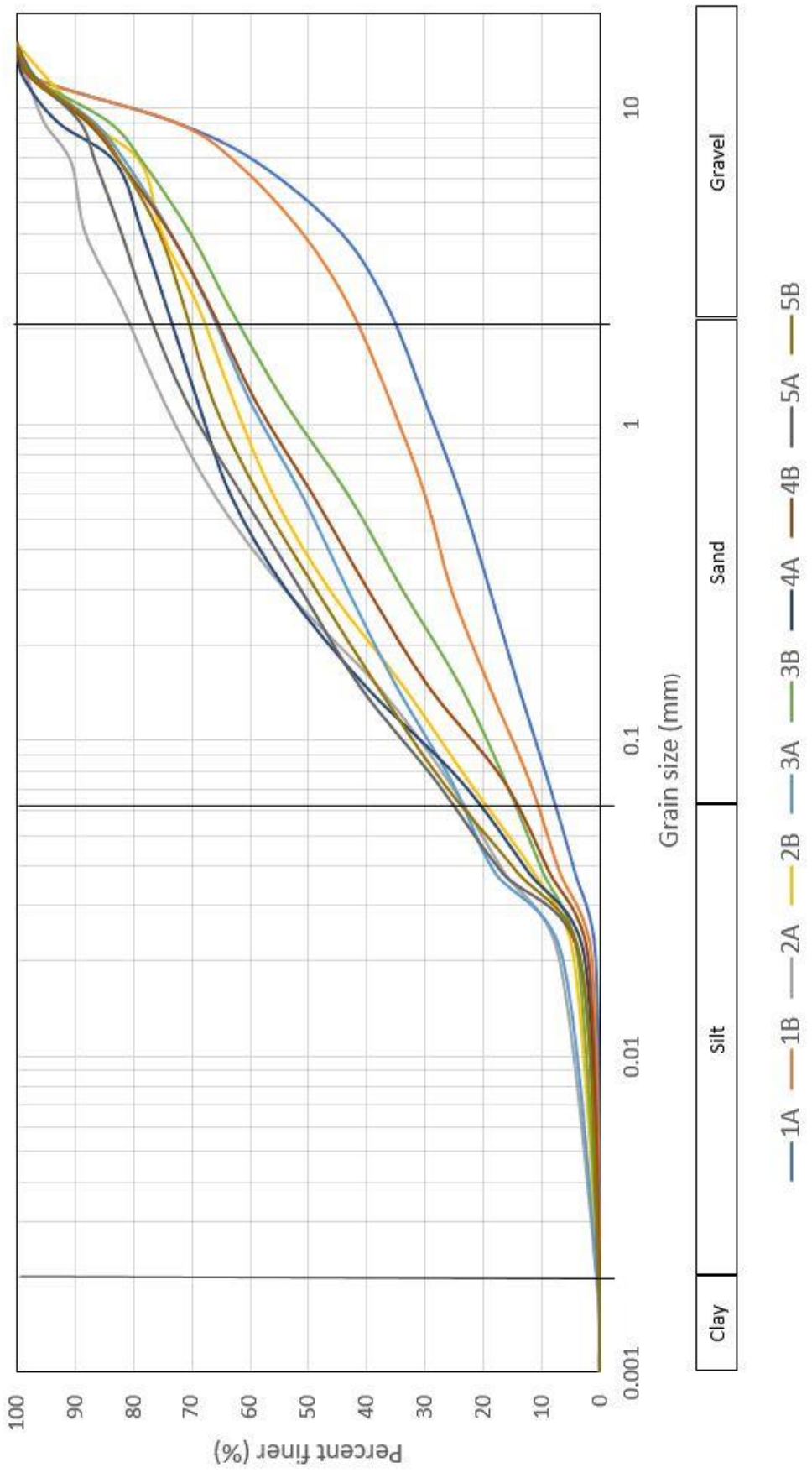

Figure 5.5: Grain size distribution of all samples. Given in cumulative percentage.

Table 5.3 Grain size distribution in non-cumulative percentage.

Fraction (%)	1A	1B	2A	2B	3A	3B	4A	4B	5A	5B
Clay	0	0	1	0	1	0	2	0	0	0
Fine silt	0	0	1	1	1	1	0	0	1	1
Medium silt	1	1	5	3	5	3	0	2	3	3
Coarse silt	7	9	16	15	16	10	18	12	21	20
Silt	8	10	22	19	23	14	18	14	24	23
Fine sand	8	11	21	19	15	13	25	19	20	19
Medium Sand	9	9	23	18	14	16	19	17	17	17
Coarse sand	10	11	13	11	13	17	9	15	14	11
Sand	27	30	57	48	42	47	52	50	51	47
Fine gravel	22	20	10	11	15	16	10	16	10	11
Medium gravel	43	39	10	22	20	23	18	19	14	19
Gravel	65	59	20	33	35	39	27	35	24	30

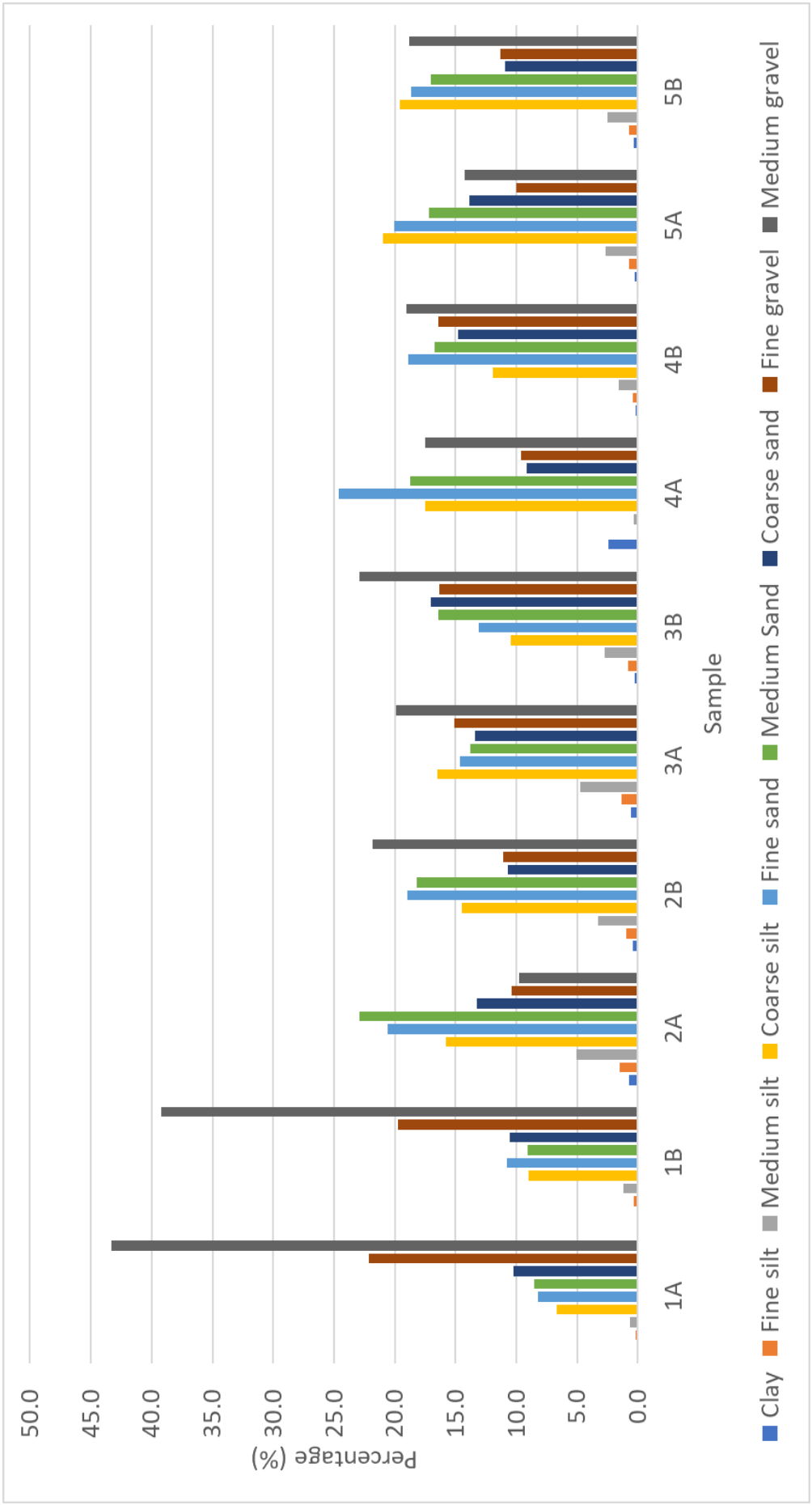

Figure 5.6 Non cumulative percentage of each fraction.

Table 5.4 Degree of grading.

Sample	Cu (Q_{60}/Q_{10})	Grading
1A	78	Well graded
1B	100	Well graded
2A	13	Graded
2B	26	Well graded
3A	36	Well graded
3B	43	Well graded
4A	13	Graded
4B	33	Well graded
5A	15	Well graded
5B	23	Well graded

The degree of grading of the samples is given in Table 5.4. All samples, except the sample 2A and 4A are well graded.

5.3 Particle shape investigations and mineralogical analysis

Microscopic investigations

Material which only had been dried in an oven were investigated too look for signs of cementation. The samples were not sieved, and thus contained several fractions. The greater part of the grains was covered by fine material, which made it difficult to observe any signs of fracture surfaces on the grains. Except for the fines, little surface coating was observed on the finer grains. A selection of the coarse grains from the samples collected in Gauldalen was covered by a layer of rust.

5.3.1 Particle shape and surface texture

The flakiness index **(**FI), Shape index (SI), angularity and surface texture are given in Table 5.5. The samples from Gauldalen and from location 1 in Innfjorden show the highest flakiness and shape index values. The dominating grain shapes is sub angular. All samples contained grains with a rough surface texture.

Table 5.5 The flakiness index (FI), Shape index (SI), angularity and surface texture of the samples.

Sample	FI (%)	SI (%)	Angularity	Surface texture
1A	21.0	35.0	Sub angular	Rough
1B	13.0	22.0	Sub angular	Rough
2A	6.0	5.0	Sub angular	Rough
2B	7.0	7.0	Sub angular	Rough
3A	2.0	3.0	Sub angular	Rough
3B	1.0	1.0	Sub angular	Rough
4A	38.0	39.0	Angular	Rough
4B	9.0	8.0	Sub angular	Rough
5A	23.0	46.0	Sub angular	Rough
5B	23.0	27.0	Sub angular	Rough

5.3.2 Mineralogical analysis

The fraction 6.3/8mm was studied in relation to rock type. The samples from Innfjorden consisted of particles of gneiss. The rock types within the samples from Gauldalen were more variable.

Table 5.6: Rock types in the fraction 6.3/8mm.

Sample	Rock / Mineral type (%)
1A	Gneiss (100%)
1B	Gneiss (100%)
2A	Gneiss (100%)
2B	Gneiss (100%)
3A	Gneiss (100%)
3B	Gneiss (100%)
4A	Mica schist (79%), Meta sandstone (10%), Amphibolite (8%), Undefined (3%)
4B	Metasandstone (28%), Amphibolite (27%), Mica schist (15%), Mica gneiss (10%), Greenstone (10%), Undefined (5%)
5A	Meta sandstone (54%), Mica schist (40%), Undefined (6%)
5B	Metasandstone (50%), Mica schist (46%), Undefined (4%)

5.3.3 XRD-analysis

The results from the XRD-analysis of material <38µm are listed in Table 5.7. The results of analysis of material 38-61µm are found in Table 5.8 .

There is not a large variation in the type of minerals occurring in the samples from Gauldalen and Innfjorden. The samples from Innfjorden have a high content of plagioclase (32 – 40%) and quartz (24 – 31%) as the second ranging mineral. The mineralogy of the samples from Gauldalen are opposite, with a high content of quartz (33 – 57%) and less plagioclase (19 – 33%). Other dominating minerals are mica (4-18%), alkali feldspar (5-12%) and amphibole (3-16%). Chlorite is mainly found in the samples from Gauldalen, while Laumonite and Spessartine are only found in Innfjorden. The difference between the material <38µm and the material 38µm-61µm is minor. A slightly higher content of mica is found in the fraction <38µm.

Table 5.7 XRD-analysis of material <38µm.

Mineral	***1A***	***1B***	***2A***	***2B***	***3A***	***3B***	***4A***	***4B***	***5A***	***5B***
Quartz (%)	24	26	27	25	23	23	53	57	35	33
Chlorite (%)	2	1					<1	1	5	6
Alkali Feldspar (%)	10	9	10	10	12	11	10	7	5	6
Amphibole (%)	12	14	6	7	12	11	3	6	8	7
Plagioclase (%)	32	37	36	36	35	36	19	20	33	32
Mica (%)	17	10	18	18	17	16	13	6	14	15
Pyroxene (%)	<1	2	3	3	2	2	<1	2	<1	<1
Laumonite (%)	2									
Spessartine (%)				<1	<1					

Table 5.8 XRD-analysis of material 38-61µm.

Mineral	1A	1B	2A	2B	3A	3B	4A	4B	5A	5B
Quartz (%)	27	26	33	31	27	28	48	53	45	44
Chlorite (%)	<1	<1	<1	<1	<1	<1	3	<1	3	4
Alkali Feldspar (%)	8	9	10	10	10	10	6	8	5	5
Amphibole (%)	14	16	7	8	12	10	3	6	7	6
Plagioclase (%)	33	37	39	40	37	38	26	25	31	33
Mica (%)	14	9	9	7	10	10	10	4	9	8
Pyroxene (%)	1	2	3	4	3	3	3	3	1	<1
Laumonite (%)	2									
Spessartine (%)			<1	<1	1	1				

5.4 Optimum moisture content

The dry of optimum moisture content of representative parts of the samples is presented in Table 5.9. The water content is given in percentage of dry material and ranges from 10 to almost 26%. All locations, except location 1, have a higher optimum moisture content in the samples collected from the landslide channel than those collected outside of a channel. The samples collected in Gauldalen have a larger content than the samples from Innfjorden.

Table 5.9 Dry of optimum moisture content

Sample	Dry of optimum moisture content (%)
1A	15.82
1B	22.90
2A	12.28
2B	11.68
3A	11.73
3B	10.64
4A	25.81
4B	12.40
5A	19.07
5B	17.77

5.5 Shear box test

Shear box testing were performed on three samples and each sample was tested in both dry and unsaturated conditions and with three different normal loads.

Table 5.10 Results from shear testing of dry material

Sample	Initial testing density (g/cm^3)	Max. shear stress, τ			Friction angle, φ (°)	Cohesion, c (kPa)
		14.13 kPa	17.66 kPa	21.19 kPa		
2A	1.94	13.0	16.0	18.0	35.4	3.2
2B	1.87	13.0	15.0	18.0	35.4	2.8
4A	1.26	13.0	14.0	16.0	22.8	6.8

The results from testing of dry material are listed in Table 5.10. The initial testing density of the samples from location 2A and 2B were 0.68 g/cm3 and 0.61 g/cm^3 higher than the sample 4A. The results from testing of dry material shows that sample 2A and 2B have the highest friction angle (35.4°) and sample 4A the lowest (22.8°).

Table 5.11 Results from shear testing of unsaturated material

Sample	Initial testing density (g/cm^3)	Moisture content (%)	Max. shear stress, τ			Friction angle, φ (°)	Cohesion, c (kPa)
			14.13 kPa	17.66 kPa	21.19 kPa		
2A	1.42	12.28	14.0	16.0	18.0	29.7	6.0
2B	1.49	11.68	13.0	15.0	18.0	35.4	2.8
4A	1.54	25.81	14.0	16.0	18.0	29.7	6.0

The results from testing of unsaturated material is presented in Table 5.11. The largest difference in initial testing density for the unsaturated material was 0.12 g/cm^3. The largest friction angle is found in sample 2B, which had the exact same results in dry and unsaturated condition. Sample 2A and 4A exhibit the same results.

Figure 5.7 shows the results plotted by shear stress and displacement from testing of sample 2A. The red lines represent results from tests on dry material, while blue on unsaturated material. The curves from tests on unsaturated material show a trend of gradually increasing shear stress, compared to dry material which reaches maximum shear stress faster. The unsaturated material has a higher shear stress for all normal loads. The graphs from testing of dry material increases rapidly in the beginning of the test and reaches a peak, before it reaches a constant value.

The results of testing of sample 2B in Figure 5.8 show a similar trend as in Figure 5.7, with higher shear strength for dry compared to unsaturated samples. However, the samples applied with corresponding normal loads reaches the same maximum shear stress. Tests performed on sample 4A, presented in Figure 5.9 results in a higher maximum shear strength for unsaturated samples than for dry.

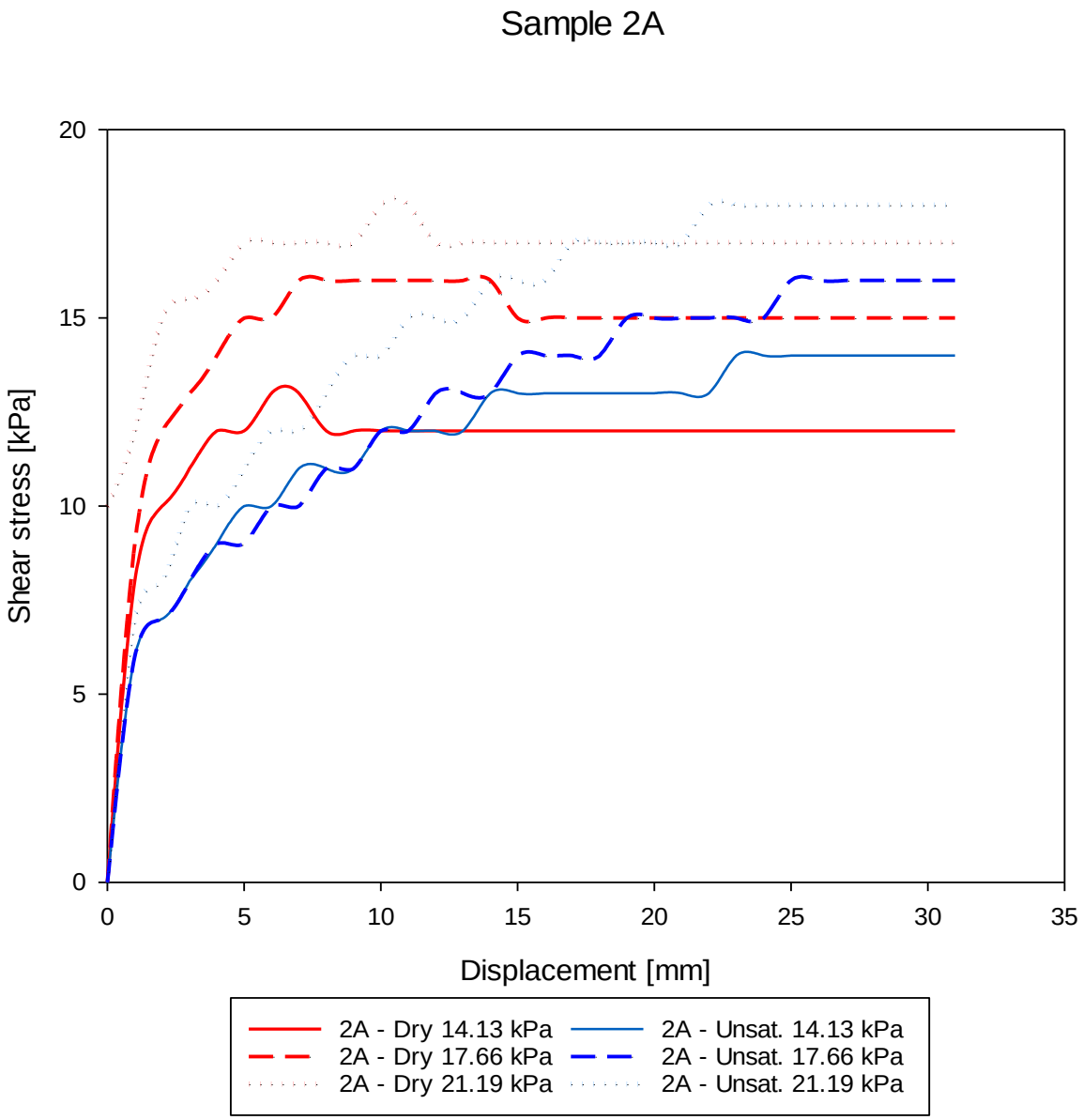

Figure 5.7 Results from shear testing of sample 2A. Red lines indicate dry sample, blue lines unsaturated sample.

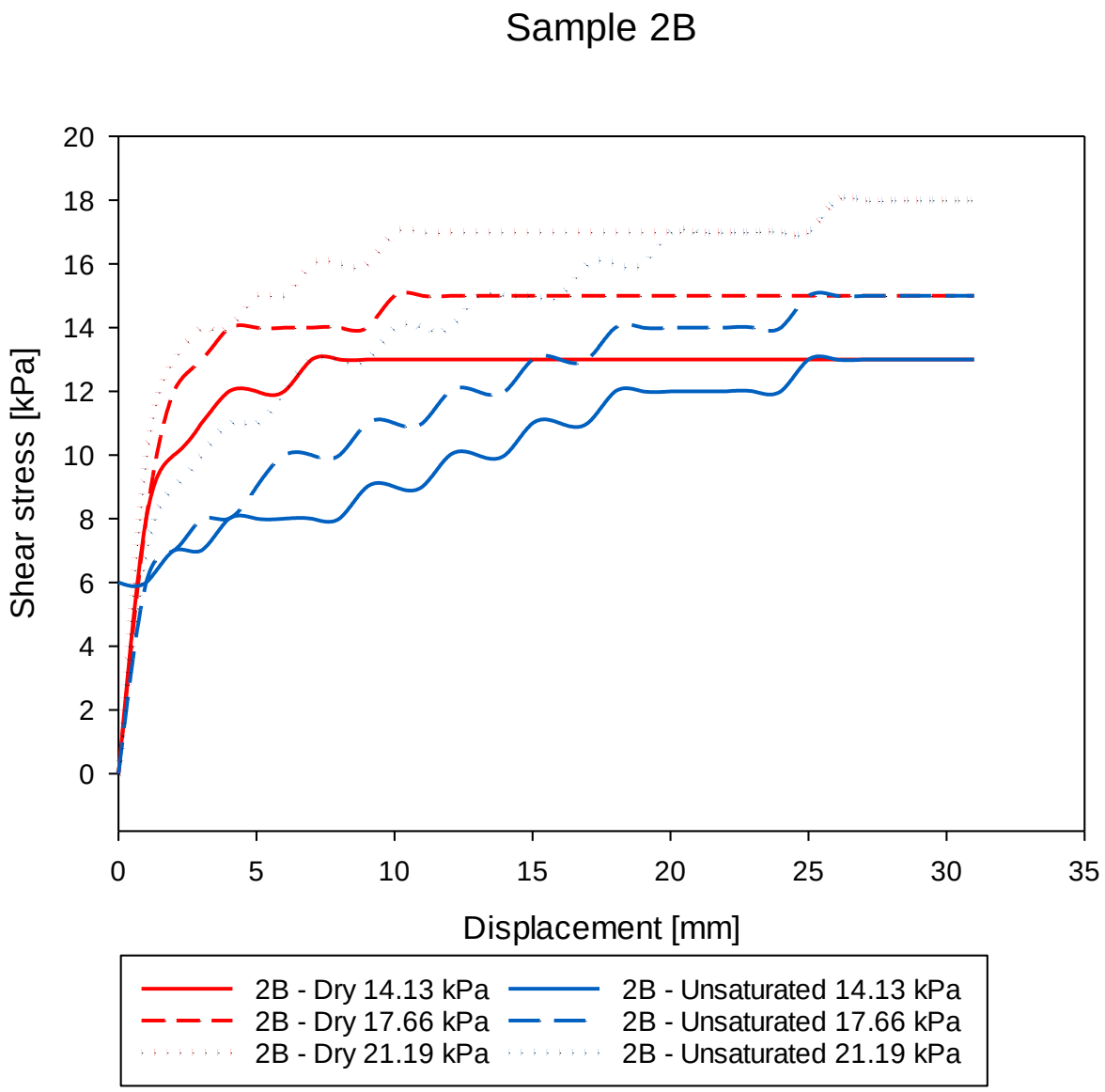

Figure 5.8: Results from shear testing of sample 2B. Red lines indicate dry sample, blue lines unsaturated sample.

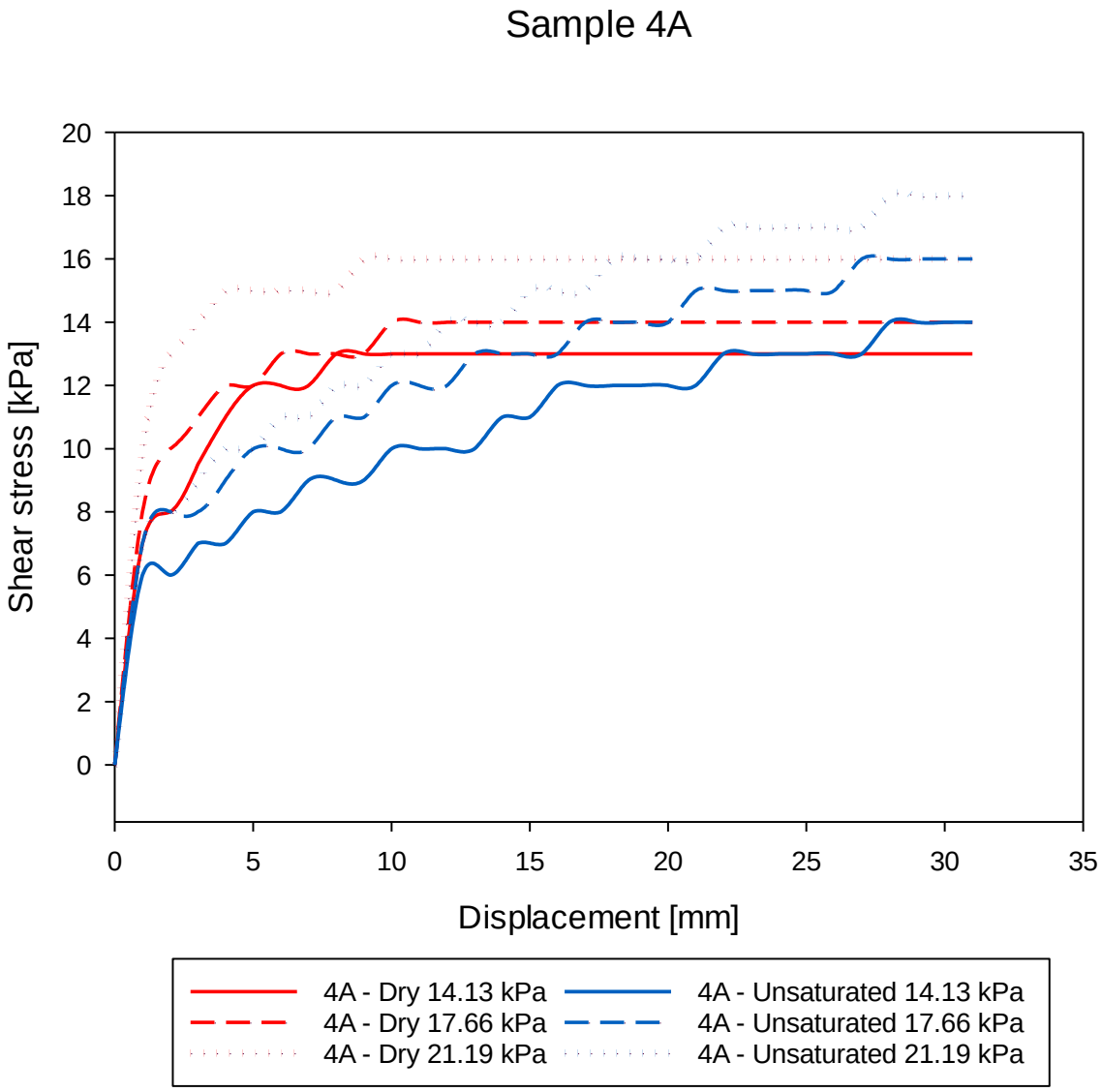

Figure 5.9 Results from shear testing of sample 4A. Red lines indicate dry sample, blue lines unsaturated sample.

6 Discussion

The main objective of this thesis is to investigate the influence of differing petrography and water content on the shear strength of two types of till soils. The field work included investigation of field sites and sample collection of ten samples from five locations.

In this section, the following subjects will be addressed:

- Analysis of field work and laboratory tests, including sources of error.
- Comparison of the mineralogical controlled properties and their effect on shear strength properties of till soils collected from Innfjorden and Gaudalen.
- Study of the connection between the water content and shear strength.
- Comparison of material properties of samples collected inside and outside of landslide channels.
- Comparison of obtained results to the results found by Opsal (2017), Opsal (2018) and other relevant research.

6.1 Field investigations and sampling

The field work was conducted in three days, two days in Innfjorden and one day in Gauldalen. Ideally, the time spent at field work should have been extended to achieve a more detailed description of influencing properties. Including description of general grain orientation and a more detailed inspection of layers, fractures and signs of cementation. Measurement of the soil density was intended, but proved difficult due to a high degree of compaction. During the selection of sampling locations depositional processes of the soils were not considered. This has a significant influence on soil properties, but is difficult to determine (Haldorsen and Kruger, 1990).

To achieve a more representative result, the number of samples should have been increased. Samples were only collected from two locations in Gauldalen due to difficulty finding a representative third location. Only two samples were collected from each location. The samples should also have been of a larger volume. Shear box testing was not intended at the time of sampling. Thus, the sample sizes were not scaled for this. Preferably, the collected samples should have been undisturbed. However, this is difficult to obtain due to the unsorted characteristic of till soils. As the samples are collected from slopes where landslide activity is apparent, the soil samples might be affected by slope processes. This is obvious in location 1, where the rock fall hazard is evident.

The depth of sampling ranged from 10 to 200 cm below the vegetation (Table 5.2). The upper part of the soil profile is within the "active layer" and thus modified by weathering and biologic activity (Bargel et al., 2011). The degree of compaction was subjectively estimated in the field and varied from loose to compact. The soil in Gauldalen was generally of a looser character compared to the soil in Innfjorden. Older and deep penetrating vegetation in Gauldalen might influence on the lower degree of compaction. Missing registration of the landslide event in location 1 creates a source of uncertainty regarding the type of landslide or avalanche.

The absence of observed fractures in the soil is probably a result of poorly conducted excavation and inspection of the profiles. Red colored layers were observed at depths of 40-50cm at location 2B, 4A and 5B. This might indicate precipitation of iron oxides in the leached horizon.

6.2 Grain size distribution analysis

The results from the grain size analysis show some errors resulting from the combination of the results from the sieving and laser diffraction into one curve. The two methods measure the grain size in different ways, resulting in an anomaly in the curve seen at 38µm in Figure 5.5. Furthermore, the laser diffraction measures with a higher frequency, which might have an emphasizing effect of the flattening in the finest part of the curve.

The grain size analysis had to be performed in three stages, as the analysis of the optimum moisture content were performed beforehand. During the optimum water content analysis, the samples were separated in two parts; material coarser than 6.68 mm and material finer. When sieving the material, the two parts were investigated separately and the results combined by calculation of the weight of each fraction to the weight of the total mass. The material coarser than 16mm were not included in the analysis, which is typical for analysis of till soils due to the large sample volume required for a more extensive analysis (Jørgensen, 1977). The observations regarding the approximate amount of removed rocks, which is listed in Table 5.2, show that the amount of particles larger than 16mm is substantial. Particularly in the samples from the Precambrian region.

Sample 2A, 2B and 4A were tested in the shear box before grain size analysis were performed. This was not ideal, but necessary as the whole sample was required for shear box testing. During this procedure it was taken care not to lose any material, but smaller amounts of the sample might have been lost. In addition to this, it should be expected that parts of the material were lost during preparation and handling before sieving in the laboratory. The results from the laser diffraction analysis show a content of material larger than 38µm. This is probably caused by clustering of material and represents a source of error in the results of the finest material.

The grain size distribution curves show a distribution typical for till soils (Neeb, 1992). Eight out of ten samples were well graded, which also indicates glacial till soils (Brattli, 2015).

The results from sample 1A and 1B show a large content of fine and medium gravel. These samples were collected in a slope with a slope gradient of 30-40° (Figure 3.5). The overlying terrain was even steeper, which indicate that the till soil might be mixed with colluvium. The results show that all samples collected inside a landslide channel have a lower degree of grading compared to the samples collected outside a channel (Table 5.4).

Jørgensen (1977) found that the clay and silt fractions were the main dominating fractions in tills derived from Cambro-Silurian sedimentary rocks, while tills originating from Precambrian rocks have a higher content of coarser fractions. The results from the grain size analysis (Table 5.3) do not show a strong correlation with this allegation. All samples, except the samples from location 1 have sand as the dominating fraction. However, the clay content is less than 10% in all samples and correspond to the findings of (Jørgensen, 1977). The samples of Cambro-Silurian origin (4A, 4B, 5A, 5B) do not generally have a larger content of silt and clay compared to the Precambrian derived tills (1A, 1B, 2A, 2B, 3A, 3B), as found by Jørgensen (1977) and verified by Opsal (2018). This might be explained by the fact that the samples were collected in locations that might be modified by running water, slope processes or human alterations. Material at the bottom of the deposit originates from the lower part of the glacier and will normally contain a higher content of fines compared to overlying material. The mode of deposition will also influence on the grain size distribution and is not considered in this study (Selmer-Olsen, 1980). Furthermore, the number of samples is too low to draw any conclusions regarding trends in the grain size distribution.

6.3 Particle shape investigations and mineralogical analysis

The results given in section 5.3.1 and 5.3.2 are mainly based on subjective assessments. This might have an impact on the achieved results. It should be noted that the amount of analyzed material is restricted compared to the total mass of the sample.

Microscopic investigations

Material exposed to a minimum amount of alteration was studied for signs of cementation. A microscope was used to visually investigate dried material consisting of several fractions. No clear signs of cementation were observed. The reason for this might be alteration of the material during sampling and handling. Fines covering the grains increased the difficulty of observing fracture planes.

The degree of cementation in Norwegian soils is generally low. The main cementitious minerals in Norwegian tills are calcite and iron oxides (Selmer-Olsen, 1977). The XRD analysis does not show any calcite in the finest fractions of the material. This might be a result of the weak character of calcite, causing the mineral to dissolve easily in water. Iron oxides are also known to cause cementation, particularly in the leached layer in the soil profile. The red colored layers observed in the field indicate, as previously mentioned, precipitation of iron oxides (Selmer-Olsen, 1977). A red surface cover was observed on certain grains of coarser size from Gauldalen and cementation in the material is thus possible.

Flakiness index, FI

The conduction of the flakiness index analysis partly evaded from the standard (NS-EN 933-3, 2012). Hence, the results are not fully comparable to the results presented by (Opsal, 2018). However, they give an indication of the dominating grain shape. The particle shape is strongly dependent upon the grain size and is variable throughout the grain size distribution (Terzaghi et al., 1996). The flakiness index given in Table 5.5 is thus a general index for the total sample.

The results from Location 1 stand out from the rest of the samples from Innfjorden. A reason for these high values (20.5% and 13.1%) might be the influence of colluvium. Due to the short transport distance of such material the degree of angularity is typically high (Selmer-Olsen, 1977). The remaining results show a similar trend to that found by Opsal (2018), with a low FI for the samples derived from Precambrian rocks and a higher value for samples derived from Cambro-Silurian rocks. This can be explained by the difference in rock types and mineralogy. The mica-schist and phyllite found in Gauldalen is made of flaky minerals and produces flaky

rock fragments. The strong metamorphic gneiss, mainly consisting of quartz and feldspar in Innfjorden is resistant to crushing and produces rounded grains (Selmer-Olsen, 1977) (Hardin, 1985).

No significant difference in FI was observed between the samples collected inside and outside of a channel. As the distance between these sampling points is low, the material is of the same origin and a large difference in relation to flakiness was not expected.

Shape index, SI

The shape index correlate with the flakiness index for all samples. A tendency of higher values in the samples from Gauldalen (Cambro-Silurian rocks), compared to the samples from Innfjorden (Precambrian rocks) is evident. This also correlates with the results found by Opsal (2018). The samples from Gauldalen have a higher SI in the in-channel samples than in the out of channel samples. No significant difference is observed in the samples from Innfjorden.

Angularity and surface texture

The main particle shape of larger rocks was registered in the field during sampling (Table 5.2). These observations correspond well to the angularity found when studying the samples in the laboratory (Table 5.5). Similar to the results of Opsal (2018), it is the sub angular grain shape that dominates the samples. Sample 4A is the only sample with an angular grain shape, which might be explained by the prevalence of mica schist in that area. All samples are characterized by a rough surface texture. The angularity and surface roughness can, similarly to the flakiness index, be explained by the originating rock type and their minerals. The grain shape and rough surface indicate a short transport distance (Brattli, 2015).

Mineralogical analysis

The mineralogical analysis was performed by visual inspection of the fraction 6.6/8 mm. The grains consisted of rock fragments which corresponded well to the rock types within a 5 km distance of the sampling locations (NGU, 2017a). Supporting the theory of a short glacial transport distance (Selmer-Olsen, 1977). Gneiss governs in Innfjorden, while metasandstone is the dominating rock type in the samples from Gauldalen, except to mica schist at location 4A (Table 5.6).

XRD-analysis

XRD-analysis was conducted on two fractions, material <38µm and material from 38-61µm. The analysis was conducted on two fractions as the mineralogical composition might vary with particle size (Berry and Jørgensen, 1971). The results show that the difference between the mineralogy in the two fractions are minor. The mica content is slightly higher in the <38µm fraction than the 38-61µm (Table 5.7 and Table 5.8).

The results from the analysis resembles the results presented by Opsal (2018), presented in Figure 2.11. The dominating mineral in the samples from the Precambrian region is plagioclase, with quartz as the second raging mineral and amphibole as the third. In the samples from the Cambro-Silurian region the mineralogy is dominated by quartz, with a smaller amount of Plagioclase. The coincidence with the results from Opsal (2018) indicates that the differences in mineralogy between the finest fractions and the 0.5/1mm fraction is negligible.

When studying the material in the field, a lot of mica minerals were observed in the samples from Gauldalen. Hence, it was expected to find a higher content of mica in the material from Gauldalen compared to Innfjorden. However, the amount is approximately equivalent in the finest fractions. This might indicate that the difference is greater in coarser fractions and this should have been investigated.

The main minerals in gneiss is feldspar and quartz, with minor amounts of biotite and amphibole. This corresponds well with the minerals found in the analysis of the samples from Innfjorden. Quartz, plagioclase and mica are dominating in the samples from Gauldalen. These minerals are found in mica schist, phyllite and sandstone (Garmo, 1995). The results indicate that the finest fractions in Norwegian till soils mainly consist of minerals originating from local rocks. The content of clay minerals is nonexistent. No large difference was seen in the mineralogy between the samples collected from inside and outside a channel. The samples from location 4 shows a slightly higher content of mica in the in-channel sample compared to the out of channel sample.

6.4 Optimum moisture content

The dry of optimum moisture content was found for all the samples. Material coarser than 6.68mm were extracted before testing as the water content is mostly dependent on the finer fractions which have the ability to retain more water (Vanapalli et al., 1999). Soils show the weakest shear strength at dry of optimum moisture content, compared to optimum and wet of optimum (Vanapalli et al., 1996b). In relation to this and to simplify the execution of the shear box testing, it was decided to find the dry of optimum moisture content.

Apart from the samples from location 1, the samples from Innfjorden have generally a lower percentage water at the dry of optimum moisture content compared to the samples from Gauldalen. There is no visible connection between the measured optimum moisture content and the content of fines, or to the content of any type of mineral. However, the results indicate a correlation with the measured flakiness index of the samples. The samples 1B and 4A both have optimum water contents above 20% and some of the highest flakiness indexes. As described in section 2.1.3, flaky particles have a higher water absorption capacity and lower compressibility than rounded grains (Adom-Asamoah and Afrifa, 2010).

According to research presented in Chapter 2 one would expect that samples with a high content of mica minerals would have a large water absorption capacity. The lacking differences in mineralogy makes it difficult to draw any conclusions regarding this fact. However, the observed large mica content in sample 4A might be related to the high dry of optimum water content (25.81%).

6.5 Shear box test

Three samples were tested in a large-scale shear box in both dry and unsaturated conditions. The number of samples tested in the shear box was restricted by limited time. Before testing, the samples were dried and sieved on a 16mm grid. There exist some restrictions to the representativeness of the results due to the constrained grain size distribution of the tested sample. Breakage of potential cementation of grains during preparation of the material will also have an effect on the results. It should be noted that the effect of layers and fractures was not evaluated during the test. In addition, the shear plane forced in the middle of the sample during the shear box test, and does not occur in the weakest part of the soil as it would in-situ (Holtz and Kovacs, 1981). Alteration of material and absence of applied pore pressure during the shear tests causes a lower frictional angle than what is expected to find in-situ. The focus in this thesis

is however to investigate the differences between the till soil types, and not to compare the results to in-situ conditions.

The representativeness of the results from the tests are affected by several factors connected to the execution of the tests and the material tested. The height of the tested samples ranged from 5.5 to 6 cm. The sample volume was therefore low compared to in the tests performed by Opsal (2017). The samples were not of the exact same volume, which also might cause a difference in the results. The standards the procedure is based on does not recommend reusing the samples as the particles might endure crushing during testing. As the till soils consists of strong and resistant Norwegian rocks, the amount of particle crushing is expected to be minor (Opsal, 2017). The results from the grain size analysis exhibit no apparent difference in the distribution between the samples that were tested in the shear box and those who were not. Indicating no major alterations of the particles during shear box testing.

The shear box machine, SB2010 has certain limitations including a minimal vertical load of 10 kPa to shear at the given rate. This is seen in the results by a high shearing rate in the beginning of the tests. During testing, particularly when testing with a normal load of 14 kPa the shear plane lifted on one of the sides. This is seen in Figure 6.1 and is normal when conducting shear tests and not expected to have a large impact on the result (Pers. Comm. G. Vistnes, 2018).

Figure 6.1: Lifting of one of the sides of the shear box.

Compression of the sand used to fill the bottom of the shear box container might have occurred during testing and influenced on the results. Particularly on the first test that was conducted. The normal load was applied by use of steel plates. The plates were designed to be used when testing core samples and had a hole in the middle. This can have affected the stress distribution in the samples. Furthermore, the calculation of the angle of friction and cohesion is based on only three points and is thus also a source of uncertainty.

The sample testing density ranged from 1.42 to 1.94 g/cm3, which is lower than the density typical for till soils in-situ (Andersen et al., 2012, Selmer-Olsen, 1977, Terzaghi et al., 1996). The shear stress-deformation curves have shapes typical for loose soils, with no large peak. Due to the loose character of the samples the degree of dilation during testing is probably minor (Terzaghi et al., 1996). The density of the top part of till soils typically is loosened due to mechanical weathering, as described in section 2.2.1. The tested samples, with a low density, might be representative for this part of the soil profile. Mineral hardness and rock compressive strength is probably of minor importance in relation to differences in shear strength, as the degree of particle crushing during testing is expected to be negligible.

The moisture content was partly chosen due to practical considerations. The shear box SB2010 is not completely water proof and previous experience has shown that testing with a large water content results in loss of fines and a lot of spillage (Pers. Comm. Ø. Opsal, 2018). To avoid this, it was decided to use the dry of optimum water content. The samples were stored in sealed plastic bags before testing to maintain the correct amount of moisture. The unsaturated material was tested three times with different normal loads. No water was observed leaving the samples, but evaporation of smaller amounts of water might have occurred. Ideally, the samples should have been weighted both before and after testing to find the amount of water lost.

Ideally, the tests should have been conducted with monitoring or control of the matric suction. As described in section 2.1.3, the matric suction has a high influence on the shear strength of unsaturated soils. The shear box container used during testing was open to air, thus letting the pore-pressure dissipate (Fredlund et al., 2012). The share rate applied when testing the unsaturated material was low to prevent buildup of pore-pressures. Monitoring of the matric suction during shear tests on poorly graded sand at optimum water content and low normal stresses were performed by Purwana et al. (2011). The study found that the soil experienced a very low matric suction between 2-5 kPa. This indicates that a matric suction is present in the till samples during shear tests. However, as the matric suction is below 500 kPa it will probably not influence on the friction angle (Vanapalli et al., 1996a).

The cohesion parameter, c found by shear box testing does not reflect the true cohesion of the soil. It rather reflects the apparent cohesion, which represents the friction between grains due to applied stresses. The cohesion parameter found from the shear box tests is thus not a fundamental soil property, but depending on the applied stresses (Mitchell and Soga, 2005). Alteration of the material has besides destroyed any potential cohesion between grains (Schofield, 2005).

Compared to the results from samples collected by (Opsal, 2017) around the same areas (sample no. 18 and 23), the samples in this thesis show a slightly lower frictional angle. Sample 18, from the Precambrian region has a friction angle of 38°, while sample 2A and 2B both have frictional angels of 35.4°. The largest difference is found when comparing sample 23 to sample 4A with friction angles of 36.5 and 22.8, respectively. An explanation for this might be differences in testing density and material properties. Sample 23 has a higher content of fines, while particles in sample 4A have a higher degree of angularity.

The content of fines is generally low in all samples, with the highest content of 24% in sample 3A and 5A (Table 5.3). The influence of the mineralogy in this fraction is most likely minor as the controlling grain size or sizes are the ones that are dominating the sample (Vallejo and Mawby, 2000).

Comparison of samples collected inside and outside of a channel

Considering the tests performed on dry material, no major difference is observed between the results of samples 2A and 2B. The samples have similar angles of friction (Table 5.10). Considering the results from testing of unsaturated material, the frictional angle of sample 2B is larger than that for sample 2A. The difference in testing density is 0.07 g/cm^3 and most likely not a reason for the difference (Table 5.11). The petrography of both coarse and fine fractions is comparable in the two samples (Table 5.6, Table 5.7 & Table 5.8). As seen in chapter 5, there is no substantial difference in optimum water content, testing density or in flakiness and shape index values. Hence, the difference in the strength parameters is most likely related to the grain size distribution. The samples show a difference in grading, where sample 2A is defined as graded while sample 2B is well graded (Table 5.4). Sample 2A has a higher content of sand compared to 2B, which has a greater content of gravel (Figure 5.6). This correlates with the illustration in Figure 2.7 and with the fact that increased content of fine grains results in a higher density (Mitchell and Soga, 2005).

Figure 6.2 and Figure 6.3 shows the shear stress vs. displacement curves for the two samples from location 2. The curves from the test of dry material shows that the out of channel sample has a higher maximum shear stress. When water is added to the samples sample 2A exhibit the gratest shear stress. This might imply that the strengthening effect of water increases with increased content of finer grains.

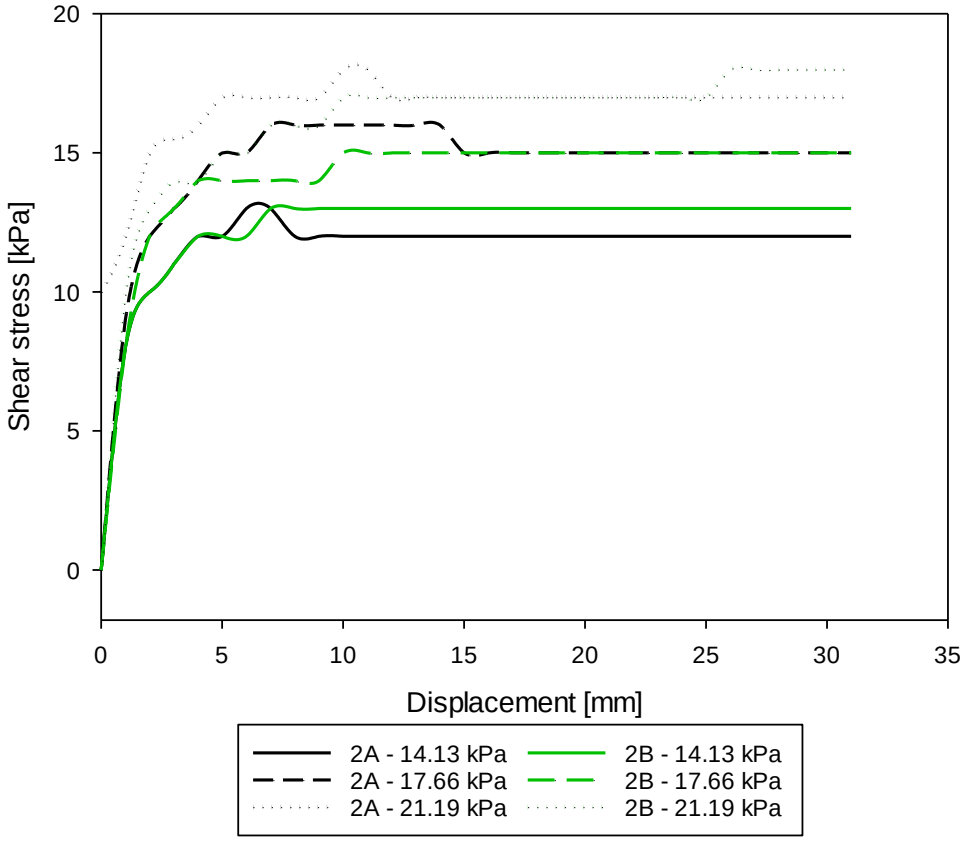

Figure 6.2 Comparison of in and outside of channel – dry samples.

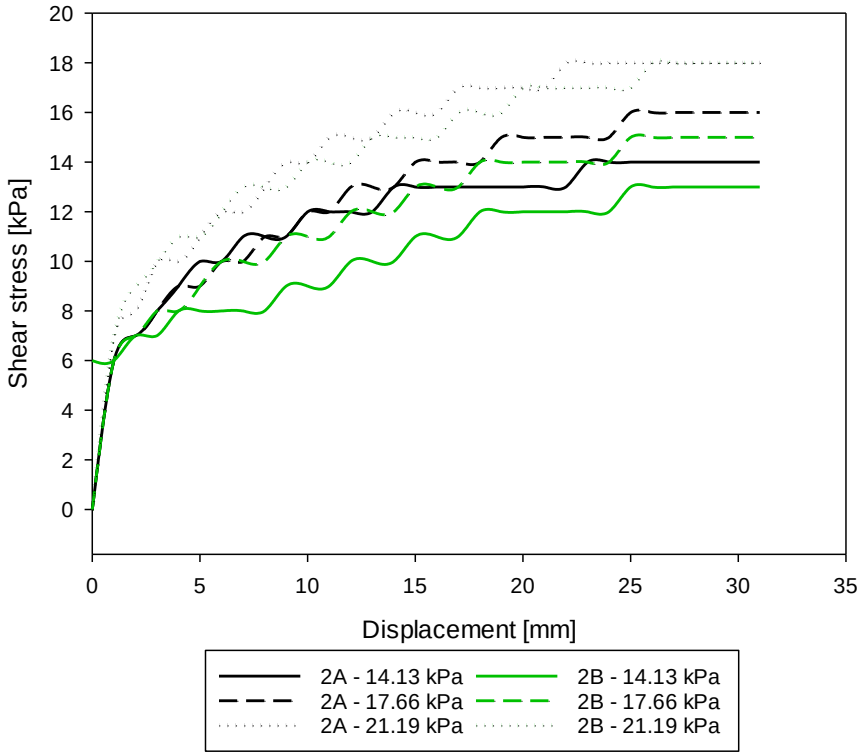

Figure 6.3 Comparison in- and outside of channel -unsaturated samples.

Comparison of results from testing of dry and unsaturated conditions

The frictional angle of sample 4A increases when water is added to the sample. In opposition, sample 2A has a reduction in frictional angle and sample 2B shows the exact same results in dry and unsaturated condition. The testing density of sample 2A and 2B decreases when water is added, while the density of sample 4A increases. Figure 5.7, Figure 5.8 and Figure 5.9 shows that the maximum shear stress of the samples is greater in unsaturated condition for sample 2A and 4A, while sample 2B shows no difference. Hence, there is no mutual tendency in the change of the shear strength parameters when water is added to the samples. The plotted results from tests of unsaturated soil show a more gradual increase in shear stress compared to dry material (Figure 5.7). The difference in shear rate might be a reason for this.

The fact that sample 4A had a higher density in unsaturated condition, indicates an effect of lubrication of particles, resulting in a denser packing (Aysen, 2002). Both the frictional angle and the testing density of sample 2A decreases. This substantiate the fact that, wetting and a higher packing density will increase the angle of friction (Vanapalli et al., 1996b). When water is added the testing density of sample 2B decreases, but the results remain constant. This might indicate a strengthening effect by water.

Comparison of samples from Innfjorden and Gauldalen

Testing of dry material

From testing of dry material, the samples from Innfjorden, 2A and 2B had a higher frictional angle compared to the sample 4A from Gauldalen (Table 5.10). It should be noted that sample 2A and 4A have different shear stress paths. Sample 2A has in general a higher shear strength in relation to displacement, compared to sample 4A (Figure 6.4) This tendency may be due to differences in material properties and was also found by Opsal (2017).

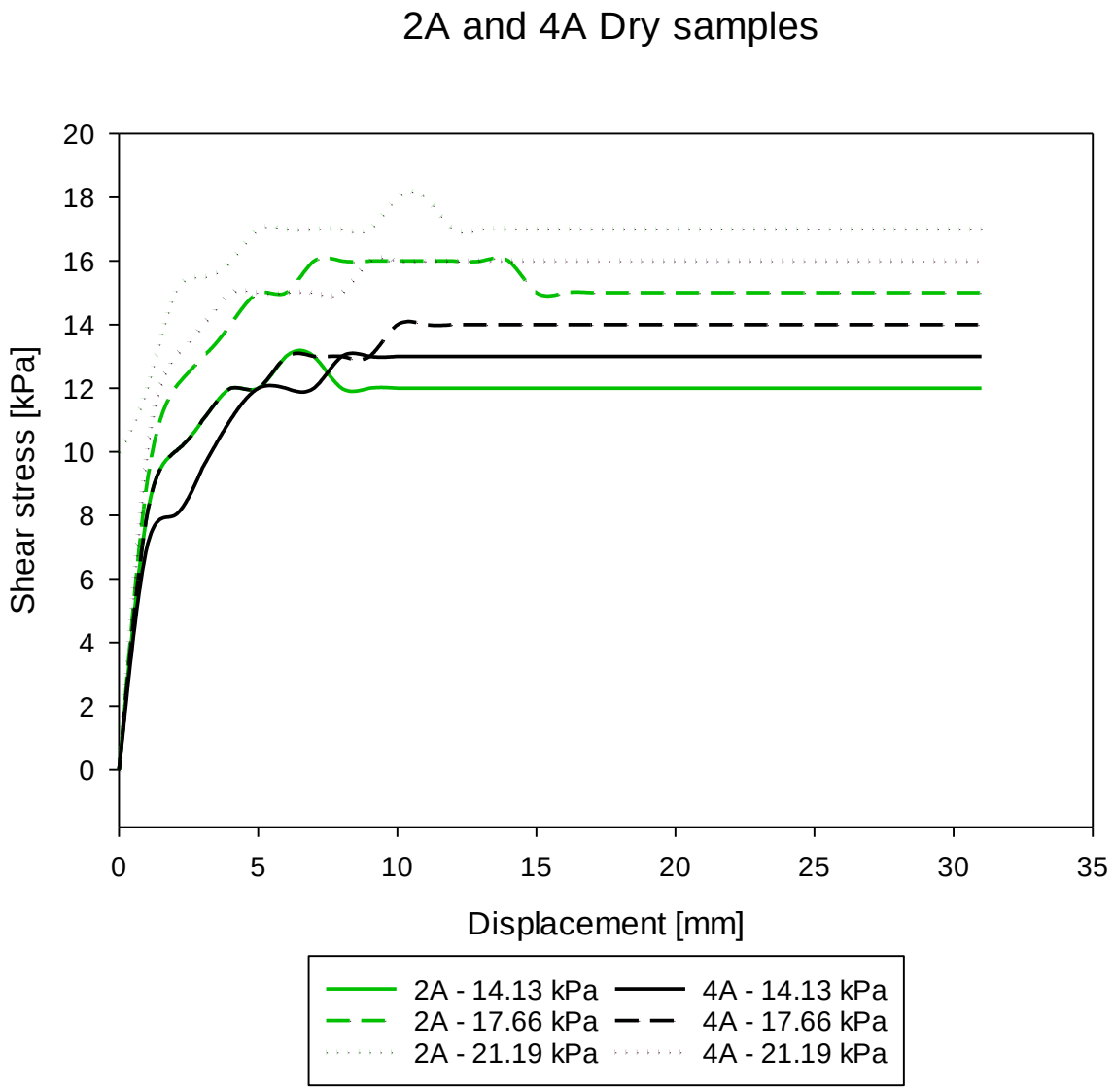

Figure 6.4 Comparison of the dry in-channel samples of location 2A and 4A.

Table 6.1 Comparison of the results of sample 2A and 4A

Parameter	2A	4A
Fines content	23 %	20 %
Grading	Cu=13, graded	Cu=13, graded
FI	6	38
SI	5	39
Angularity	Sub angular	Angular

Table 6.1 shows a comparison of the material parameters of sample 2A and 4A. A comparison of these two samples is conducted as both are collected inside a channel. The main difference is found within the grain shapes of the samples, given by FI, SI and angularity. The large amount of angular grains in sample 4A reduces the degree of compaction of the sample (Mitchell and Soga, 2005). This might be a reason for a lower testing density in 4A compared to 2A, with 1.26 g/cm^3 and 1.94 g/cm^3, respectively. Lower testing density causes reduced interparticle contact area and is thus most likely influencing on the lower frictional angle (Terzaghi et al., 1996). From analyses it is found that the sample from Gauldalen contains a higher content of flaky minerals. These minerals have smooth surfaces and can reduce the shear strength (Mitchell and Soga, 2005). The finest fractions of sample 2A have a high content of feldspar, compared to sample 4A which is dominated by quartz. According to the values listed in Table 2.1, feldspar minerals have a higher frictional angle than quartz. This might also influence on the shear strength differences.

Testing of unsaturated material

Theory presented in section 2.1.3 imply that the water content of the samples has a large influence on the shear strength. Matric suction and reduced friction between grains are the two main differences between dry and unsaturated material. As the contribution from matric suction most likely is minor in this case, the results mainly represent the influence of water on the frictional forces between grains.

The results from the tests of unsaturated soil give the exact same results for sample 2A and 4A. Sample 4A had a significantly higher moisture content of 25.81% compared to 12.28% in sample 2A. The samples have approximately the same amount of fines and the same degree of grading. Sample 4A has a greater content of flaky particles which have the ability to absorb a lot of water on the surface compared to more rounded grains (Adom-Asamoah and Afrifa, 2010). As described in section 2.1.2, the density of a soil is dependent on the water content. This might be a reason for the increase in testing density of sample 4A, and not in sample 2A and 2B. In contrast to testing of dry material, the shear strength of sample 4A is higher than sample 2A in the same displacement interval, even though they reach the same maximum value (Figure 6.5). This shows that the material properties most likely have a larger impact on the shear strength in the beginning of the tests, as implied by (Opsal, 2017).

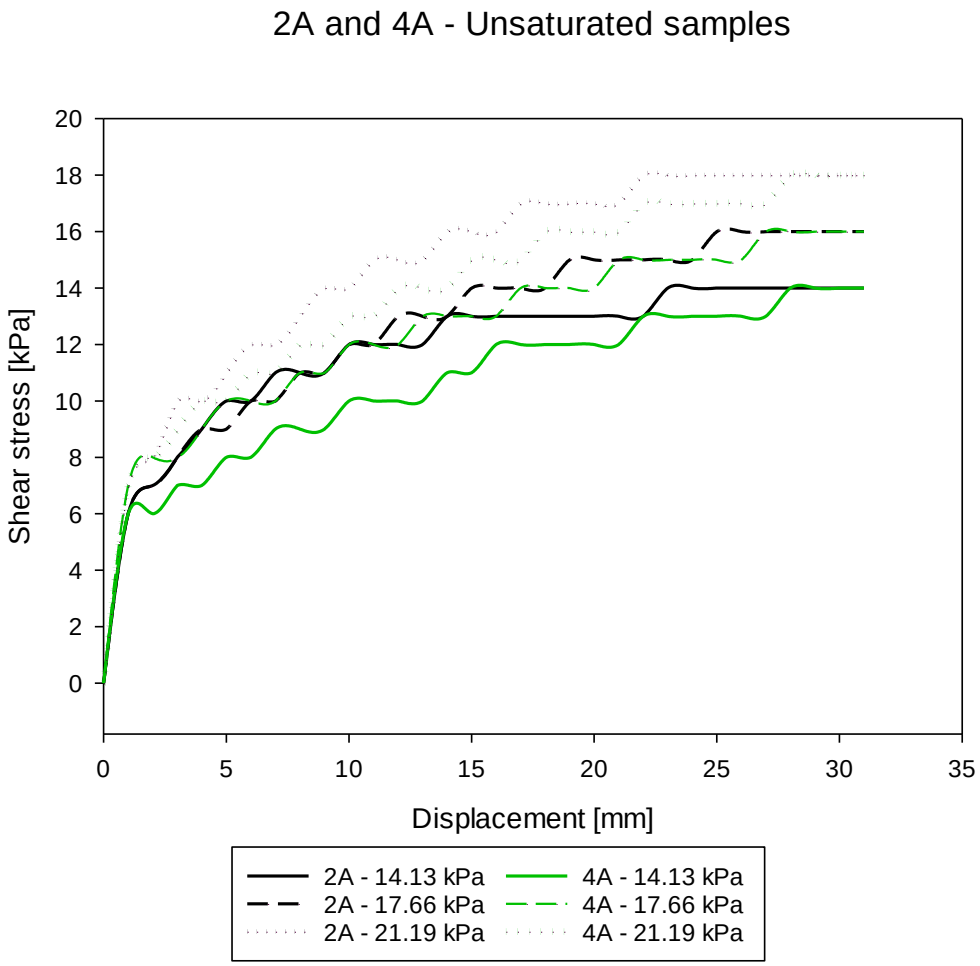

Figure 6.5 Comparison of in channel samples from Innfjorden (2A) and Gauldalen (4A).

Based on the results presented in this thesis it is difficult to say whether the likelihood for debris slides and flows is greater in one of the regions than the other. As previously mentioned, the degree of matric suction is of major importance when considering shear strength of unsaturated soils. The type of depositional process is also found to have an impact on the soil properties (Boulton, 1972). The fact that only a few of the influencing factors on the shear strength has been evaluated in this thesis limits the representativeness of the results. The climatic differences between the locations influence on the degree of weathering and modification of the soil. Variances in amount and type of vegetation will also influence on the shear strength of the soil in-situ. Investigations indicate that the degree of cementation of the soil in Gauldalen might be more extensive compared to the soil in Innfjorden. This might cause an increasing difference in shear strength. In addition to shear strength, the initiation of landslides is influenced by several factors. These include terrain shape, depth of soil and human alterations (Høeg et al., 2014).

7 Conclusion and further work

Shear tests of three samples, two originating from Innfjorden and one from Gauldalen results in frictional angles ranging from 22.8 to 35.4°. Each sample was tested two times, once in dry condition and once as unsaturated. The number of investigated samples is restricted and makes it difficult to draw any conclusions. However, the conducted analysis of the samples indicates that:

- The mineralogy of the finest fractions is presumably of minor importance in relation to shear strength as the content of fines is insignificant compared to the content of coarser grains.
- No obvious distinction was observed between the grain size distributions of samples collected at the various locations. This part from the results and conclusions made by Jørgensen (1977) and Opsal (2018). The representativeness of the samples is thus uncertain and it is difficult to determine the influence of the grain size distribution on the shear strength.
- The rock types in the regions reflect the mineralogy and particle shape found in the samples.
- The samples collected at location 1 differs from the remaining samples. This substantiates the importance of modification by slope processes in relation to material properties.
- The testing density is thought to be of great importance and influencing the frictional angle. This confirms the theory that wetting of the samples and higher packing densities results in increasing angle of friction.
- Comparison of the material properties of the samples collected inside and outside of a landslide channel shows only a small difference. The samples from inside a channel has a lower degree of grading, compared to the samples collected outside. This might be the reason for a higher frictional angle in the “out of channel” sample and thus a reason for the landslide initiation.
- No analogous reaction in the shear strength in relation to wetting of the samples is observed. A reason for this might be the different effect of water on the density of the samples.
- In dry condition the samples from Innfjorden shows a greater frictional angle than the sample from Gauldalen. This is assumed to be due to the difference in grain shape which

influences on the density, water absorption ability and the frictional resistance between grains.

- In unsaturated condition the sample from Gauldalen shows the greatest impact of added water. The samples from Innfjorden experience a reduction in density due to water, while sample 4A receives an increase.
- Unsaturated material reaches maximum shear strength at a later displacement compared to dry material and thus exerts generally a lower shear resistance. This implies that landslide failure occurs more easily in unsaturated material compared to dry.

7.1 Further work

A proposal for further work within this field of research includes;

- Sampling from several locations and include investigation of additional influencing factors, such as differentiation of different depositional types.
- Study of the influence of mica minerals in the fractions above 61µm.
- Investigation of the effect of higher water contents on the frictional angle of till soil.
- Shear box testing with control or measurement of matric suction.

8 Bibliography

Adom-Asamoah, M. & Afrifa, R. O. 2010. A study of concrete properties using phyllite as coarse aggregates. *Materials & Design,* 31**,** 4561-4566.

Amundsen, B. 2009. *Flere skred i fremtidens klima.* Oslo. Norges Forskningsråd. Available from: https://www.forskningsradet.no/servlet/Satellite?blobcol=urldata&blobheader=application%2Fpdf&blobheadername1=Content-Disposition%3A&blobheadervalue1=+attachment%3B+filename%3DNORKLIMAfaktark109web.pdf&blobkey=id&blobtable=MungoBlobs&blobwhere=1274460421951&ssbinary=true.

Andersen, R., Østvold, H. M., Rystad, V. & Hyllestad, E. 2012. *Veileder for fyllingsdammer.* Oslo. Norges Vassdrags- og Energidirektorat. Available from: http://publikasjoner.nve.no/veileder/2012/veileder2012_04.pdf.

Aysen, A. 2002. *Soil mechanics: basic concepts and engineering applications,* Lisse, A.A. Balkema.

Bargel, T. H., Fergus, Å. T., Devoli, G., Orvedal, K., Peereboom, I., Øydvin, E. K., Stalsberg, K., Sletten, K., Fischer, L., Rubensdotter, L. & Eilertsen, R. 2011. *Plan for skredfarekartlegging: Delrapport jordskred og flomskred.* Norges Vassdrags- og Energidirektorat. Available from: http://publikasjoner.nve.no/rapport/2011/rapport2011_16.pdf.

Berry, R. W. & Jørgensen, P. 1971. Grain size, mineralogy and chemistry of a quick-clay sample from the Ullensaker slide, Norway. *Engineering Geology,* 5**,** 73-84.

Boulton, G. S. 1972. Modern Arctic glaciers as depositional models for former ice sheets. *Journal of the Geological Society,* 128**,** 361-393.

Brattli, B. 2009. *Fysisk og kjemisk hydrogeologi,* Trondheim, Norwegian University of Science and Technology.

Brattli, B. 2015. *Ingeniørgeologi løsmasser,* Trondheim, Norwegian University of Science and Technology.

Dahl, R., Berg, K. & Nålsund, R. 1981. *Stabilitetsforholdene i skråninger med morene og lignende jordarter : sluttrapport vedrörende et NTNF-stöttet prosjekt.* Trondheim. Geologisk institutt.

Dannevig, P. & Harstveit, K. E. 2013. *Klima i Norge* [Online]. Store Norske Leksikon. Available: https://snl.no/Klima_i_Norge [Accessed 08.12. 2017].

Das, B. M. & Sawicki, A. 2001. Fundamentals of Geotechnical Engineering. *Applied Mechanics Reviews,* 54**,** B103.

Emdal, A. 2013. *Introduksjon til geoteknikk,* Trondheim, NTNU, Geoteknikk Tapir akademisk forlag, Kompendieforlaget.

Fragaszy, R. J., Su, J., Siddiqi, F. H. & Ho, C. L. 1992. Modeling strength of sandy gravel. *Journal of Geotechnical Engineering,* 118**,** 920-935.

Fredlund, D. G. & Morgenstern, N. R. 1977. Stress state variables for unsaturated soils. *Journal of Geotechnical and Geoenvironmental Engineering,* 103.

Fredlund, D. G., Morgenstern, N. R. & Widger, R. A. 1978. The shear strength of unsaturated soils. *Canadian Geotechnical Journal,* 15**,** 313-321.

Fredlund, D. G., Rahardjo, H. & Fredlund, M. D. 2012. Unsaturated soil mechanics in engineering practice. Wiley.

Furseth, A. 2006. *Skredulykker i Norge,* Oslo, Tun.

Garmo, T. T. 1995. *Norsk steinbok : norske mineral og bergartar,* Oslo, Universitetsforl.

Haldorsen, S. 1983. Mineralogy and geochemistry of basal till and their relationship to till-forming processes *Norsk Geologisk Tidsskrift,* 63**,** 15-25.

Haldorsen, S., Jenssen, P. D., Koler, J. C. & Myhr, E. 1983. Some hydraulic properties of Sandy-silty Norweigan Tills. *Acta geológica hispánica,* 18.

Haldorsen, S. & Kruger, J. 1990. Till genesis and hydrogeological properties. *Nordic Hydrology,* 21**,** 81-94.

Hanssen-Bauer, I. 2015. Klima i Norge 2100 : kunnskapsgrunnlag for klimatilpasning oppdatert 2015. Oslo: Norsk klimaservicesenter.

Hardin, B. O. 1985. Crushing of soil particles. *Journal of geotechnical engineering,* 111**,** 1177-1192.

Hauge, E. O. 2017. Influencing factors on threshold values for rainfall induced landslides in Norwegian tills. *Department of Geoscience and Petroleum.* Trondheim: Norwegian University of Science and Technology, NTNU. (Unpublished).

Holtz, R. D. & Kovacs, W. D. 1981. *An introduction to geotechnical engineering,* Englewood Cliffs, N.J, Prentice-Hall.

Horn, H. & Deere, D. 1962. Frictional characteristics of minerals. *Geotechnique,* 12**,** 319-335.

Høeg, K., Lied, K., Karlsrud, K., Gregory, T. & Norges geotekniske, i. 2014. *Skred : skredfare og sikringstiltak : praktiske erfaringer og teoretiske prinsipper,* Oslo, NGI Universitetsforl.

ISO 17892-10 2004. Geotechnical investigation and testing: Laboratory testing of soil: Part 10: Direct shear tests. Geneva: International Organization for Standardization.

Jørgensen, P. 1977. Some properties of Norwegian tills. *Boreas,* 6**,** 149-157.

Kartverket. 2017. *Norgeskart* [Online]. Available: www.norgeskart.no [Accessed 25.11 2017].

Krinsley, D. H. & Doornkamp, J. C. 2011. *Atlas of quartz sand surface textures,* Cambridge University Press.

Li, Y. 2013. Effects of particle shape and size distribution on the shear strength behavior of composite soils. *Bulletin of Engineering Geology and the Environment,* 72**,** 371-381.

Lu, N. & Godt, J. W. 2013. *Hillslope hydrology and stability,* Cambridge, Cambridge University Press.

Lu, N. & Likos, W. J. 2004. *Unsaturated soil mechanics,* Hoboken, N.J, Wiley.

Lu, N. & Likos, W. J. 2006. Suction stress characteristic curve for unsaturated soil. *Journal of geotechnical and geoenvironmental engineering,* 132**,** 131-142.

MalvernPanalytical. 2018. *Mastersizer 3000* [Online]. Available: https://www.malvernpanalytical.com/en/products/product-range/mastersizer-range/mastersizer-3000/index.html [Accessed 09.04 2018].

Mitchell, J. K. & Soga, K. 2005. Fundamentals of soil behavior. 3rd ed. ed. Hoboken, NJ: John Wiley & Sons.

Neeb, P.-R. 1992. *Byggeråstoffer : kartlegging, undersøkelse og bruk,* Trondheim, Tapir.

NGI. 2017. *Bratte områder Norge* [Online]. The Norwegian Geotechnical Institute. Available: https://geodata.ngi.no/arcgisportal/apps/webappviewer/index.html?id=fd597e0179fe479b9274d95a90b00931 [Accessed 13.11].

NGU. 2017a. *Bedrock geology* [Online]. The Geological Survey of Norway. Available: https://www.ngu.no/en/topic/bedrock-geology-0# [Accessed 09.12 2017].

NGU. 2017b. *Bedrock map* [Online]. Geological Survey of Norway. Available: http://geo.ngu.no/kart/berggrunn/ [Accessed 13.11 2017].

NGU. 2017c. *Marin limit map* [Online]. Geological survey of Norway. Available: http://geo.ngu.no/kart/losmasse/?lang=Norsk&Box=-268657:6427000:1299257:7965000&map=Marin%2Egrense [Accessed 06.12 2017].

NGU. 2017d. *Quarternary map* [Online]. Geological Survey of Norway. [Accessed 13.11 2017].

Novikov, E. & Miskovsky, K. 2009. The Capillarity of Mica-Rich Base-Course Aggregates. *Journal of Materials Engineering and Performance,* 18**,** 420-423.

Novotný, J. & Klimeš, J. 2014. Grain size distribution of soils within the Cordillera Blanca, Peru: an indicator of basic mechanical properties for slope stability evaluation. *Journal of Mountain Science,* 11**,** 563-577.

NRK. 2017. *Yr* [Online]. NRK, Meteorological-institute. Available: www.yr.no [Accessed 03.12 2017].

NS-EN 933-3 2012. Tests for geometrical properties of aggregates - Part 3: Determination of particle shape - Flakiness index Lysaker: Standard Norge.

NS-EN 933-4 2008. Tests for geometrical properties of aggregates - Part 4: Determination of particle shape - Shape index. Lysaker: Standard Norge.

NS-EN 12670 2001. Naturstein - Terminologi. Lysaker: Norsk Standard.

NS-EN ISO 14688-1 2002. Geotechnical investigation and testing - Identification and classification of soil - Part 1: Identification and description (ISO 14688-1:2002). Lysaker: Standard Norge.

NVE. 2014. *Sikkerhet mot skred i bratt terreng.* Oslo. The Norwegian water resources and energy directorate. Available from: http://publikasjoner.nve.no/veileder/2014/veileder2014_08.pdf.

NVE. 2017. *NVE Atlas* [Online]. The Norwegian Water Resources and Energy Directorate. Available: https://atlas.nve.no/Html5Viewer/index.html?viewer=nveatlas# [Accessed 13.11 2017].

Opsal, Ø. 2017. Shear strength of dry tills from the southern half of Norway in relation to bedrock geology. *Norw. J. Geol.,* 97**,** 145-169.

Opsal, Ø. 2018. Geological parameters in relation to bedrock geology and shear strength of dry tills: samples from the southern half of Norway. *Bulletin of Engineering Geology and the Environment***,** 1-12.

Ottesen, D., Dowdeswell, J. A. & Rise, L. 2005. Submarine landforms and the reconstruction of fast-flowing ice streams within a large Quaternary ice sheet: The 2500-km-long Norwegian-Svalbard margin (57°–80°N). Boulder, Colo.

Price, M., Walsh, K., Gabrielsen, S. & Schomacker, E. R. 2012. *Bergarter og mineraler*, Oslo, Cappelen Damm faktum.

Purwana, Y., Jitsangiam, P., Nikraz, H. & Jotisankasa, A. Experimental Studies of Suction-Monitored Direct Shear Apparatus on Perth Poorly Graded Sand. Proceedings of the International Conference on Advances in Geotechnical Engineering, 2011. Australian Geomechanics Society, 273-278.

Raade, G. 2017. *Leirmineraler* [Online]. Store Norske leksikon. Available: https://snl.no/leirmineraler [Accessed 21.04 2018].

Ramberg, I. B., Bryhni, I., Nøttvedt, A. & Norsk geologisk, f. 2007. *Landet blir til : Norges geologi*, Trondheim, Norsk geologisk forening.

Reite, A. J. 1994. *Weichselian and Holocene geology of Sør-Trøndelag and adjacent parts of Nord-Trøndelag county, Central Norway*, Norges geologiske undersøkelse.

Santamarina, J. & Cho, G. Soil behaviour: The role of particle shape. Advances in geotechnical engineering: The skempton conference, 2004. Thomas Telford, London, 604-617.

Santamarina, J. C. 2003. Soil behavior at the microscale: particle forces. *Soil behavior and soft ground construction.*

Schofield, A. N. 2005. *Disturbed soil properties and geotechnical design*, Thomas Telford.

Selmer-Olsen, R. 1977. *Ingeniørgeologi : D. 2 : De løse jordlag*, Trondheim, Tapir.

Selmer-Olsen, R. 1980. *Ingeniørgeologi : 1 : Generell geologi*, Trondheim, Tapir.

SFI. 2017. *About KLIMA 2050* [Online]. Centre for Research-based Innovation. Available: http://www.klima2050.no/what-we-do/ [Accessed 17.10 2017].

Sidle, R. C. & Ochiai, H. 2006. *Landslides : processes, prediction, and land use*, Washington, D.C, American Geophysical Union.

SVV 2016. Laboratorieundersøkelser - Håndbok R210. Statens Vegvesen - Vegdirektoratet.

Terzaghi, K. 1943. Theoretical Soil Mechanics. John Wiley & Sons Incorporated.

Terzaghi, K., Peck, R. B. & Mesri, G. 1996. Soil mechanics in engineering practice. 3rd ed. ed. New York: Wiley.

Testconsult. 2012. *Operation Manual: SB2010.*

Vallejo, L. E. & Mawby, R. 2000. Porosity influence on the shear strength of granular material–clay mixtures. *Engineering Geology*, 58**,** 125-136.

Vanapalli, S., Fredlund, D. & Pufahl, D. 1999. The influence of soil structure and stress history on the soil-water characteristics of a compacted till.

Vanapalli, S., Fredlund, D., Pufahl, D. & Clifton, A. 1996a. Model for the prediction of shear strength with respect to soil suction. *Canadian Geotechnical Journal*, 33**,** 379-392.

Vanapalli, S. K., Fredlund, D. G. & Pufahl, D. E. 1996b. The relationship between the soil-water characteristic curve and the unsaturated shear strength of a compacted glacial till. *Geotechnical Testing Journal*, 19**,** 259-268.

Whitlow, R. 2001. *Basic soil mechanics*, Harlow, Prentice Hall.

Appendices

Appendix A – Coordinates of sampling locations

Appendix B – Results from grain size analysis

Appendix C – Results from investigations of mineralogy and particle shape

Appendix D – Results from analysis of optimum water content

Appendix E – Results from shear box testing

Appendix A - Coordinates of sampling locations

Table A-1 Coordinates of sampling locations (Euref89, UTM33).

Sample	N	E
1A	6945498	111639
1B	6945476	111685
2A	6951704	116135
2B	6951384	115697
3A	6952200	115989
3B	6952216	115980
4A	6993814	269616
4B	6993825	269426
5A	6990343	294083
5B	6990195	294458

Appendix B Results from the grain size analysis

Table B-1 : Data from grain size analysis given as the cumulative sum, in grams.

Fraction (mm)	1A	1B	2A	2B	3A
Total weight (g)	6597	6374	2688.2	3192.3	9935
12.5	6425.9	6234.1	2638.4	3031.9	9665.9
9	4820.9	4660.1	2561.6	2793.9	8619.9
6.68	3873.9	3976.1	2434.6	2511.1	8065.9
4	2929.9	3256.1	2370.6	2396.3	7309.9
2.326	2400.4	2739.1	2200.4	2196.3	6656.5
1.168	1978.8	2293.8	2007.4	2002.1	5951.3
0.589	1579.3	1914.0	1773.3	1783.9	5062.2
0.295	1250.5	1627.1	1444.7	1474.8	4285.5
0.147	929.8	1215.6	1021.7	1074.8	3462.8
0.074	594.9	778.8	698.3	720.6	2527.7
0.038	292.3	449.6	442.5	364.4	1791.8
0.035	102.7	166.9	260.8	206.2	887.4
0.03080544	92.3	152.1	246.1	193.6	834.0
0.02711357	81.6	136.3	229.7	179.3	776.6
0.02386415	71.2	120.2	212.4	164.2	717.6
0.02100416	61.5	104.8	194.9	148.9	658.9
0.01848692	52.7	90.5	177.7	134.0	601.9
0.01627136	45.1	77.9	161.2	120.0	547.4
0.01432133	38.7	67.0	145.7	107.1	495.7
0.01260499	33.3	57.8	131.2	95.3	446.8
0.01109435	28.8	50.1	117.7	84.6	400.5
0.00976475	25.0	43.7	105.1	74.8	356.9
0.0085945	21.7	38.3	93.4	66.0	315.8
0.00756449	18.9	33.7	82.6	57.9	277.4
0.00665793	16.4	29.6	72.6	50.6	241.9
0.00586001	14.3	26.1	63.4	44.0	209.4
0.00515772	12.4	22.9	55.1	38.1	180.3

0.0045396	10.7	20.2	47.7	32.8	154.4
0.00399555	9.3	17.8	41.1	28.2	131.8
0.0035167	8.1	15.7	35.3	24.2	112.3
0.00309525	7.1	14.0	30.3	20.8	95.5
0.0027243	6.2	12.4	25.9	17.8	81.0
0.0023978	5.4	11.0	22.0	15.2	68.7
0.00211044	4.7	9.8	18.7	13.0	58.2
0.00185752	4.1	8.7	15.9	11.1	49.5
0.0016349	3.6	7.6	13.5	9.5	42.2
0.00143897	3.1	6.6	11.3	8.1	35.9
0.00126652	2.5	5.5	9.3	6.7	29.8
0.00111473	2.0	4.3	7.2	5.3	23.3
0.00098114	1.4	3.1	5.1	3.7	16.5
0.00086355	0.8	1.9	3.0	2.2	9.9
0.00076006	0.4	0.9	1.3	1.0	4.5
0.00066897	0.1	0.3	0.4	0.3	1.2
0.0005888	0.0	0.0	0.0	0.0	0.0

Table B-2 : Data from the grain size analysis given as the cumulative sum, in grams.

Fraction (mm)	3B	4A	4B	5A	5B
Total weight (g)	9635	3498.6	9276	6155	9157
12.5	9387.6	3465.0	9063.0	5959.3	8914.1
9	8113.6	3259.4	8157.0	5485.3	7993.1
6.68	7541.6	2908.8	7623.0	5318.3	7517.1
4	6761.6	2750.4	6835.0	5046.3	6914.1
2.326	6114.2	2601.8	6195.5	4781.8	6521.4
1.168	5207.4	2415.0	5471.1	4358.1	6066.4
0.589	4144.0	2216.0	4557.6	3766.5	5344.5
0.295	3251.5	1879.7	3680.9	3145.7	4444.5
0.147	2297.3	1406.1	2730.7	2530.2	3495.0
0.074	1566.2	838.5	1539.0	1730.8	2486.2
0.038	944.3	430.9	814.5	1032.6	1299.4
0.035	517.1	170.1	331.5	363.8	488.4
0.030805	484.4	153.1	301.5	330.1	449.9
0.027114	449.1	135.1	270.2	295.1	409.4
0.023864	412.6	117.2	239.2	260.4	369.0
0.021004	376.1	100.4	209.9	227.7	330.4
0.018487	340.7	85.4	183.3	197.8	294.6
0.016271	307.0	72.6	159.8	171.4	262.1
0.014321	275.1	61.9	139.6	148.4	233.1
0.012605	245.2	53.1	122.2	128.6	207.3
0.011094	217.3	46.0	107.3	111.6	184.1
0.009765	191.3	40.1	94.5	96.9	163.1
0.008594	167.2	35.1	83.1	84.2	144.1
0.007564	145.0	30.7	73.1	73.0	126.8
0.006658	124.9	26.9	64.0	63.1	110.9
0.00586	106.8	23.4	55.9	54.4	96.6
0.005158	90.8	20.4	48.7	46.7	83.8
0.00454	76.9	17.7	42.4	40.1	72.4

0.003996	65.0	15.4	37.0	34.5	62.4
0.003517	55.0	13.5	32.3	29.7	53.8
0.003095	46.5	11.9	28.3	25.6	46.3
0.002724	39.3	10.5	24.9	22.1	39.8
0.002398	33.2	9.4	21.9	19.1	34.1
0.00211	28.0	8.4	19.3	16.5	29.1
0.001858	23.5	7.4	16.9	14.2	24.9
0.001635	19.8	6.6	14.8	12.3	21.3
0.001439	16.4	5.7	12.7	10.5	18.1
0.001267	13.2	4.8	10.6	8.6	14.9
0.001115	9.9	3.7	8.2	6.7	11.7
0.000981	6.5	2.6	5.8	4.7	8.2
0.000864	3.5	1.5	3.5	2.7	4.9
0.00076	1.2	0.7	1.6	1.2	2.2
0.000669	0.0	0.2	0.4	0.3	0.6
0.000589	0.0	0.0	0.0	0.0	0.0

Table B-3 The degree of grading. D60 and d10 is found by use of figure ø.

Sample	d60	d10	Cu	Grading
1A	7	0.09	78	Well graded
1B	6	0.06	100	Well graded
2A	0.4	0.03	13	Graded
2B	0.9	0.035	26	Well graded
3A	1	0.028	36	Well graded
3B	1.3	0.03	43	Well graded
4A	0.45	0.035	13	Graded
4B	1.3	0.04	33	Well graded
5A	0.45	0.03	15	Well graded
5B	0.7	0.03	23	Well graded

Appendix C Results from investigations of mineralogy and particle shape

Table C-1: Results from the flakiness index analysis

	6.68-8mm		8-9.5mm		9.5-12.5mm				
Weight sieved material [g]	Weight total [g]	Weight sieved material [g]	Weight total [g]	Weight sieved material [g]	Weight total [g]	Weight sieved material [g]	SUM weight total [g]	SUM weight sieved material [g]	FI
2.1	141.1	25.6	164.2	43.7	485.4	94.3	812.5	166.9	20.5
1.3	221.8	22.6	317.1	40.4	338.6	52.8	898.6	117.9	13.1
6.2	64	12	70.1	2	127	3.7	431.4	25.7	6.0
3.2	57.5	4.3	74.4	2.7	141.4	15.4	373.3	26.3	7.0
0.6	76	2.3	127.6	5	250.9	1.5	467.1	9.4	2.0
0.2	139.8	1.9	211.3	1.5	454.4	7.4	818.3	11	1.3
16.3	78.9	18.7	106.8	50.7	203.5	83.3	463.5	174.6	37.7
0.9	146.2	9.3	208.4	20.6	532.6	45.1	897.4	76.3	8.5
1.1	115.9	32.8	130.6	48.9	360.7	55.4	615.9	139.2	22.6
1.1	131.6	23.4	139.8	28	118.2	36.7	395.6	89.5	22.6

Table C-2: Results from the shape index analysis

Fraction	4-5mm			5-6.68mm			6.68-8mm			8-9.5mm			9.5-12.5mm					
Sample	Weight total [g]	Weight of non-cubical grains [g]	SI	Weight total [g]	Weight of non-cubical grains [g]	SI	Weight total [g]	Weight of non-cubical grains [g]	SI	Weight total [g]	Weight of non-cubical grains [g]	SI	Weight total [g]	Weight of non-cubical grains [g]	SI	Sum weight	Sum of non cubical grians	SI
1A	10.7	3.8	36	10.9	4.5	41	37.4	16.6	44	56.1	29.4	52	140.6	36	26	255.7	90.3	35
1B	7.6	2.1	28	13.3	3.7	28	71.2	22	31	75.1	22.3	30	142.8	19	13	310	69.1	22
2A	49	0.7	1	121.3	4.6	4	63	3.9	6	70	4	6	122.7	7	6	426	20.2	5
2B	27.2	0.3	1	72.6	1.7	2	56.5	4.9	9	74.3	0.7	1	141.4	16.7	12	372	24.3	7
3A	4.5	0	0	8.2	0.8	10	75	4.5	6	64.3	2.1	3	147.1	2.5	2	299.1	9.9	3
3B	4.6	0	0	8.3	0.7	8	60.7	1.1	2	68.1	0	0	154.5	0	0	296.2	1.8	1
4A	21.6	4.7	22	52.4	14.7	28	73.4	15.3	21	106.7	41.2	39	203.2	101.5	50	457.3	177.4	39
4B	3	0.5	17	7.2	1.5	21	76.3	10.1	13	56.2	7.6	14	152.1	2.7	2	294.8	22.4	8
5A	4.2	1.7	40	4.2	2	48	75.9	30	40	61.6	35.5	58	118.2	51.7	44	264.1	120.9	46
5B	2.3	0.5	22	4	1.5	38	76.6	18.1	24	74.7	18.6	25	158.2	47.8	30	315.8	86.5	27

Appendix D Results from Optimum moisture content

Table D-1 Data from the optimum moisture content analysis

Sample	Wet weight incl. Tara	tara	Wet weight [g]	Dry weight [g]	Moisture [g]	% moisture content of wet weight	% moisture content of dry weight	Packing
1A	299.57	90.00	209.57	180.95	28.62	13.65	15.82	3
1B	281.78	92.85	188.93	153.73	35.20	18.63	22.90	3
2A	215.75	69.41	146.34	130.34	16.00	10.93	12.28	3
2B	220.39	67.51	152.88	136.89	15.99	10.45	11.68	3
3A	316.24	88.06	228.18	204.23	23.95	10.49	11.73	3
3B	328.17	89.05	239.12	216.12	23.00	9.61	10.64	3
4A	203.87	72.78	131.09	104.20	26.89	20.51	25.81	3
4B	303.12	89.33	213.79	190.21	23.58	11.02	12.40	3
5A	283.65	90.66	192.99	162.08	30.91	16.01	19.07	3
5B	292.12	86.36	205.76	174.71	31.05	15.09	17.77	3

Appendix E Results from Shear box testing

Calculation of initial density

$$\rho = \frac{m}{V}$$

ρ = density

m = mass of dry/unsaturated sample

V = volume of sample

Area of shear box

30.50 cm * 30.50 cm = 930.25 cm^2

Calculation of normal load

1 kPa = 102 kg/m^2

Area: 930.25 cm2 = 0.093 m2

$$\frac{134kg}{0.093m2} = \frac{1440.86\frac{kg}{m2}}{102} = \ 14.13kPa$$

$$\frac{167.5kg}{0.093m2} = \frac{1801.08\frac{kg}{m2}}{102} = 17.66kPa$$

$$\frac{201kg}{0.093m2} = \frac{2161.29\frac{kg}{m2}}{102} = \ 21.19kPa$$

Table E-1 Data and calculations in relation to the shear box tests of dry samples

Sample	Mass (g)	Height in box (cm)	Volume (m3)	Initial dry density (g/cm3)
2A	9909.4	5.5	5116.375	1.94
2B	10440	6	5581.5	1.87
4A	6443.91	5.5	5116.375	1.26

	Max shear stress dry (kPa) at normal stress, σ					
Sample	14.13	17.66	21.19	Gradient	Angle of friction (°)	Cohesion,c (kPa)
2A	13.0	16.0	18.0	0.71	35.4	3.2
2B	13.0	15.0	18.0	0.71	35.4	2.8
4A	13.0	14.0	16.0	0.42	22.8	6.8

Table E-2 Data and calculations in relation to the shear box tests of unsaturated material

Sample	Mass (g)	Height in box (cm)	Volume (m3)	Initial testing density (g/cm3)	Moisture (% of dry)
2A	7245.4	5.5	5116.375	1.42	12.28
2B	7634	5.5	5116.375	1.49	11.68
4A	7865.97	5.5	5116.375	1.54	25.81

Sample	Max shear stress wet (kPa) at normal stress, σ 14.13	17.66	21.19	Gradient	Angle of friction (°)	Cohesion, c (kPa)
2A	14.0	16.0	18.0	0.57	29.7	6.0
2B	13.0	15.0	18.0	0.71	35.4	2.8
4A	14.0	16.0	18.0	0.57	29.7	6.0

Results 2A dry

Table E-3 Data from the shear box tests of sample 2A in dry condition

σ_n = 14.3 kPa		σ_n =17.6 kPa		σ_n = 21.19 kPa	
Displacement (mm)	Shear kPa	Displacement mm	Shear kPa	Disp mm	Shear kPa
0,00	0	0,00	0	0,00	0
0,10	5	0,10	5	0,10	5
0,20	6	0,20	6	0,20	6
0,30	6	0,30	6	0,31	7
0,40	7	0,41	7	0,41	7
0,50	7	0,51	7	0,51	8
0,61	7	0,61	8	0,61	8
0,71	8	0,71	8	0,71	9
0,81	8	0,81	9	0,82	9
0,91	8	0,91	9	0,92	10
1,01	8	1,02	9	1,02	10
1,11	9	1,12	10	1,12	10
1,22	9	1,22	10	1,18	11
1,32	9	1,32	10	1,18	11
1,42	9	1,42	10	1,18	11
1,52	9	1,48	10	1,18	11

1,62	9	1,48	11	1,18	11
1,72	9	1,48	11	1,18	11
1,83	10	1,48	11	1,18	11
1,93	10	1,48	11	1,18	11
2,03	10	1,48	11	1,18	11
2,13	10	1,48	11	1,18	11
2,23	10	1,48	11	1,18	11
2,34	10	1,48	11	1,18	11
2,44	10	1,48	11	1,18	11
2,53	10	1,48	11	1,38	12
2,64	10	1,48	11	1,59	12
2,70	10	1,68	12	1,80	13
2,70	10	1,89	12	2,01	13
2,90	11	2,10	12	2,22	13
3,11	11	2,31	12	2,43	14
3,32	11	2,52	13	2,64	14
3,53	11	2,73	13	2,85	14
3,74	12	2,94	13	3,06	15
3,95	12	3,15	14	3,27	15
4,16	12	3,36	14	3,48	15
4,37	12	3,57	14	3,69	15
4,58	12	3,78	14	3,90	15
4,79	12	3,99	14	4,11	16
5,00	12	4,20	14	4,32	16
5,21	12	4,41	15	4,53	16
5,42	12	4,62	15	4,74	16
5,63	13	4,83	15	4,95	16
5,84	13	5,04	15	5,16	16
6,05	13	5,25	15	5,37	16
6,26	13	5,46	15	5,58	17
6,46	13	5,67	15	5,79	17
6,67	12	5,88	15	6,00	17
6,88	13	6,09	15	6,21	17
7,09	13	6,30	15	6,42	17
7,30	13	6,51	16	6,63	17
7,51	13	6,72	16	6,84	17
7,72	13	6,93	16	7,05	17
7,93	13	7,14	15	7,26	17
8,14	13	7,35	16	7,47	17
8,35	13	7,56	16	7,68	17
8,56	13	7,77	16	7,89	17
8,77	12	7,98	16	8,10	17
8,98	13	8,19	16	8,31	17
9,19	13	8,40	16	8,52	17
9,40	12	8,61	16	8,73	17
9,61	12	8,82	16	8,94	17
9,82	13	9,03	16	9,15	17
10,03	12	9,24	16	9,36	17

10,24	12	9,45	16	9,56	18
10,45	12	9,66	16	9,77	17
10,66	12	9,87	16	9,98	17
10,87	12	10,08	16	10,19	18
11,08	12	10,29	16	10,40	18
11,29	12	10,50	16	10,61	18
11,50	12	10,71	16	10,82	18
11,71	12	10,92	16	11,03	18
11,92	12	11,13	16	11,24	18
12,13	12	11,34	16	11,45	17
12,34	12	11,55	16	11,66	17
12,55	12	11,76	16	11,87	18
12,76	12	11,97	16	12,08	17
12,97	12	12,18	16	12,29	17
13,18	12	12,39	16	12,50	17
13,39	12	12,60	16	12,71	18
13,60	12	12,81	16	12,92	18
13,81	12	13,02	16	13,13	18
14,02	12	13,23	16	13,34	17
14,23	12	13,44	16	13,55	17
14,44	12	13,65	15	13,76	17
14,65	12	13,86	16	13,97	17
14,86	12	14,07	16	14,18	17
15,07	12	14,28	15	14,39	17
15,28	12	14,49	15	14,60	17
15,49	12	14,70	16	14,81	17
15,70	12	14,91	16	15,02	17
15,91	12	15,12	16	15,23	17
16,12	12	15,33	16	15,44	17
16,33	12	15,54	16	15,65	17
16,54	12	15,75	16	15,86	17
16,75	12	15,96	15	16,07	17
16,96	12	16,17	15	16,28	17
17,17	12	16,38	15	16,49	17
17,38	12	16,59	15	16,70	17
17,59	12	16,80	15	16,91	17
17,80	12	17,01	15	17,12	17
18,01	12	17,22	15	17,33	17
18,22	12	17,43	15	17,54	17
18,43	12	17,64	15	17,75	17
18,64	12	17,85	15	17,96	17
18,85	12	18,06	15	18,17	17
19,06	12	18,27	15	18,38	17
19,27	12	18,48	15	18,59	17
19,48	12	18,69	15	18,80	17
19,69	12	18,90	15	19,01	17
19,90	12	19,11	15	19,22	17
20,11	12	19,32	15	19,43	17

20,32	12	19,53	15	19,64	17
20,53	12	19,74	15	19,85	17
20,74	12	19,95	15	20,06	17
20,95	12	20,16	15	20,27	17
21,16	12	20,37	15	20,48	17
21,37	12	20,58	15	20,69	17
21,58	12	20,79	15	20,90	17
21,79	12	21,00	15	21,11	17
22,00	12	21,21	15	21,32	17
22,21	12	21,42	15	21,53	17
22,42	12	21,63	15	21,74	17
22,63	12	21,84	15	21,95	17
22,84	12	22,05	15	22,16	17
23,05	12	22,26	15	22,37	17
23,26	12	22,47	15	22,58	17
23,47	12	22,68	15	22,79	17
23,68	13	22,89	15	23,00	17
23,89	12	23,10	15	23,21	17
24,10	12	23,31	15	23,42	17
24,31	12	23,52	15	23,63	17
24,52	12	23,73	15	23,84	17
24,73	12	23,94	15	24,05	17
24,94	12	24,15	15	24,26	17
25,15	12	24,36	15	24,47	17
25,36	12	24,57	15	24,68	17
25,57	12	24,78	15	24,89	17
25,78	12	24,99	15	25,10	17
25,99	12	25,20	15	25,31	17
26,20	12	25,41	15	25,52	17
26,41	12	25,62	15	25,73	17
26,62	12	25,83	15	25,94	17
26,83	12	26,04	15	26,15	17
27,04	12	26,25	15	26,36	17
27,25	12	26,46	15	26,57	17
27,46	12	26,67	15	26,78	17
27,67	13	26,88	15	26,99	17
27,88	12	27,09	15	27,20	17
28,09	12	27,30	15	27,41	17
28,30	12	27,51	15	27,62	17
28,51	12	27,72	15	27,83	17
28,71	13	27,93	15	28,04	17
28,92	13	28,14	15	28,25	17
29,14	12	28,35	16	28,46	17
29,34	13	28,56	15	28,67	17
29,72	13	28,77	15	28,88	17
29,93	13	28,98	15	29,09	17
30,14	13	29,19	15	29,30	17
30,35	13	29,72	15	29,51	17

30,56	13	29,93	15	29,72	17
30,77	13	30,14	15	29,93	17
30,98	13	30,35	15	30,14	17
31,19	13	30,56	15	30,35	17
31,40	13	30,77	15	30,56	17
		30,98	15	30,77	17
		31,19	15	30,98	18
		31,40	15	31,19	18
				31,40	17

Results 2A – Moist

Table E-4 Data from the shear box tests of sample 2A with dry of optimum water content

σ_n = 14.3 kPa		σ_n =17.6 kPa		σ_n = 21.19 kPa	
Disp (mm)	Shear kPa	Disp (mm)	Shear kPa	Disp (mm)	Shear kPa
0,00	0	0,00	0	0,00	0
0,10	5	0,09	5	0,10	5
0,20	5	0,20	5	0,20	5
0,30	5	0,30	5	0,31	6
0,40	5	0,40	6	0,41	6
0,50	5	0,51	6	0,51	6
0,61	6	0,61	6	0,61	6
0,71	6	0,70	6	0,71	6
0,81	6	0,81	6	0,81	7
0,91	6	0,91	6	0,92	7
1,01	6	1,01	6	1,02	7
1,11	6	1,11	6	1,12	7
1,21	6	1,21	6	1,22	7
1,32	6	1,31	6	1,32	7
1,42	6	1,42	7	1,42	8
1,52	6	1,52	7	1,53	8
1,62	7	1,62	7	1,63	8
1,72	7	1,72	7	1,73	8
1,82	7	1,82	7	1,83	8
1,93	7	1,92	7	1,93	8
2,03	7	2,02	7	2,03	8
2,13	7	2,13	7	2,14	9
2,23	7	2,23	7	2,24	9
2,33	7	2,33	7	2,34	9
2,43	7	2,43	7	2,44	9
2,53	7	2,53	8	2,54	9
2,64	7	2,63	8	2,64	9
2,74	8	2,74	8	2,75	9
2,84	8	2,84	8	2,85	9
2,94	8	2,94	8	2,95	9

3,04	8	3,04	8	3,05	10
3,15	8	3,14	8	3,15	10
3,25	8	3,24	8	3,25	10
3,35	8	3,34	8	3,36	10
3,45	8	3,45	8	3,46	10
3,55	8	3,55	8	3,56	10
3,65	8	3,65	8	3,62	10
3,76	8	3,75	8	3,62	10
3,86	9	3,85	9	3,62	10
3,96	9	3,95	9	3,62	10
4,06	9	4,06	9	3,62	10
4,16	9	4,16	9	3,62	10
4,26	9	4,26	9	3,62	10
4,37	9	4,36	9	3,62	10
4,47	9	4,46	9	3,62	10
4,57	9	4,57	9	3,62	10
4,67	9	4,67	9	3,62	10
4,77	10	4,77	9	3,82	10
4,87	10	4,87	9	4,03	10
4,98	10	4,97	9	4,23	10
5,07	10	5,07	9	4,44	11
5,18	10	5,18	9	4,64	11
5,28	10	5,28	9	4,85	11
5,38	10	5,38	10	5,05	11
5,44	10	5,48	10	5,26	11
5,44	10	5,58	10	5,46	11
5,44	10	5,68	10	5,67	11
5,44	10	5,79	10	5,87	12
5,44	10	5,89	10	6,08	12
5,44	10	5,99	10	6,28	12
5,44	10	6,09	10	6,49	12
5,44	10	6,19	10	6,69	12
5,44	10	6,29	10	6,90	12
5,44	10	6,40	10	7,10	12
5,65	10	6,49	10	7,31	13
5,86	10	6,60	10	7,51	13
6,07	10	6,66	10	7,72	13
6,28	11	6,66	10	7,92	13
6,49	11	6,66	10	8,13	13
6,70	11	6,66	10	8,33	13
6,91	11	6,66	10	8,53	13
7,12	11	6,66	10	8,74	13
7,33	11	6,66	10	8,94	13
7,54	11	6,66	10	9,15	14
7,75	11	6,66	9	9,35	14
7,96	11	6,66	9	9,56	14
8,17	11	6,66	9	9,76	14
8,38	11	6,66	9	9,97	14

8,59	11	6,86	10	10,17	14
8,80	11	7,07	10	10,38	14
9,01	11	7,27	10	10,58	14
9,22	12	7,48	10	10,79	14
9,43	12	7,68	11	10,99	15
9,64	12	7,89	11	11,20	15
9,85	12	8,09	11	11,40	15
10,06	12	8,30	11	11,61	15
10,27	12	8,50	11	11,81	15
10,48	12	8,71	11	12,02	15
10,69	12	8,91	11	12,22	15
10,90	12	9,12	11	12,43	15
11,11	12	9,32	11	12,63	15
11,31	12	9,53	11	12,84	15
11,53	12	9,73	12	13,04	15
11,73	12	9,94	12	13,25	15
11,94	12	10,14	12	13,45	15
12,15	12	10,35	12	13,66	15
12,36	12	10,55	12	13,86	16
12,57	12	10,75	12	14,07	16
12,78	12	10,96	12	14,27	16
12,99	12	11,16	12	14,47	16
13,20	12	11,37	12	14,68	16
13,41	12	11,57	12	14,89	16
13,62	13	11,78	12	15,09	16
13,83	13	11,98	12	15,30	16
14,04	13	12,19	13	15,50	16
14,25	13	12,39	13	15,71	16
14,46	13	12,60	13	15,91	16
14,67	13	12,80	13	16,12	16
14,88	13	13,01	13	16,32	16
15,09	13	13,21	13	16,52	16
15,30	13	13,42	13	16,73	16
15,51	13	13,62	13	16,93	16
15,72	13	13,83	13	17,14	17
15,93	13	14,03	13	17,34	17
16,14	13	14,24	13	17,55	17
16,35	13	14,44	13	17,75	17
16,56	13	14,65	14	17,96	17
16,77	13	14,85	14	18,16	17
16,98	13	15,06	14	18,37	17
17,19	13	15,26	14	18,57	17
17,40	13	15,47	14	18,78	17
17,61	13	15,67	14	18,98	17
17,82	13	15,88	14	19,19	17
18,03	13	16,08	14	19,39	17
18,24	13	16,29	14	19,60	17
18,45	13	16,49	14	19,80	17

18,66	13	16,69	14	20,01	17
18,87	13	16,90	14	20,21	17
19,08	13	17,10	14	20,42	17
19,29	13	17,31	14	20,62	17
19,50	13	17,51	14	20,83	17
19,71	13	17,72	14	21,03	17
19,92	13	17,92	14	21,24	17
20,13	13	18,13	14	21,44	17
20,34	13	18,33	14	21,65	17
20,55	13	18,54	15	21,85	17
20,76	13	18,74	15	22,06	17
20,97	13	18,95	15	22,26	18
21,18	13	19,15	15	22,46	18
21,39	13	19,36	15	22,67	18
21,60	13	19,56	14	22,87	18
21,81	13	19,77	15	23,08	18
22,02	13	19,97	15	23,28	18
22,23	13	20,18	15	23,49	18
22,44	14	20,38	15	23,69	18
22,65	14	20,59	15	23,90	18
22,86	13	20,79	15	24,10	18
23,07	14	21,00	15	24,31	18
23,28	14	21,20	15	24,51	18
23,49	13	21,41	15	24,72	18
23,70	13	21,61	15	24,92	18
23,91	13	21,82	15	25,13	18
24,12	14	22,02	15	25,33	18
24,33	14	22,23	15	25,54	18
24,54	14	22,43	15	25,74	18
24,75	14	22,63	15	25,95	18
24,96	14	22,84	15	26,15	18
25,17	14	23,04	15	26,36	18
25,38	14	23,25	15	26,56	18
25,59	14	23,45	15	26,77	18
25,80	14	23,66	15	26,97	18
26,01	14	23,86	15	27,18	18
26,22	14	24,07	15	27,38	18
26,43	14	24,27	16	27,59	18
26,64	14	24,48	16	27,79	18
26,85	14	24,68	16	28,00	18
27,06	14	24,89	15	28,20	18
27,27	14	25,09	16	28,40	18
27,48	14	25,30	16	28,61	18
27,69	14	25,50	16	28,81	18
27,90	14	25,71	16	29,02	18
28,11	14	25,91	16	29,22	18
28,32	14	26,12	16	29,43	18
28,53	14	26,32	16	29,63	18

28,74	14	26,53	16	29,84	18
28,95	14	26,73	16	30,04	18
29,16	14	26,94	16	30,25	18
29,37	14	27,14	16	30,45	18
29,58	14	27,35	16	30,66	18
29,79	14	27,55	16		
30,00	14	27,76	16		
30,21	14	27,96	16		
30,42	14	28,17	16		
30,63	14	28,37	16		
30,84	14	28,57	16		
31,05	14	28,78	16		
31,27	14	28,98	16		
31,48	14	29,19	16		
31,69	14	29,39	16		
31,90	14	29,60	16		
32,11	14	29,80	16		
32,32	14	30,01	16		
32,53	14	30,21	16		
32,74	14				

Results 2B - Dry

Table E-5 Data from the shear box tests of sample 2B in dry condition

σ_n = 14.3 kPa		σ_n =17.6 kPa		σ_n = 21.19 kPa	
Disp (mm)	Shear kPa	Disp (mm)	Shear kPa	Disp (mm)	Shear kPa
0,00	0	0,00	0	0,00	0
0,10	5	0,10	5	0,09	5
0,20	6	0,20	6	0,20	6
0,30	6	0,31	6	0,30	7
0,40	6	0,41	7	0,40	7
0,51	7	0,51	7	0,51	8
0,61	7	0,61	8	0,60	8
0,71	7	0,71	8	0,70	9
0,81	8	0,81	8	0,81	9
0,91	8	0,92	8	0,91	10
1,01	8	1,02	8	1,01	10
1,12	8	1,12	9	1,08	11
1,22	8	1,22	9	1,08	11
1,32	9	1,32	10	1,08	11
1,42	9	1,42	10	1,08	11
1,52	9	1,53	10	1,08	11
1,62	9	1,63	11	1,08	11
1,73	9	1,73	11	1,08	11
1,83	9	1,83	11	1,08	11

1,93	9	1,93	12	1,08	11
2,03	10	2,03	12	1,08	11
2,13	10	2,14	12	1,28	12
2,23	10	2,24	12	1,49	12
2,33	10	2,34	12	1,70	12
2,40	10	2,44	13	1,91	13
2,39	10	2,54	13	2,12	13
2,39	10	2,64	13	2,33	13
2,39	10	2,75	13	2,54	13
2,39	10	2,85	13	2,75	14
2,39	10	2,95	13	2,96	14
2,39	10	3,05	13	3,18	14
2,39	10	3,15	13	3,39	14
2,39	10	3,25	13	3,60	14
2,39	10	3,36	13	3,81	14
2,39	10	3,46	13	4,02	14
2,39	10	3,56	13	4,23	15
2,39	10	3,62	14	4,44	15
2,39	10	3,62	14	4,65	15
2,59	11	3,82	14	4,86	15
2,80	11	4,03	14	5,07	15
3,01	11	4,23	14	5,28	15
3,22	11	4,44	14	5,49	15
3,43	12	4,64	14	5,70	15
3,64	12	4,85	14	5,91	15
3,86	12	5,05	14	6,12	15
4,07	12	5,26	14	6,32	16
4,28	12	5,46	14	6,53	16
4,49	12	5,67	14	6,74	16
4,70	12	5,87	14	6,95	16
4,91	12	6,08	14	7,16	16
5,12	12	6,28	14	7,37	16
5,33	12	6,49	14	7,58	16
5,54	12	6,69	14	7,79	16
5,75	12	6,90	14	8,00	16
5,96	12	7,10	14	8,21	16
6,17	12	7,31	14	8,42	16
6,38	12	7,51	14	8,63	16
6,59	12	7,72	14	8,84	16
6,80	13	7,92	14	9,05	16
7,01	13	8,13	14	9,26	16
7,22	12	8,33	14	9,47	16
7,43	12	8,53	14	9,68	16
7,64	12	8,74	14	9,89	17
7,85	13	8,94	14	10,10	17
8,06	13	9,15	14	10,31	17
8,27	13	9,35	14	10,52	17
8,48	13	9,56	14	10,73	17

8,69	13	9,76	14	10,94	17
8,90	13	9,97	15	11,15	17
9,11	13	10,17	15	11,36	17
9,32	13	10,38	15	11,57	17
9,53	13	10,58	15	11,78	17
9,74	13	10,79	15	11,99	16
9,95	13	10,99	15	12,20	16
10,16	13	11,20	15	12,41	16
10,37	13	11,40	15	12,62	16
10,58	13	11,61	15	12,83	17
10,79	13	11,81	15	13,04	17
11,00	13	12,02	15	13,25	16
11,21	12	12,22	15	13,46	17
11,42	13	12,43	15	13,67	16
11,63	13	12,63	15	13,88	16
11,84	13	12,84	15	14,09	16
12,05	13	13,04	15	14,30	16
12,26	13	13,25	15	14,51	16
12,47	13	13,45	15	14,72	17
12,68	13	13,66	15	14,93	17
12,89	13	13,86	15	15,14	16
13,10	13	14,07	15	15,35	17
13,31	13	14,27	15	15,56	17
13,52	13	14,47	15	15,77	16
13,73	13	14,68	15	15,98	17
13,94	13	14,89	15	16,19	17
14,15	13	15,09	15	16,40	17
14,36	13	15,30	15	16,61	16
14,57	13	15,50	15	16,82	16
14,78	13	15,71	15	17,03	16
14,99	12	15,91	15	17,24	16
15,20	13	16,12	15	17,45	17
15,41	12	16,32	15	17,66	17
15,62	12	16,52	15	17,87	17
15,83	13	16,73	15	18,08	16
16,04	13	16,93	15	18,29	17
16,25	13	17,14	15	18,50	17
16,46	13	17,34	15	18,71	17
16,67	13	17,55	15	18,92	17
16,88	13	17,75	15	19,13	17
17,09	13	17,96	15	19,34	17
17,30	13	18,16	15	19,55	17
17,51	13	18,37	15	19,76	17
17,71	13	18,57	15	19,97	17
17,92	13	18,78	15	20,18	17
18,13	13	18,98	15	20,39	17
18,34	13	19,19	15	20,60	17
18,55	13	19,39	15	20,81	17

18,76	13	19,60	15	21,02	17
18,97	13	19,80	15	21,23	17
19,18	13	20,01	15	21,44	17
19,39	13	20,21	15	21,65	17
19,60	13	20,42	15	21,86	17
19,81	13	20,62	15	22,07	17
20,02	13	20,83	15	22,28	17
20,23	13	21,03	15	22,49	17
20,44	13	21,24	15	22,70	17
20,65	13	21,44	15	22,91	17
20,86	13	21,65	15	23,12	17
21,07	13	21,85	15	23,33	17
21,28	13	22,06	15	23,54	18
21,49	13	22,26	15	23,75	18
21,70	13	22,46	15	23,96	18
21,91	13	22,67	15	24,17	18
22,12	13	22,87	15	24,38	18
22,33	13	23,08	15	24,59	18
22,54	13	23,28	15	24,80	17
22,75	13	23,49	15	25,01	17
22,96	13	23,69	15	25,22	17
23,17	13	23,90	15	25,43	17
23,38	12	24,10	15	25,64	17
23,59	13	24,31	15	25,85	17
23,80	13	24,51	15	26,06	18
24,01	13	24,72	15	26,27	18
24,22	13	24,92	15	26,48	18
24,43	13	25,13	15	26,69	18
24,64	13	25,33	15	26,90	18
24,85	13	25,54	15	27,11	18
25,06	13	25,74	15	27,32	18
25,27	13	25,95	15	27,53	18
25,48	13	26,15	15	27,74	18
25,69	13	26,36	15	27,95	18
25,90	13	26,56	15	28,16	18
26,11	13	26,77	15	28,37	18
26,32	13	26,97	15	28,57	18
26,53	13	27,18	15	28,78	18
26,74	13	27,38	15	28,99	18
26,95	13	27,59	15	29,20	18
27,16	13	27,79	15	29,41	18
27,37	13	28,00	15	29,62	18
27,58	13	28,20	15	29,83	18
27,79	13	28,40	15	30,04	18
28,00	13	28,61	15	30,25	18
28,21	13	28,81	15	30,46	18
28,42	13	29,02	15	30,67	18
28,63	13	29,22	15	30,88	18

28,84	13	29,43	15	31,09	18
29,05	13	29,63	15	31,30	18
29,26	13	29,84	15	31,51	18
		30,04	15		
		30,25	15		
		30,45	15		
		30,66	15		

Results 2B – Moist

Table E-6: Data from the shear box tests of sample 2B in unsaturated condition

σ_n = 14.3 kPa		σ_n =17.6 kPa		σ_n = 21.19 kPa	
Disp (mm)	Shear kPa	Disp (mm)	Shear kPa	Disp (mm)	Shear kPa
0,00	0	0,00	0	0,00	0
0,10	5	0,11	5	0,11	5
0,21	5	0,21	5	0,21	6
0,31	5	0,31	5	0,31	6
0,41	5	0,41	6	0,41	6
0,51	5	0,51	6	0,51	6
0,61	5	0,61	6	0,61	7
0,71	5	0,72	6	0,72	7
0,82	5	0,82	6	0,82	7
0,92	5	0,92	6	0,92	7
1,02	6	1,02	6	1,02	8
1,12	6	1,12	6	1,12	8
1,22	6	1,22	6	1,22	8
1,32	6	1,34	6	1,33	8
1,43	6	1,43	7	1,42	8
1,53	6	1,53	7	1,53	8
1,63	6	1,63	7	1,63	8
1,73	6	1,73	7	1,73	9
1,83	6	1,83	7	1,83	9
1,93	6	1,95	7	1,93	9
2,03	6	2,04	7	2,03	9
2,14	6	2,14	7	2,13	9
2,24	6	2,24	7	2,24	9
2,34	6	2,34	7	2,34	9
2,44	6	2,44	7	2,44	9
2,54	6	2,55	7	2,54	9
2,64	6	2,65	7	2,64	10
2,75	6	2,75	7	2,74	10
2,85	7	2,85	8	2,85	10
2,95	7	2,95	8	2,95	10
3,05	7	3,05	8	3,05	10
3,15	7	3,16	8	3,15	10

3,26	7	3,26	8	3,21	10
3,36	7	3,36	8	3,21	10
3,46	7	3,46	8	3,21	10
3,56	7	3,56	8	3,21	10
3,66	7	3,66	8	3,21	10
3,76	7	3,77	8	3,21	10
3,87	7	3,87	8	3,21	10
3,97	7	3,97	8	3,21	10
4,07	7	4,07	8	3,21	10
4,17	7	4,17	9	3,21	10
4,27	7	4,27	9	3,21	10
4,37	7	4,37	9	3,41	10
4,48	7	4,47	9	3,62	10
4,57	7	4,57	9	3,82	10
4,68	7	4,68	9	4,03	11
4,78	7	4,78	9	4,23	11
4,88	7	4,88	9	4,44	11
4,98	7	4,98	9	4,64	11
5,08	8	5,08	9	4,85	11
5,18	8	5,18	9	5,05	11
5,29	8	5,29	9	5,26	12
5,39	8	5,39	9	5,46	11
5,49	8	5,49	9	5,67	12
5,59	8	5,59	9	5,87	12
5,69	8	5,69	9	6,08	12
5,79	8	5,79	9	6,28	12
5,89	8	5,90	9	6,49	12
6,00	8	6,00	10	6,69	12
6,10	8	6,10	10	6,90	13
6,20	8	6,20	10	7,10	13
6,30	8	6,30	10	7,30	13
6,40	8	6,40	10	7,51	13
6,50	8	6,50	10	7,71	13
6,61	8	6,61	10	7,92	13
6,71	8	6,71	10	8,12	13
6,81	8	6,81	10	8,33	13
6,91	8	6,91	10	8,53	13
7,01	8	7,01	10	8,74	13
7,11	8	7,08	10	8,94	13
7,21	8	7,08	10	9,15	13
7,32	8	7,08	10	9,35	13
7,42	8	7,08	10	9,56	13
7,52	8	7,08	10	9,76	14
7,62	8	7,08	10	9,97	14
7,72	8	7,08	10	10,17	14
7,82	8	7,08	10	10,38	14
7,93	8	7,08	10	10,58	14
8,03	8	7,08	9	10,79	14

8,13	8	7,08	9	10,99	14
8,23	8	7,08	9	11,20	14
8,33	8	7,28	10	11,40	14
8,43	8	7,49	10	11,61	14
8,54	9	7,69	10	11,81	14
8,64	9	7,90	10	12,02	14
8,74	9	8,10	10	12,22	14
8,84	9	8,31	11	12,43	15
8,94	9	8,51	11	12,63	14
9,04	9	8,71	11	12,84	15
9,15	9	8,92	11	13,04	15
9,25	9	9,12	11	13,24	15
9,35	9	9,33	11	13,45	15
9,45	9	9,53	11	13,65	15
9,55	9	9,74	11	13,86	15
9,66	9	9,94	11	14,06	15
9,76	9	10,15	11	14,27	15
9,86	9	10,35	11	14,47	15
9,96	9	10,56	11	14,68	15
10,06	9	10,76	11	14,88	15
10,16	9	10,97	11	15,09	15
10,26	9	11,17	11	15,29	15
10,37	9	11,38	12	15,50	15
10,46	9	11,58	12	15,70	15
10,57	9	11,79	12	15,91	15
10,67	9	11,99	12	16,11	15
10,77	9	12,20	12	16,32	16
10,87	9	12,40	12	16,52	15
10,97	9	12,61	12	16,73	16
11,07	9	12,81	12	16,93	16
11,18	9	13,02	12	17,14	16
11,28	9	13,22	12	17,34	16
11,38	9	13,43	12	17,55	16
11,48	10	13,63	12	17,75	16
11,58	10	13,84	12	17,96	16
11,68	10	14,04	12	18,16	16
11,79	10	14,24	12	18,37	16
11,89	10	14,45	13	18,57	16
11,99	10	14,65	13	18,78	16
12,09	10	14,86	13	18,98	16
12,19	10	15,06	13	19,18	16
12,29	10	15,27	13	19,39	16
12,39	10	15,47	13	19,59	17
12,50	10	15,68	13	19,80	17
12,60	10	15,88	13	20,00	17
12,70	10	16,09	13	20,21	17
12,80	10	16,29	13	20,41	17
12,90	10	16,50	13	20,62	17

13,00	10	16,70	13	20,82	17
13,11	10	16,91	13	21,03	17
13,21	10	17,11	13	21,23	17
13,27	10	17,32	13	21,44	17
13,27	10	17,52	13	21,64	17
13,27	10	17,73	14	21,85	17
13,27	10	17,93	13	22,05	17
13,27	10	18,14	14	22,26	17
13,27	10	18,34	13	22,46	17
13,27	10	18,55	14	22,67	17
13,27	10	18,75	14	22,87	17
13,27	10	18,96	14	23,08	17
13,27	10	19,16	14	23,28	17
13,27	10	19,37	14	23,49	17
13,47	10	19,57	14	23,69	17
13,68	10	19,78	14	23,90	17
13,88	10	19,98	14	24,10	17
14,09	10	20,19	14	24,31	17
14,29	10	20,39	14	24,51	17
14,50	11	20,59	14	24,72	17
14,70	10	20,80	14	24,92	17
14,91	11	21,00	14	25,13	17
15,11	11	21,21	14	25,33	17
15,32	11	21,41	14	25,53	17
15,52	11	21,62	14	25,74	17
15,72	11	21,82	14	25,94	18
15,93	11	22,03	14	26,15	18
16,13	11	22,23	14	26,35	18
16,34	11	22,44	14	26,56	18
16,54	11	22,64	14	26,76	18
16,75	11	22,85	14	26,97	18
16,95	11	23,05	14	27,17	18
17,16	11	23,26	14	27,38	18
17,36	11	23,46	14	27,58	18
17,57	12	23,67	14	27,79	18
17,77	12	23,87	14	27,99	18
17,98	12	24,08	14	28,20	18
18,18	12	24,28	14	28,40	18
18,39	12	24,49	14	28,61	18
18,59	12	24,69	14	28,81	18
18,80	12	24,90	15	29,02	18
19,00	12	25,10	14	29,22	18
19,21	12	25,31	14	29,43	18
19,41	12	25,51	15	29,63	18
19,62	12	25,72	15	29,84	18
19,82	12	25,92	15	30,04	18
20,03	12	26,13	14	30,25	18
20,23	12	26,33	15		

20,44	12	26,53	15	
20,64	12	26,74	15	
20,85	12	26,94	15	
21,05	12	27,15	15	
21,26	12	27,35	15	
21,46	12	27,56	15	
21,66	12	27,76	15	
21,87	12	27,97	15	
22,08	12	28,17	15	
22,28	12	28,38	15	
22,49	12	28,58	15	
22,69	12	28,79	15	
22,90	12	28,99	15	
23,10	12	29,20	15	
23,31	12	29,40	15	
23,51	12	29,61	15	
23,72	12	29,81	15	
23,92	12	30,02	15	
24,13	13	30,22	15	
24,33	12			
24,54	13			
24,74	13			
24,95	13			
25,15	13			
25,36	13			
25,56	13			
25,76	13			
25,97	13			
26,17	13			
26,38	13			
26,58	13			
26,79	13			
26,99	13			
27,20	13			
27,40	13			
27,61	13			
27,81	13			
28,02	13			
28,22	13			
28,43	13			
28,63	13			
28,84	13			
29,04	13			
29,25	13			
29,45	13			
29,66	13			
29,86	13			
30,07	13			

30,27	13		
30,48	13		
30,68	13		

Results 4A – Dry

Table E-7: Data from the shear box tests of sample 4A in dry condition

σ_n = 14.3 kPa		σ_n =17.6 kPa		σ_n = 21.19 kPa	
Disp (mm)	Shear kPa	Disp (mm)	Shear kPa	Disp (mm)	Shear kPa
0,00	0	0,00	0	0,00	0
0,10	5	0,10	5	0,11	6
0,21	6	0,20	6	0,21	6
0,31	6	0,31	6	0,31	7
0,41	6	0,41	7	0,41	7
0,51	6	0,51	7	0,51	8
0,61	6	0,61	7	0,62	8
0,71	6	0,71	7	0,72	9
0,82	6	0,82	7	0,82	9
0,92	6	0,92	8	0,92	9
1,02	7	1,01	8	1,02	10
1,12	7	1,12	8	1,12	10
1,22	7	1,22	8	1,19	11
1,32	7	1,32	9	1,18	11
1,43	7	1,42	9	1,18	11
1,52	7	1,52	9	1,18	11
1,63	7	1,62	9	1,18	11
1,73	8	1,73	9	1,18	11
1,83	8	1,83	9	1,18	11
1,93	8	1,93	10	1,18	11
2,03	8	2,03	10	1,18	11
2,13	8	2,13	10	1,18	11
2,24	8	2,23	10	1,38	12
2,34	9	2,29	10	1,59	12
2,44	9	2,29	10	1,80	13
2,54	9	2,29	10	2,01	13
2,64	9	2,29	10	2,22	13
2,74	9	2,29	10	2,43	13
2,84	9	2,29	10	2,64	14
2,95	9	2,29	10	2,85	14
3,05	10	2,29	10	3,06	14
3,15	10	2,29	10	3,27	14
3,25	10	2,29	10	3,48	14
3,35	10	2,29	10	3,69	14
3,45	10	2,29	10	3,90	14
3,56	10	2,49	11	4,11	15

3,62	10	2,70	11	4,32	15
3,62	10	2,91	11	4,53	15
3,62	10	3,12	11	4,74	15
3,62	10	3,33	11	4,95	15
3,62	10	3,54	12	5,16	15
3,62	10	3,75	12	5,37	15
3,62	10	3,96	12	5,58	15
3,62	10	4,17	12	5,79	15
3,62	10	4,38	12	6,00	15
3,62	10	4,59	12	6,21	15
3,62	10	4,80	12	6,42	15
3,82	11	5,01	12	6,63	15
4,03	11	5,22	12	6,84	15
4,24	11	5,43	13	7,05	15
4,45	12	5,64	13	7,26	15
4,66	12	5,85	13	7,47	15
4,87	12	6,06	13	7,68	15
5,08	12	6,27	13	7,89	15
5,29	12	6,48	13	8,10	15
5,50	12	6,69	13	8,31	16
5,71	12	6,90	13	8,52	15
5,92	12	7,11	13	8,73	15
6,13	12	7,32	13	8,94	16
6,34	12	7,53	13	9,15	15
6,55	12	7,74	13	9,36	16
6,77	12	7,95	13	9,57	16
6,98	13	8,16	13	9,78	16
7,19	12	8,37	13	9,99	16
7,40	12	8,58	13	10,20	16
7,61	12	8,79	13	10,41	16
7,82	13	9,00	13	10,62	16
8,03	13	9,21	13	10,83	16
8,24	13	9,42	13	11,04	16
8,45	13	9,63	13	11,25	16
8,66	13	9,84	14	11,46	16
8,87	13	10,05	14	11,67	16
9,08	13	10,26	14	11,88	16
9,29	13	10,47	14	12,09	16
9,50	13	10,68	14	12,30	16
9,71	13	10,89	14	12,51	16
9,92	13	11,10	14	12,72	16
10,13	13	11,31	14	12,93	16
10,34	13	11,52	13	13,14	16
10,55	13	11,73	13	13,35	16
10,76	13	11,94	14	13,56	16
10,97	13	12,15	14	13,77	16
11,18	13	12,36	13	13,98	16
11,39	13	12,57	14	14,19	16

11,60	13	12,78	13	14,40	16
11,81	13	12,99	14	14,61	16
12,02	13	13,20	13	14,82	16
12,23	13	13,41	13	15,03	16
12,44	13	13,62	14	15,24	16
12,65	13	13,83	14	15,45	16
12,86	13	14,04	13	15,66	16
13,07	13	14,25	13	15,87	16
13,28	13	14,46	13	16,08	16
13,49	13	14,67	13	16,29	16
13,70	13	14,88	13	16,50	16
13,91	13	15,09	13	16,71	16
14,12	13	15,30	14	16,92	16
14,33	13	15,51	13	17,13	16
14,54	13	15,72	13	17,34	16
14,75	13	15,93	13	17,55	16
14,96	13	16,14	13	17,76	16
15,17	13	16,35	13	17,97	16
15,38	13	16,56	13	18,18	16
15,59	13	16,77	14	18,39	16
15,80	13	16,98	13	18,60	16
16,01	13	17,19	13	18,81	16
16,22	13	17,40	13	19,02	16
16,43	13	17,61	14	19,23	16
16,64	13	17,82	14	19,44	16
16,85	13	18,03	14	19,65	16
17,06	13	18,24	14	19,86	16
17,26	13	18,45	13	20,07	16
17,47	13	18,66	13	20,28	16
17,68	13	18,87	13	20,49	16
17,89	13	19,08	13	20,70	16
18,10	13	19,29	13	20,91	16
18,31	13	19,50	13	21,12	16
18,52	13	19,71	13	21,33	16
18,73	13	19,92	13	21,53	16
18,94	13	20,13	13	21,75	16
19,15	13	20,34	13	21,95	16
19,36	13	20,55	13	22,16	16
19,57	13	20,76	13	22,37	16
19,78	13	20,96	13	22,58	16
19,99	13	21,17	13	22,79	16
20,20	13	21,38	13	23,00	16
20,41	13	21,59	13	23,21	16
20,62	13	21,80	13	23,42	16
20,83	13	22,01	13	23,63	16
21,04	13	22,22	13	23,84	16
21,25	13	22,43	13	24,05	16
21,46	13	22,64	13	24,26	16

21,67	13	22,85	13	24,47	16
21,88	13	23,06	13	24,68	16
22,09	13	23,27	13	24,89	16
22,30	13	23,48	13	25,10	16
22,51	13	23,69	13	25,31	16
22,72	13	23,90	13	25,52	16
22,93	13	24,11	13	25,73	16
23,14	13	24,32	13	25,94	16
23,35	13	24,53	13	26,15	16
23,56	13	24,74	13	26,36	16
23,77	13	24,95	13	26,57	16
23,98	13	25,16	13	26,78	16
24,19	13	25,37	14	26,99	16
24,40	13	25,58	14	27,20	16
24,61	13	25,79	14	27,41	16
24,82	13	26,00	14	27,62	16
25,03	13	26,21	14	27,83	16
25,24	13	26,42	14	28,04	16
25,45	13	26,63	14	28,25	16
25,66	13	26,84	14	28,46	16
25,87	13	27,05	14	28,67	16
26,08	13	27,26	14	28,88	16
26,29	13	27,47	14	29,10	16
26,50	13	27,68	14	29,31	16
26,71	13	27,89	14	29,52	16
26,92	13	28,10	14	29,73	16
27,13	13	28,31	14	29,94	16
27,34	13	28,52	14	30,15	16
27,55	13	28,73	14	30,36	16
27,76	13	28,94	13	30,57	16
27,97	13	29,15	14	30,78	16
28,18	13	29,36	13	30,99	16
28,39	13	29,57	14	31,20	16
28,60	13	29,78	14	31,41	16
28,81	13	29,99	14	31,62	16
29,02	13	30,20	14	31,83	16
29,23	13	30,41	14	32,04	16
29,44	13	30,62	14	32,25	16
29,65	13	30,83	14		
29,86	13	31,04	14		
30,07	13	31,25	14		
30,28	13	31,46	14		
30,49	13	31,67	14		
30,70	13	31,88	14		
30,91	13	32,09	14		
31,12	13	32,30	14		
31,33	13	32,51	14		
		32,72	14		

Results 4A – Moist

Table E-8 Data from the shear box tests of sample 4A in unsaturated condition

σ_n = 14.3 kPa		σ_n =17.6 kPa		σ_n = 21.19 kPa	
Disp (mm)	Shear kPa	Disp (mm)	Shear kPa	Disp (mm)	Shear kPa
0,00	0	0,00	0	0,00	0
0,10	5	0,10	5	0,10	5
0,20	5	0,21	5	0,20	5
0,31	5	0,31	6	0,30	6
0,41	5	0,41	6	0,41	6
0,51	5	0,51	6	0,51	6
0,61	5	0,61	6	0,61	6
0,71	6	0,71	6	0,71	6
0,81	6	0,82	6	0,81	6
0,92	6	0,92	6	0,91	7
1,02	6	1,02	7	1,02	7
1,12	6	1,12	7	1,12	7
1,22	6	1,22	7	1,22	7
1,32	6	1,33	7	1,32	7
1,42	6	1,43	7	1,42	7
1,53	6	1,53	7	1,52	7
1,63	6	1,63	7	1,63	7
1,73	6	1,73	7	1,73	8
1,83	6	1,83	7	1,83	8
1,93	6	1,93	8	1,93	8
2,03	6	2,04	8	2,03	8
2,13	6	2,13	8	2,13	8
2,24	7	2,24	8	2,24	8
2,34	7	2,34	8	2,33	8
2,44	7	2,44	8	2,44	8
2,54	7	2,54	8	2,54	8
2,64	7	2,65	8	2,64	8
2,75	7	2,74	8	2,74	9
2,85	7	2,85	8	2,84	9
2,95	7	2,95	8	2,94	9
3,05	7	3,05	8	3,05	9
3,15	7	3,16	9	3,15	9
3,25	7	3,25	9	3,25	9
3,36	7	3,35	9	3,35	9
3,46	7	3,46	9	3,45	9
3,69	7	3,56	9	3,55	9
3,76	7	3,66	9	3,66	9
3,86	7	3,76	9	3,76	10
3,97	7	3,86	9	3,86	10

4,07	7	3,96	9	3,96	10
4,17	8	4,07	9	4,06	10
4,27	8	4,17	9	4,16	10
4,37	8	4,27	9	4,26	10
4,47	8	4,38	9	4,37	10
4,57	8	4,47	9	4,47	10
4,67	8	4,57	9	4,54	10
4,78	8	4,67	9	4,54	10
4,88	8	4,78	9	4,54	10
4,98	8	4,88	9	4,54	10
5,08	8	4,98	9	4,54	10
5,18	8	5,08	10	4,54	10
5,28	8	5,18	10	4,54	10
5,38	8	5,28	10	4,54	9
5,49	8	5,39	10	4,54	9
5,59	8	5,49	10	4,54	9
5,69	8	5,59	10	4,54	9
5,79	8	5,69	10	4,54	9
5,89	8	5,79	10	4,54	9
5,99	8	5,89	10	4,74	10
6,10	8	6,00	10	4,94	10
6,20	8	6,10	10	5,15	10
6,30	8	6,20	10	5,35	10
6,40	8	6,26	10	5,56	10
6,50	8	6,26	10	5,76	10
6,60	8	6,26	10	5,97	11
6,70	9	6,26	10	6,17	11
6,81	9	6,26	10	6,38	11
6,91	9	6,26	10	6,58	11
7,01	9	6,26	9	6,79	11
7,11	9	6,26	9	6,99	11
7,21	9	6,26	9	7,20	11
7,31	9	6,26	9	7,40	12
7,42	9	6,26	9	7,61	12
7,52	9	6,46	10	7,81	12
7,62	9	6,66	10	8,02	12
7,72	9	6,87	10	8,22	12
7,82	9	7,07	10	8,43	12
7,92	9	7,28	10	8,63	12
8,03	9	7,48	10	8,84	12
8,13	9	7,69	10	9,04	12
8,23	9	7,89	10	9,25	13
8,33	9	8,10	11	9,45	13
8,57	9	8,30	11	9,66	13
8,64	9	8,51	11	9,86	13
8,74	9	8,71	11	10,07	13
8,84	9	8,92	11	10,27	13
8,94	9	9,12	11	10,47	13

9,04	9	9,33	11	10,68	13
9,14	9	9,53	11	10,88	13
9,25	9	9,74	12	11,09	13
9,35	9	9,94	11	11,29	13
9,45	9	10,15	12	11,50	14
9,55	9	10,35	12	11,70	14
9,65	9	10,56	12	11,91	14
9,75	9	10,76	12	12,11	14
9,86	10	10,97	12	12,32	14
9,95	10	11,17	12	12,52	14
10,06	10	11,38	12	12,73	14
10,16	10	11,58	12	12,93	14
10,26	10	11,79	12	13,14	14
10,36	10	11,99	12	13,34	14
10,46	10	12,19	12	13,55	14
10,56	10	12,40	12	13,75	14
10,67	10	12,60	12	13,96	15
10,77	10	12,81	12	14,16	14
10,87	10	13,01	13	14,37	14
10,97	10	13,22	13	14,57	15
11,07	10	13,42	13	14,78	15
11,13	10	13,63	13	14,98	15
11,13	10	13,83	13	15,19	15
11,13	10	14,04	13	15,39	15
11,13	10	14,24	13	15,60	15
11,13	10	14,45	13	15,80	15
11,13	10	14,65	13	16,01	15
11,13	9	14,86	13	16,21	15
11,13	9	15,06	13	16,41	15
11,13	9	15,27	13	16,62	15
11,13	9	15,47	13	16,82	15
11,13	9	15,68	13	17,03	16
11,13	9	15,88	13	17,23	16
11,13	9	16,09	13	17,44	16
11,33	10	16,29	13	17,64	16
11,54	10	16,50	14	17,85	16
11,74	10	16,70	14	18,05	16
11,95	10	16,91	14	18,26	16
12,15	10	17,11	14	18,46	16
12,36	10	17,32	14	18,67	16
12,56	10	17,52	14	18,87	16
12,77	10	17,73	14	19,08	16
12,97	10	17,93	14	19,28	16
13,18	10	18,13	14	19,49	16
13,38	11	18,34	14	19,69	16
13,59	11	18,54	14	19,90	16
13,79	11	18,75	14	20,10	16
14,00	11	18,95	14	20,31	16

14,20	11	19,16	14	20,51	16
14,41	11	19,36	14	20,72	16
14,61	11	19,57	14	20,92	16
14,82	11	19,77	14	21,13	16
15,02	11	19,98	14	21,33	16
15,22	11	20,18	14	21,54	16
15,43	11	20,39	14	21,74	16
15,63	11	20,59	14	21,95	17
15,84	12	20,80	15	22,15	17
16,05	12	21,00	14	22,36	17
16,25	12	21,21	14	22,56	17
16,46	12	21,41	15	22,77	17
16,66	12	21,62	15	22,97	17
16,86	12	21,82	15	23,18	17
17,07	12	22,03	15	23,38	17
17,27	12	22,23	15	23,59	17
17,48	12	22,44	15	23,79	17
17,68	12	22,64	15	24,00	17
17,89	12	22,85	15	24,20	17
18,09	12	23,05	15	24,40	17
18,30	12	23,26	15	24,61	17
18,50	12	23,46	15	24,81	17
18,71	12	23,67	15	25,02	17
18,91	12	23,87	15	25,22	17
19,12	12	24,07	15	25,43	17
19,32	12	24,28	15	25,63	17
19,53	12	24,48	15	25,84	17
19,74	12	24,69	15	26,04	17
19,94	12	24,89	15	26,25	17
20,15	12	25,10	15	26,45	17
20,35	12	25,30	15	26,66	17
20,56	12	25,51	15	26,86	17
20,76	12	25,71	15	27,07	18
20,97	12	25,92	15	27,27	17
21,17	12	26,12	15	27,48	17
21,38	13	26,33	15	27,68	17
21,58	13	26,53	16	27,89	17
21,79	13	26,74	16	28,09	18
21,99	13	26,94	16	28,30	18
22,20	13	27,15	16	28,50	18
22,40	13	27,35	16	28,71	18
22,61	13	27,56	16	28,91	18
22,81	13	27,76	16	29,12	18
23,02	13	27,97	16	29,32	18
23,22	13	28,17	16	29,53	18
23,43	13	28,38	16	29,73	18
23,63	13	28,58	16	29,94	18
23,84	13	28,79	16	30,14	18

24,04	13	28,99	16	30,34	18
24,25	13	29,20	16	30,55	18
24,45	13	29,40	16	30,75	18
24,66	13	29,61	16	30,96	18
24,86	13	29,81	16	31,16	18
25,07	13	30,01	16	31,37	18
25,27	13	30,22	16		
25,48	13	30,42	16		
25,68	13	30,63	16		
25,89	13				
26,09	13				
26,30	13				
26,50	13				
26,71	13				
26,91	13				
27,11	13				
27,32	13				
27,52	14				
27,73	14				
27,93	14				
28,14	14				
28,34	14				
28,55	14				
28,75	14				
28,96	14				
29,16	14				
29,37	14				
29,57	14				
29,78	14				
29,98	14				
30,19	14				
30,39	14				
30,60	14				